Summer 7-16-2013

Remote Sensing of Green Leaf Area Index in Maize and Soybean: From Close-Range to Satellite

Anthony L. Nguy-Robertson
University of Nebraska-Lincoln, anthony.robertson@huskers.unl.edu

REMOTE SENSING OF GREEN LEAF AREA INDEX IN MAIZE AND SOYBEAN: FROM CLOSE-RANGE TO SATELLITE

by

Anthony Lawrence Nguy-Robertson

A DISSERTATION

Presented to the Faculty of

The Graduate College at the University of Nebraska

In Partial Fulfillment of Requirements

For the Degree of Doctor of Philosophy

Major: Natural Resource Sciences

Under the Supervision of Professor Anatoly A. Gitelson

Lincoln, Nebraska

July, 2013

REMOTE SENSING OF GREEN LEAF AREA INDEX IN MAIZE AND SOYBEAN: FROM CLOSE-RANGE TO SATELLITE

Anthony Lawrence Nguy-Robertson, Ph.D.

University of Nebraska, 2013

Advisor: Anatoly A. Gitelson

This dissertation seeks to explore alternative methodologies for estimating green leaf area index (LAI) and crop developmental stages. Specifically this research [1] developed an approach for creating a Moderate Resolution Imaging Spectroradiometer (MODIS) high spatial resolution product for estimating green LAI on the base of data collected using two different close-range sensors. It was determined that the vegetation indices (VIs) Wide Dynamic Range Vegetation Index (WDRVI) and Enhanced Vegetation Index 2 (EVI2) were capable of accurate estimation of green LAI from MODIS 250 m data using models developed from hyperspectral (RMSE < 0.69 m^2 m^{-2}; CV < 33%) or multispectral sensors (RMSE < 0.69 m^2 m^{-2}; CV < 34%). [2] Explored a new approach for maximizing the sensitivity of VIs to green LAI. Rather than use one VI, we suggested using multiple VIs in different LAI dynamic ranges. Thus, the sensitivity of the VI to the green LAI was preserved and simpler linear models could be used instead of complex non-linear ones. Two combined vegetation indices (CVI) were presented using near infrared and either the red or red edge bands and were accurate in estimating green LAI. While the red band is more common in satellite sensors, the indices use red edge band were found to be species independent for maize and soybean. The two species-independent VIs used in the CVI were Red Edge Normalized Difference

Index (Red Edge NDVI) and Red Edge Chlorophyll Index ($CI_{red\ edge}$). [3] Algorithms were developed for estimating green LAI in four vastly different crops (maize, potato, soybean, and wheat) that do not require re-parameterization. The most promising VIs for developing a unified algorithm utilized either a green or red edge bands. [4] It was found that, in addition to traditionally used (VIs), the 2-dimensional spectral spaces (e.g. red vs. green reflectance) were capable of identifying four distinct stages of crop development (e.g. soil/residue, green-up, vegetative, and senescence).

Dedicated to my lovely wife, Karen Nguy-Robertson, without her support and understanding, this work would have not been possible. Her willingness to come home after working all day to take care of our newborn son, Jacoby has allowed me to finish my dissertation in a timely manner.

Acknowledgements

There are many individuals who have helped me along on this road to a Ph.D. I could have never completed so much without their support. First and foremost, I must thank my advisor and chairman of my supervisory committee, Dr. Anatoly Gitelson. His passion for science was unmatched and is an inspiration to all who follow. I enjoyed our discussions and occasional disagreements. Dr. Gitelson always encouraged us to develop ideas even when contrary to his line of thought. He stimulated deep thought into concepts rather than focusing on the surface, easy-to-obtain answers. I am disheartened to be one of Dr. Gitelson's last students here at the University of Nebraska-Lincoln. I wish him the best in his future endeavors.

My committee members, in alphabetical order: Drs. Timothy J. Arkebauer, Donald C. Rundquist, Andrew E. Suyker, and Brian D. Wardlow, have also progressed my research through discussions, manuscript revisions, providing data, and classroom instruction. Their collective expertise has influenced my writing and improved my skills in research design. Thanks to Dr. Rundquist, I will never view the word 'this' the same way.

I would like to thank Dr. Elizabeth Walter-Shea for the use of her 4-band radiometers for my project and her suggestions for my manuscripts. I also appreciate the innovations that Dr. Arthur Zygielbaum has brought to the sensor platform, Hercules, and the wireless backpack system. This has allowed our research group to explore some topics of interest without having to run cables everywhere. I am also thankful for the assistance in processing some of the MODIS imagery and the use of his digital cameras from Dr. Toshi Sakamoto.

I would like to thank Bryan Leavitt for his technical assistance. He was extremely valuable in assisting in the development of the calibration procedure for the 4-band radiometers. He also assisted with solving various field and computer problems.

I have had many thoughtful discussions with my Gitelson Lab colleagues, Yi Peng, Daniela Gurlin, Tarlan Razzaghi, and Wesley Moses. There was no competition between us and I appreciated the friendly advice and assistance provided even after graduation. All four of them are very intelligent and excellently trained by Dr. Gitelson. I look forward to collaborating with all of them in the future. I must also provide an extra thanks to Yi and Tarlan for house-sitting my pets when I was away.

I am extremely thankful for the assistance of the staff, graduate, and undergraduate students involved in the carbon sequestration project. I would like to specifically thank Dave Scoby and Tommy Lowman who are responsible for collecting the ground data which I base my models. I would also like to thank Drs. David Bonfil, Agustin Pimstein, Ittai Herrmann, and Arnon Karnieli for their wheat and potato data used in Chapter 5.

I appreciate the opportunity to teach several different classes at varying degree levels. I want to specifically thank Drs. Tala Awada, Anatoly Gitelson, Ayse Kilic, and Arthur Zygielbaum for serving as a mentor in the classroom. I want to thank Bryan Leavitt for trusting me to teach one of his lectures for his course.

I would like to thank Dr. James Brandle for supporting the School of Natural Resources Graduate Student Association. His dedication to improving conditions for graduate students in SNR is an inspiration to remember to be kind to my future students.

I am thankful for the support of my friends and family, primarily my parents Bruce and Christine, my brother Doug and sister Rebecca.

Grant Information

This research was supported partially by the by the NASA NACP program, U.S. Department of Energy EPSCoR program, Grant Office of Science (BER), NASA EPSCoR “Aerial” grant, Nebraska Space Grant program, BARD Senior Research Fellowship program, and funds provided through the Hatch Act.

My graduate assistantship and money for travel for presentations of the results at international conferences was supported through the School of Natural Resources Graduate Assistantship, University of Nebraska Chancellor's Fellowship, Farmers National Company Fellowship, Nebraska Space Grant Fellowship and Travel Grant, and the Larrick Travel Grant. I am grateful to be supported by the resources, facilities, and equipment by the Center for Advanced Land Management Information Technologies (CALMIT), Carbon Sequestration Program, and the School of Natural Resources located within the University of Nebraska-Lincoln.

TABLE OF CONTENTS

LIST OF FIGURES

LIST OF TABLES

LIST OF EQUATIONS

Chapter 1 : Introduction and background

One of the most commonly utilized vegetation biophysical characteristics is leaf area index, LAI (Buermann et al., 2001; Bulcock & Jewitt, 2010; Fang et al., 2011). LAI is the ratio of leaf area per ground area typically reported with the units m^2 m^{-2} (Watson, 1947). The green LAI is the ratio of green photosynthetically active leaf area per ground area (Daughtry et al., 1992) and is typically utilized instead of LAI since it is a measure of leaf area participating in photosynthesis. Green LAI is a metric commonly used in climate (Buermann et al., 2001), ecological (Bulcock & Jewitt, 2010; Richardson et al., 2011), and crop models (Casa et al., 2012), as well as for estimating crop vegetation status (Bobée et al., 2012), light-use efficiency (Claverie et al., 2012; Garbulsky et al., 2011), and yield (Fang et al., 2011; Guindin-Garcia et al., 2012).

Various techniques based on remotely sensed data have been employed for assessing green LAI (Doraiswamy et al., 2003; Hatfield et al., 2004, 2008; le Maire et al., 2008; Pinter et al., 2003). Vegetation indices (VIs) are a widely employed remote sensing technique for monitoring various crop characteristics (Hatfield & Prueger, 2010; Huang et al., 2012) including green LAI, primarily due to their simplicity in application and ease of data processing. Most VIs incorporate reflectance in a few wavebands that can be collected mainly by satellite broadband sensors (e.g., Moderate Resolution Imaging Spectroradiometer, MODIS, and Medium Resolution Imaging Spectrometer, MERIS, among others). While narrow band and hyperspectral data can be used, it is often not necessary (Broge & Leblanc, 2001) except in cases of sparse canopy and high background reflectance (Elvidge & Chen, 1995), or to distinguish between similar classes, as is the case in monitoring crop P and K content (Pimstein et al., 2011) or weed

identification (Shapira et al., 2013). This is usually not the case in many managed agricultural systems (e.g. treated with herbicides, irrigated) after the initial stages of crop growth. Several studies have examined the relationship between VIs and green LAI (Broge & Leblanc, 2001; J. Liu et al., 2012); however, few studies have examined this relationship in the context of multiple crops with a wide range of leaf structures and canopy architectures.

VIs, particularly the normalized difference vegetation index, NDVI (Rouse et al., 1974) and the simple ratio, SR (Jordan, 1969), are the most widely used. However, NDVI is prone to saturation at moderate-to-high green LAI values (Asrar et al., 1984; Baret & Guyot, 1991; Buschmann & Nagel, 1993; Curran & Steven, 1983; Gitelson, 2004; González-sanpedro et al., 2008; Huete et al., 2002; Kanemasu, 1974; Myneni et al., 1995, 2002; Sellers, 1985; Wu et al., 2007) and requires re-parameterization for different crops/species. The saturation of NDVI has been attributed to insensitivity of reflectance in the red region at moderate-to-high green LAI values due to the high absorption coefficient of chlorophyll. For green LAI below 3 $m^2 m^{-2}$, total absorption by a canopy in the red range reaches 90-95% and further increases in green LAI do not bring additional changes in absorption and reflectance (Gitelson, 2011; Hatfield et al., 2008). Another reason for the decrease in sensitivity of NDVI to moderate-to-high green LAI values is the mathematical formulation of that index. At moderate-to-high green LAI, the NDVI is dominated by near infrared (NIR) reflectance. Because scattering by cellular/leaf structure causes the NIR reflectance to be high and the absorption by chlorophyll causes the red reflectance to be low, NIR reflectance is considerably greater than red reflectance:

e.g., for green LAI = 3 $m^2 m^{-2}$, NIR reflectance is around 40%, while red reflectance is below 5%. Thus, NDVI becomes insensitive to changes in both red and NIR reflectances.

In contrast to NDVI, VIs such as the simple ratio (SR), MEdium Resolution Imaging Spectrometer (MERIS) terrestrial chlorophyll index (MTCI), and chlorophyll indices (CIs) are less sensitive to low values of green LAI; however, they show an increase in sensitivity to moderate to high green LAI (Nguy-Robertson et al., 2012; Viña et al., 2011). It also has been demonstrated that the red-edge inflection point (REIP) is a good predictor of widely variable green LAI in potato and wheat (Herrmann et al., 2011).

Other commonly used VIs include the enhanced vegetation index, EVI (Huete et al., 1997, 2002), its alternative form, EVI2 (Jiang et al., 2008), and the triangular vegetation index, TVI (Broge & Leblanc, 2001). While the EVI is more sensitive to moderate-to-high LAI than NDVI, it was also found to be sensitive to canopy architecture (Gao et al., 2000), and it does not relate well to LAI during the senescence stages (Wang et al., 2005). The TVI relates the difference between reflectance in the NIR and red regions to the magnitude of reflectance in the green region, thus, defining a triangle in a three dimensional spectral space. While the TVI is less affected by atmospheric properties when compared to typical vegetation indices, it is sensitive to differences in canopy structure and soil background (Broge & Leblanc, 2001). To minimize the sensitivities of TVI, a soil adjustment factor has been introduced in a modified version of the TVI, MTVI (Haboudane et al., 2004). The same study found that a second modified version (MTVI2) was accurate in estimating green LAI in different canopy structures that were simulated through radiative transfer models. Another investigation, aimed at examining green LAI in wheat, found that MTVI2 was more sensitive than NDVI to

green LAI at higher green LAI values; however, it was sensitive to heading (i.e. flowering), which is not a component of green LAI, but nevertheless affects the reflectance of crop canopies (Smith et al., 2008).

VIs that incorporate bands in the spectral transition zone between absorption by pigments and scattering by leaves/canopies, termed the "red edge region" (between 700 and 740 nm), were introduced to increase the sensitivity to moderate-to high vegetation densities and estimate total chlorophyll content and green LAI (Dash & Curran, 2004; Gitelson & Merzlyak, 1994; Gitelson et al., 2003b). Radiation in the red edge region penetrates deeper into the leaves and canopies than radiation in the visible region due to a lower absorption coefficient in the former than in the latter. Thus, higher values of chlorophyll content and green LAI are required to decrease the sensitivity of red edge VIs to green LAI (Ciganda et al., 2008; Dash & Curran, 2004; Gitelson, 2011). Some of the red edge VIs constitute transformations of existing VIs, such as the red edge NDVI (Gitelson & Merzlyak, 1994), which replaces the red band with one in the red edge region. Others constitute semi-analytical procedures for estimating pigment content in diffuse media, such as the Chlorophyll Indices, CI (Gitelson et al., 2003a). While the CIs were developed for estimating chlorophyll content, they also correlate closely with green LAI since total canopy chlorophyll content has been shown to be closely related to green LAI (Ciganda et al., 2008; Peng et al., 2011). Therefore, CIs are suitable for estimating green LAI (Brantley et al., 2011; Gitelson et al., 2003b), but particularly for moderate-to-high green LAI values. For instance, it was found that VIs utilizing the red edge region (710-730 nm) were more accurate for estimating moderate-to-high green LAI in shrub canopies than normalized difference indices (Brantley et al., 2011). However, this study

also found that at low-to-moderate green LAI values, normalized difference indices (e.g., NDVI) perform better than the $CI_{red\ edge}$. The MERIS Terrestrial Chlorophyll Index (MTCI) also contains a red-edge band, and was developed for the remote estimation of total canopy chlorophyll content (Dash & Curran, 2004, 2007). It has been shown that the MTCI closely relates with green LAI (Gitelson, 2011).

Canopy reflectance of several crop species can be influenced by the presence of reproductive organs (Pimstein et al., 2009; Viña et al., 2004; Yang & Chen, 2004), thus this is likely to reduce the accuracy of the models using VIs sensitive to these changes. For green LAI estimation using VIs, it is ideal that the VI selected is not sensitive to canopy architecture (e.g. leaf angle distribution), leaf structure (e.g. foliar chlorophyll distribution), reproductive organs (e.g. tassels in maize, heading in wheat) and heliotropism (e.g. sun-avoidance), such that the relationships green LAI vs. VI would be applicable to different vegetation types without requiring algorithm re-parameterization. The VIs selected should also be insensitive to soil background and atmospheric effects.

To minimize the effects of soil background and maximize the sensitivity to foliar chlorophyll, it was suggested to combine two VIs by taking a ratio of a VI sensitive to chlorophyll and a VI insensitive to soil background, canopy architecture, and LAI variability (Daughtry et al., 2000). Thus, combination of indices based on the Transformed Chlorophyll Absorption Reflectance Index (TCARI), the MCARI, and the OSAVI, such as, TCARI/OSAVI and MCARI/OSAVI, were used to estimate leaf chlorophyll content in crops, minimizing the effects of the soil background and the green LAI variation (Daughtry et al., 2000; Haboudane et al., 2002). However, the goal of these studies was to remove the effect of LAI on the estimation of leaf chlorophyll content

(Daughtry et al., 2000; Eitel et al., 2008, 2009; Haboudane et al., 2002), therefore, for this study, that particular set of VIs was not considered for estimating green LAI.

Viña et al., (2011) evaluated the potential effects of soil background on the remote estimation of green LAI. For this, they used reflectance spectra of spherical and planophile canopies with different green LAI values under two contrasting soil backgrounds (i.e., dark and bright), as simulated by the New Advanced Discrete Model (Gobron et al., 1997), and used them for calculating three vegetation indices - EVI, MTCI and $CI_{red\ edge}$. The EVI has been suggested to be less sensitive to background effects (Huete et al., 1997), however, the uncertainties of green LAI estimation due to soil background effects by all three indices were very similar. In the spherical canopy, the errors of EVI, MTCI and $CI_{red\ edge}$ were 0.25, 0.18, and 0.21 $m^2\,m^{-2}$, respectively, while in the planophile canopy they were 0.21, 0.20, 0.14 $m^2\,m^{-2}$, respectively.

Maize and soybean plants have contrasting canopy architectures (i.e., maize has a predominantly spherical leaf angle distribution while soybean has a predominantly planophile/heliotropic leaf angle distribution), and leaf structures (i.e., maize is a monocot while soybean is a dicot) that exhibit different chlorophyll distributions along the leaf depth (De Wit, 1965; Ehleringer & Forseth, 1980; Idso & de Wit, 1970). Additionally, these two species have different physiological pathways (C3 vs. C4). Based on contrasting anatomical and physiological traits, these crops are representative of many crops types, and most VIs have been shown to respond to them, thus are species- or crop-specific (Curran & Milton, 1983; Gao et al., 2000; González-sanpedro et al., 2008). However, some indices that use red edge bands in their formulation have been shown to

be less sensitive to differences among species (Brantley et al., 2011; Gitelson, 2011; Gitelson et al., 2005; Viña et al., 2011).

In addition to estimating green LAI, there is a strong interest in real-time monitoring of the plant stage of development as defined by the USA phenological network (Betancourt et al., 2005) and SpecNet (Gamon et al., 2006) for detecting the impacts of climate change (Hufkens et al., 2012; Richardson et al., 2009; Zhang et al., 2003). This definition of plant stage of development should not be confused with the definition of phenology as defined for identifying plant developmental and reproductive status (Abendroth et al., 2011; Hanway, 1963). VIs have been used to determine plant stage of development (Baghzouz et al., 2010; Eklundh et al., 2011; Hmimina et al., 2013; Huete, 2012; Soudani et al., 2012). However, this approach has some limitations when applied out of context of the data set or to ancillary data. For example, with the same crop greenness, the values of most typically utilized VIs (e.g. Normalized Difference Vegetation Index, NDVI; Enhanced Vegetation Index, EVI) are similar in both the green-up/leaf-on and senescence stages. Therefore, having reflectance data taken with low temporal resolution it is difficult to differentiate between plant stages of development without any other ancillary data. In crop systems in Nebraska and most agricultural areas of the USA, the date of acquisition is likely enough ancillary information to determine crop stage of development (e.g. green-up vs. senescence) using VIs. However, in some areas of the world, multiple cropping patterns are common. It is in these regions that it is necessary to examine alternative methods for identifying plant stage of development.

Earlier studies have attempted to achieve near-continuous data sets for monitoring plant stage of development by collecting data frequently (2-3 per week) using a close-

range spectroradiometer (Gitelson et al., 2003b; Goodin & Henebry, 1997; Viña et al., 2004). However, even with these frequent measurements, changes in plant stage of development may be missed. Therefore, instruments that are capable of collecting data continuously are commonly used in monitoring plant stage of development and physiological status of vegetation. They include light emitting diodes, LEDs (Ryu et al., 2010), radiometers (Eklundh et al., 2011; Gamon et al., 2006; Sakamoto et al., 2012), and digital cameras (Sakamoto et al., 2010, 2011).

In addition to VIs, spectral spaces, or the relationship between reflectances in different spectral bands, can be informative to plant stage of development and physiological status of vegetation. The tasseled cap methodology uses various reflectance bands in 3-dimensional (3-D) space (Crist & Cicone, 1984a; Crist & Kauth, 1986) for a variety of applications such as estimating plant stage of development (Crist & Cicone, 1984b), differentiating between sagebrush species (Sivanpillai & Ewers, 2013), and use in models for predicting wildlife corridors (Squires et al., 2013). Even comparisons of reflectances in just two bands can provide information such as the impacts of background on reflectance (Broge & Leblanc, 2001; Gobron et al., 1999), land cover estimates (Hansen et al., 1998), and estimating vegetation fraction (Gitelson et al., 2002). 2-D spectral spaces have been used to estimate periods in plant stage of development, primarily by using near infrared (NIR) vs. red reflectance space (Ayyangar et al., 1980). Little attention was paid to the use of 2-D spectral spaces with visible spectral bands where, in addition to the soil line, the vegetation line is clearly defined (Gitelson et al., 2002).

The purposes of the research presented in this thesis are to:

1) Demonstrate the use of close-range sensors for monitoring crop stage of development
2) Explore the sensitivity and accuracy of different vegetation indices for estimating green LAI in maize and soybean
3) Determine if the green LAI vs. VI relationships found for maize and soybean are similar to those in potato and wheat
4) Develop green LAI products from close-range sensors
5) Apply the green LAI products developed using close-range sensors to a satellite sensor

Chapter 2 : Materials and methods

2.1 Study area

The primary study area included three approximately 65-ha fields involved in the Carbon Sequestration Program (Verma et al., 2005) located at the University of Nebraska-Lincoln (UNL) Agricultural Research and Development Center near Mead, Nebraska, U.S.A (41°10"46.8'N, 96°26"22.7'W, 361 m above mean sea level) under different management conditions (Figure 2.1). From 2001-2009, one of the fields was irrigated maize, the other two were under a maize/soybean rotation either irrigated (via center pivots) or rainfed. In 2010, the irrigated maize/soybean field was converted to continuous maize. All fields were fertilized and treated with herbicide/pesticides following UNL's best management practices for eastern Nebraska. A summary of the

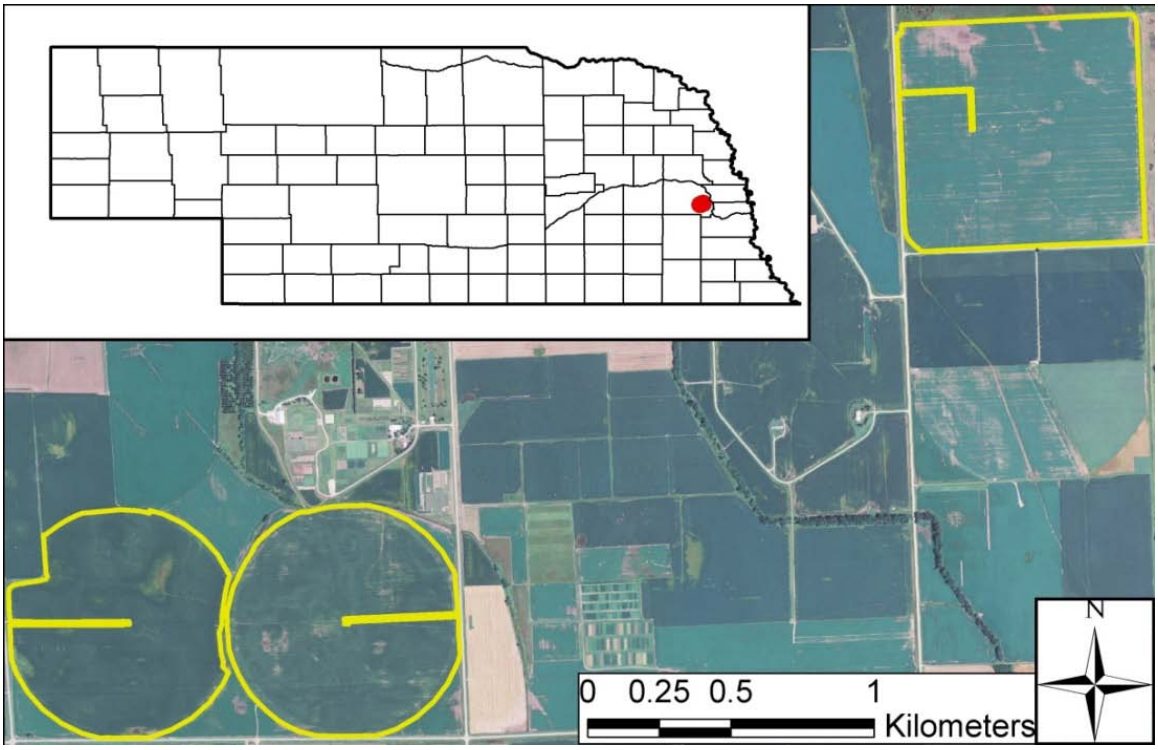

Figure 2.1: Map of the study area in Nebraska, USA

Table 2.1: Hybrid, planting density and maximum green leaf area index (green LAI) in the three sites studied. Sites 1 and 2 were irrigated with center pivots. Site 3 was rainfed.

Year	Site	Crop	Hybrid	Planting Density (plants ha^{-1})	Maximum green LAI (m^2 m^{-2})
2001	1	Maize	Pioneer 33P67	82,000	6.1
	2	Maize	Pioneer 33P67	83,314	6.1
	3	Maize	Pioneer 33B51	62,236	3.9
2002	1	Maize	Pioneer 33P67	81,000	6.0
	2	Soybean	Asgrow 2703	370,644	5.5
	3	Soybean	Asgrow 2703	370,644	3.0
2003	1	Maize	Pioneer 33B51	77,000	5.5
	2	Maize	Pioneer 33B51	86,667	5.5
	3	Maize	Pioneer 33B51	64,292	4.3
2004	1	Maize	Pioneer 33B51	84,012	5.2
	2	Soybean	Pioneer 93B09	370,644	4.4
	3	Soybean	Pioneer 93B09	370,644	4.5
2005	1	Maize	DeKalb 63-75	82,374	5.2
	2	Maize	Pioneer 33B51	83,200	4.8
	3	Maize	Pioneer 33G68	59,184	4.3
2006	1	Maize	Pioneer 33B53	84,012	5.3
	2	Soybean	Pioneer 31N28	370,644	5.0
	3	Soybean	Pioneer 93M11	370,644	4.5
2007	1	Maize	Pioneer 31N30	80,697	6.3
	2	Maize	Pioneer 31N28	78,740	5.7
	3	Maize	Pioneer 33H26	62,088	4.1
2008	1	Maize	Pioneer 31N30	84,469	6.5
	2	Soybean	Pioneer 93M11	369,508	4.7
	3	Soybean	Pioneer 93M11	369,508	3.6
2009	1	Maize	Pioneer 32N73	81,108	6.4
	2	Maize	Pioneer 32N72	81,108	6.6
	3	Maize	Pioneer 33T57	61,446	4.9
2010	1	Maize	DeKalb 65-63 VT3	81,675	5.7
	2	Maize	DeKalb 65-63 VT3	82,382	4.5
	3	Soybean	Pioneer 93M11	370,644	3.8
2011	1	Maize	Pioneer 32T88	80,153	5.8
	2	Maize	Pioneer 32T88	81,112	6.1
	3	Maize	DeKalb 61-69 VT3	56,834	3.5
2012	1	Maize	DeKalb 62-97 VT3	84,015	4.7
	2	Maize	DeKalb 62-97 VT3	84,015	5.0
	3	Soybean	Pioneer 93M43	370,644	3.3

hybrids, planting densities, and maximal green leaf area index (green LAI) is in Table 2.1. Additional details on the study sites in Nebraska can be found in Suyker et al. (2004, 2010) and Verma et al. (2005).

A secondary research site growing wheat and potato was located in northwestern Negev, Israel (Figure 2.2). All fields consisted of irrigated plots under different nitrogen management strategies from 2004 through 2007. The green LAI for potato ranged from 0.68 to 3.3 $m^2 m^{-2}$ in 2006 and 0.17 to 4.1 $m^2 m^{-2}$ in 2007. The green LAI for wheat ranged from 0.12 to 4.5 $m^2 m^{-2}$ in 2004 and 2.77 to 6.4 $m^2 m^{-2}$ in 2005. The nitrogen treatment for potato consisted of applications of 0, 100, 215, 335, or 400 kg N ha^{-1} in 2006 and 0, 100, 200, 300, or 400 kg N ha^{-1} in 2007 (Cohen et al., 2010). The nitrogen

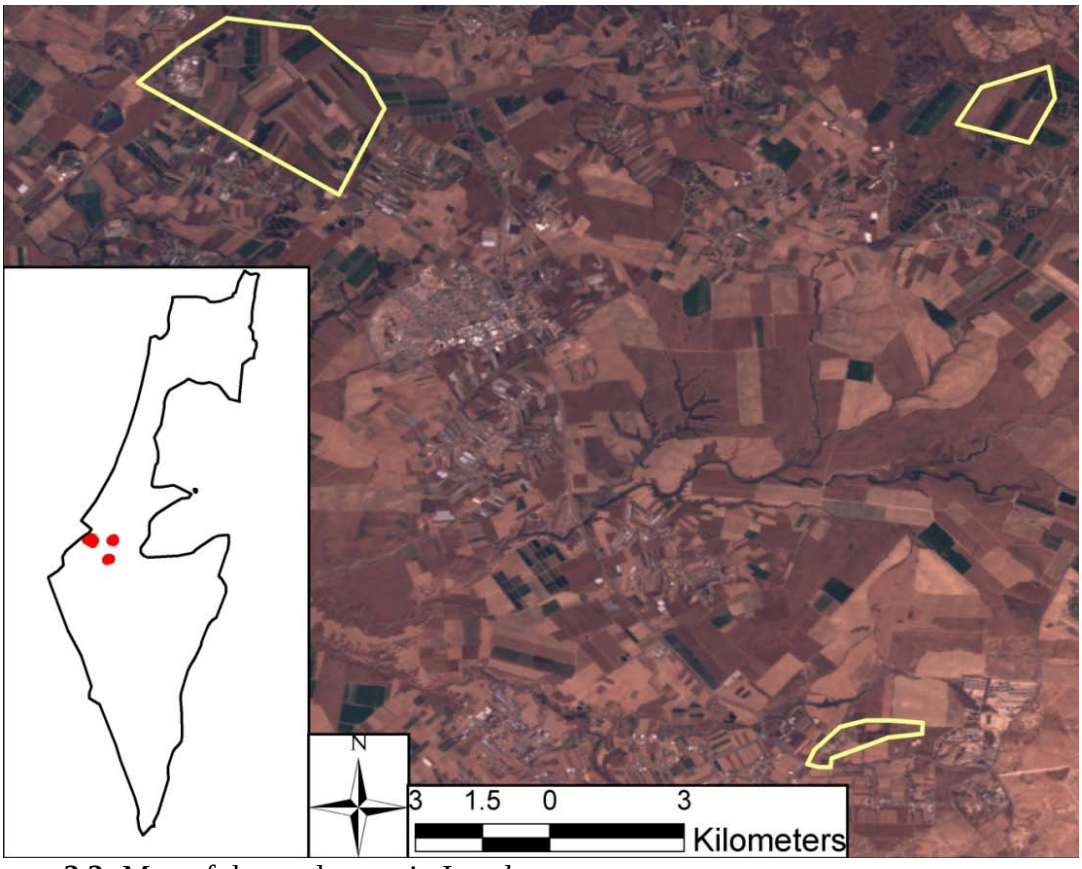

Figure 2.2: Map of the study area in Israel

treatment for wheat was either 50 or 100 kg N ha^{-1} in both 2004 and 2005. There were a total of 11 and 4 field-years for potato and wheat, respectively. Specific details of this study site can be found in the papers of Pimstein et al., (2007); Pimstein et al., (2009) and Herrmann et al., (2011).

2.2 Ground-truth measurements

2.2.1 Field measurements

For the sites located in Nebraska, the green LAI was calculated from the leaf area determined from plants harvested from a 1 m length of one or two rows (6 ± 2 plants) from six small (20 m x 20 m) plots established in each field. These plots represented all major soil types within the field. The plants were collected every 10-14 days from each field between emergence and crop maturity (with the exception of the 2010 season which ended after DOY 255 due to power failure to the instruments and heavy crop damage following a hail storm). The plants collected were transported on ice to the laboratory for visual separation into green and dead leaves. The leaf area of the green leaves per plant was measured using an area meter (LI-3100, Li-Cor, Inc., Lincoln, NE, USA). Green LAI was determined by multiplying the green leaf area per plant by the plant population (plants m^{-2}) within the sampling plot. The green LAI values from all six plots were averaged to provide a field-level green LAI. Crop phenological stage (Abendroth et al., 2011) was also recorded for each plot on each LAI sampling date.

For the sites located in Israel, LAI measurements were an average of three measurements taken in the same field of view (FOV) as the spectral measurements using an AccuPAR LP80 ceptometer (Decagon Devices, Inc.) programmed differently

according to the manufacturer's instructions for potato and wheat. The leaf distribution parameter was set to 2.00 for potato and 0.96 for wheat. Since the ceptometer measurements used transmittance to estimate LAI, the study was limited to only the green up stage where the LAI measurements were a good proxy of green LAI. The values of replicate plots (same treatment) were averaged to create a field level green LAI value for each sampling date.

2.2.2 Lab measurements

Total canopy chlorophyll (Chl) was determined during the 2001-2005 field campaigns for maize (n = 189) and soybean (n = 72). Firstly, we determined leaf chlorophyll *a* content using non-destructive leaf reflectance measurements (Ciganda et al., 2009; Gitelson et al., 2003a), collected with an USB2000 (Ocean Optics, Inc.) fitted with a leaf clip and a bifurcated fiber attached to a LS-1 tungsten halogen light source (Ocean Optics, Inc.). The leaf was held at 60° angle relative to the fiber and calibrated using a Spectralon coated 99% reflectance panel (Labsphere, Inc.). The following equation was used to determine the leaf chlorophyll *a* content in the upper canopy leaf for soybean and either the collar or ear leaf for maize (Ciganda et al., 2009):

$$\text{Leaf Chlorophyll (mg m}^{-2}) = 37.9 + 1353.70 * CI_{\text{red edge}} \quad (2.1)$$

The $CI_{\text{red edge}}$ is the same formulation as in Table 2.3 using the spectral ranges of 725±5 and 785±15 nm for red edge and NIR, respectively. Equation 2.1 was calibrated with leaf pigment content determined analytically from circular punches and extracted

with 100% acetone (Lichtenthaler, 1987). A root mean square error (RMSE) of Chl estimation was less than 51 mg m^{-2} in the range of Chl content 2.44-918 mg m^{-2} for both crops (Ciganda et al., 2009).

Total canopy Chl content was then determined as a product of leaf chlorophyll *a* content and green LAI:

$$\text{Canopy Chlorophyll (Chl, g } m^{-2}) = \text{Leaf Chlorophyll} * \text{green LAI} \quad (2.2)$$

2.3 Canopy reflectance

2.3.1 Hyperspectral reflectance

For the sites located in Nebraska, canopy reflectance was collected using an all-terrain sensor platform (Figure 2.3), with a dual-fiber system and two Ocean Optics USB2000 radiometers (Rundquist et al., 2004). One fiber was fitted with a cosine diffuser to measure incoming downwelling irradiance, and the second one measured upwelling radiance. The field of view of the upwelling sensor was kept constant along the growing season (approximately 2.4 m in diameter) by placing the radiometer at a height of 5.5 m above the top of the canopy. Ten reflectance spectra were measured at each of 36 collection points along access roads into each of the fields, and average reflectance represented each collection point. Measurements took about 5 minutes per plot and about 30 minutes per field. The two radiometers were inter-calibrated immediately before and immediately after measurement in each field.

Using hyperspectral aerial imagery, acquired over the study site by an AISA Eagle hyperspectral imaging spectrometer, it was shown that the canopy reflectance in

Figure 2.3: Image of the all-terrain field sensor Hercules

the fields was spatially homogeneous; thus, reflectance spectra taken along access roads were representative of the field (Viña et al., 2011). Therefore, the remotely estimated green LAI may be compared with measured field level green LAI.

For the sites located in Israel, canopy reflectance of potato and wheat were collected in clear sky conditions in a nadir orientation ±2 h from solar noon using an Analytical Spectral Devices (ASD) FieldSpec Pro FR spectrometer with a spectral range of 350-2500 nm and 25° field of view (FOV). For the purpose of this study, we only utilized the visible/near-infrared region with a spectral resolution of 1.4 nm. Measurements were an average of 20 readings taken 1.5 m above the ground with a FOV of approximately 0.35 m^2 at the start of the season. Due to crop growth, the FOV was reduced to 0.13-0.26 m^2 and 0.08 m^2 for potato and wheat, respectively. Barium sulfate

($BaSO_4$) was used as the white reference for potato reflectance and a standard white reference panel (Spectralon Labsphere Inc.) was utilized for wheat reflectance.

2.3.2 Multispectral reflectance

The multispectral instruments were only used in Nebraska. Seven SKYE radiometers (SKR 1850, SKYE Instruments Ltd, Llandrindod Wells, UK), were used with four spectral bands: green (536.5-561.5 nm), red (664.5-675.5 nm), red edge (704.5-715.5 nm), and NIR (862-874 nm). SKYE radiometers can measure downwelling irradiance with the aid of a cosine corrector. When used without the cosine collector, upwelling radiance can be measured within a 25° field of view.

All SKYE instruments were mounted 6 m above the ground on a tower located in the middle of each field (Figure 2.4). For the irrigated fields, one downwelling and one upwelling instrument was installed. For the rainfed field, two upwelling instruments were installed 30 cm apart to monitor the impact of sensor placement on reflectance. This instrument orientation provided one set of measurements centered above the row and one set of measurements centered between the rows. Responses from the radiometers were recorded every second between 0500 and 1900 h (CDT) from which thirty minute averages were determined. Reflectance was determined by using a ratio of incoming irradiance and upwelling radiance collected by two four-band radiometers (see 2.4.3 Multispectral reflectance for details).

There were two different calibrations procedures applied. For the 2003-2005 data set pairs of instruments (downwelling and upwelling for each site) were assigned and calibrated together. These pairs were mounted on a goniometer; henceforth named as the

Figure 2.4: SKYE instruments mounted on the radiation tower over maize (Above) and a close-up image of the sensors (Below)

goniometer calibration, in the same orientation as that installed on each site (e.g. downwelling was facing upward, upwelling was facing the calibration panel). A large 1.22 m x 1.22 m halon reference panel was used. Instruments were calibrated under clear sky conditions. The goniometer was inclined using a series of angle inclinations (15-75° at 5° increments). The calibration coefficient (CC) for each date is an average of the measurements collected.

For the 2009-2012 data sets, the SKYE radiometers were calibrated based on their response to a National Institute of Standards and Technology (NIST) traceable light source in a uniform light source integrating sphere calibration system (OCL-61, Labsphere, Inc.); henceforth named the calibrated light source. Each SKYE sensor was placed flush with the integrating sphere exit port with the light output maintained at 64,475 cd m^{-2}. The output of spectral radiance at the band centers of the green, red, red edge, and NIR bands was 793.5, 1,236, 1,333, and 1,455 W m^{-2} sr^{-1} nm^{-1} respectively. The output (in mV) of the SKYE sensors for each spectral band is proportional to the spectral radiance received. As part of the calibration process, the SKYE sensor was rotated 90° between readings to account for alignment bias in the calibration. An average of four alignment readings, in mV, for each waveband (e.g. green, red, red edge, or NIR) was recorded for each instrument. Each radiometer was calibrated with and without the cosine corrector at the start of the 2010 season and either with or without the cosine corrector based on their installation orientation for subsequent years. A calibration coefficient was determined for each band based upon the mV response to the integrating sphere output. Sensors were calibrated prior to installation in the field and upon completion of the field season. They were calibrated after their removal from the field in their post-field

Table 2.2: Percent change in radiometer sensitivity to a calibrated light source prior to installation and after removal from the site for the A) 2010, B) 2011, and C) 2012 growing seasons for each spectral band of seven radiometers tested. The post-season calibration included calibration before cleaning the sensor channels, filters, and cosine collectors (mentioned in Table as "dirty") and after cleaning these parts ("clean"). The view of the instrument is also listed: downward (D) or upward (U) facing.

A) 2010 growing season

Instrument	Field	View	Green		Red		Red Edge		NIR	
			dirty	clean	dirty	clean	dirty	clean	dirty	clean
A	1	U	-4.99	-2.84	-3.25	2.35	-2.75	-2.24	-4.91	-5.04
B	1	D	-2.39	-2.83	-2.79	1.77	-3.73	0.74	-5.54	-3.48
C	2	U	-5.77	-4.79	-9.50	9.00	-5.07	-5.04	-7.34	-7.60
D	2	D	-11.03	-1.18	-4.42	0.70	-3.43	-1.23	-18.09	-3.55
E	3	U	-2.45	-0.75	-0.07	0.01	-0.28	-0.29	-2.57	-2.33
F	3	D	-1.51	1.61	-0.02	6.07	0.29	1.37	-3.33	4.35
G	3	D	-2.87	0.10	-2.79	0.94	-3.76	-0.13	-2.87	0.07

B) 2011 growing season

Instrument	Field	View	Green		Red		Red Edge		NIR	
			dirty	clean	dirty	clean	dirty	clean	dirty	clean
A	1	U	-5.94	1.49	-3.56	0.74	-0.67	2.02	-5.88	-4.54
B	1	D	-23.87	-0.03	-3.39	-1.12	-2.2	-0.5	-8.08	-3.00
C	2	U	-2.79	-0.28	-0.19	0.29	0.84	1.12	-2.4	-1.89
D	2	D	-10.02	-1.38	-5.23	0.36	-1.57	0.89	-8.29	-3.92
E	3	U	-7.26	-2.4	-1.76	-0.32	-1.18	0.67	-3.41	-1.67
F	3	D	-12.00	-1.67	-3.79	-1.74	-3.18	-0.67	-6.09	-3.32
G	3	D	-5.94	1.49	-3.56	0.74	-0.67	2.02	-5.88	-4.54

C) 2012 growing season

Instrument	Field	View	Green		Red		Red Edge		NIR	
			dirty	clean	dirty	clean	dirty	clean	dirty	clean
A	1	U	-7.62	-4.30	-4.46	-4.11	-3.81	-3.73	-9.49	-8.92
B	1	D	-4.94	-1.26	-3.24	-0.27	-3.93	-0.05	-10.66	-5.63
C	2	U	-6.81	-3.73	-6.08	-3.96	-4.42	-2.23	-5.04	-4.21
D	2	D	-3.76	5.15	-3.11	5.51	-42.06	-5.52	-8.01	-8.44
E	3	U	-4.51	-1.75	-4.59	-2.83	-2.28	-1.59	-4.28	-3.92
F	3	D	-3.16	-1.34	-2.58	1.28	-2.47	1.54	-6.16	-1.16
G	3	D	-3.87	-0.96	-3.88	-0.24	-37.41	-0.81	-9.02	-6.57

condition ("dirty") and again after being thoroughly cleaned ("clean") by wiping down the cosine corrector, removing spider silk in the sensor channels and washing the filters. The variation between the "dirty" and "clean" states each year is in Table 2.2. A marine sealant was applied around the cosine corrector to prevent water infiltration for the sensors used in the downwelling measurements so that the calibration values were relevant to the entire measurement period (otherwise, the periodic saturation and drying of sensors added noise that could not be corrected by the calibration procedure).

Measurements of incoming photosynthetically active radiation (PARin) were obtained using point quantum sensors (Li-Cor, Inc., Lincoln, NE, USA). A second point quantum sensor in the nadir direction was used as a quality control tool by examining the ratio of the SKYE and PARin sensors in the same orientation (i.e. ratio of downwelling instruments or ratio of upwelling instruments). The ratio for each SKYE band and the respective PARin sensor determined near solar noon (1330 CDT) was compared to the previous day's ratio. Deviances of 50% or greater between these ratios were flagged and provide an indication of change for the calibration coefficients (see 2.4.3 Multispectral reflectance for details).

2.4 Data Processing

2.4.1 Ground-data

Since the green LAI of crops changes gradually during the growing season (Nguy-Robertson et al., 2012), destructive green LAI measurements for maize and soybean were interpolated either linearly (Chapter 4 and Chapter 5) or using a spline function (Chapter 3 and Chapter 6) using known values of green LAI on sampling dates

for each field in each year. Interpolated green LAI values were then obtained for the dates when reflectance measurements did not coincide with the dates of destructive green LAI measurements.

2.4.2 Hyperspectral reflectance

Reflectance for maize and soybean was calculated as the median value of the 36 collected reflectance measurements. Reflectance measurements were carried out during the growing season each year over the eight-year period. This resulted in a total of 314 reflectance spectra for maize (47 in 2001, 30 in 2002, 92 in 2003, 30 in 2004, 53 in 2005, 13 in 2006, 40 in 2007 and 9 in 2008) and 145 spectra for soybean (54 in 2002, 49 in 2004, 26 in 2006 and 16 in 2008), which were representative of a wide range of green LAI variation found in maize and soybean cropping systems. A total of 54 spectra for potato and 20 for wheat were collected.

Since a goal of this research was to find approaches applicable to satellite sensors (e.g. MODIS and MERIS), the collected field reflectance spectra were resampled by averaging the Ocean Optics data to simulate the spectral bands of MODIS (band 3/green: 545 - 565 nm, band 1/red: 620 - 670 nm, and band 2/NIR: 841 - 876 nm) and of MERIS (band 5/green: 555 - 565 nm, band 7/red: 660 - 670 nm, band 8/red: 677.5-685, band 9/red edge: 703.8 - 713.8 nm, band 10 NIR: 750 - 757.5 nm, and band 12/NIR: 771.3 - 786.3). While the satellite hosting the MERIS sensor failed, the bands are still relevant since the ESA satellite Sentinel-2 will contain a sensor with the same bands. The launch data is currently estimated to be in 2014.

2.4.3 Multispectral reflectance

To remove short-term variation in the data from rapidly changing environmental conditions in which the radiometers were exposed by unforeseen circumstances (e.g. birds, insects, spiders, etc.), the spectral band radiometer responses, in mV, were averaged over a 30 minute period. These 30-minute average responses were converted to irradiance and radiance values using the appropriate band calibration coefficients. Two different procedures were used depending on the calibration procedure described in 2.3.2 Multispectral reflectance.

For the goniometer calibration data collected in 2003-2005, pre- and post-field season calibration coefficients (CC) were compared for each individual band. If the difference between the pre- and post-field season calibration was less than 5%, then the pre-season CC was used. If not, the two coefficients were averaged and this averaged CC was applied

For the calibrated light source data collected in 2009-2012, dates flagged by SKYE/PARin ratios were examined to determine if the change was related to major differences in sky conditions or if an outside factor was involved. For periods where the ratio changed due to overcast sky conditions, the ratio returned to the values achieved under sunny conditions as illumination conditions changed. These points were also identified by examining the raw PARin values, which were much lower during cloudy conditions. Points where the ratio did not return to similar values after monitoring sky conditions were marked as the point where the "dirty" calibration coefficient for that particular band may be applied. In cases where the "dirty" calibration varied less than 5% from the pre-season calibration, only the initial calibration coefficient was used. In the

instances where the difference between the "dirty" and "clean" calibrations was greater than 5%, the errors were assumed to be introduced by contaminants. The date where the largest difference between the SKYE/PARin ratio from the previous day occurs was utilized as the point where the post-season "dirty" calibration was applied. This method is preferable over a gradual application or an average of the corrected calibration from pre- to post-season coefficients since most changes occurred abruptly and could be identified as such in combination with the PAR albedo values. The contaminants consisted of primarily spider threads or insects blocking the sensor channels (Figure 2.5).

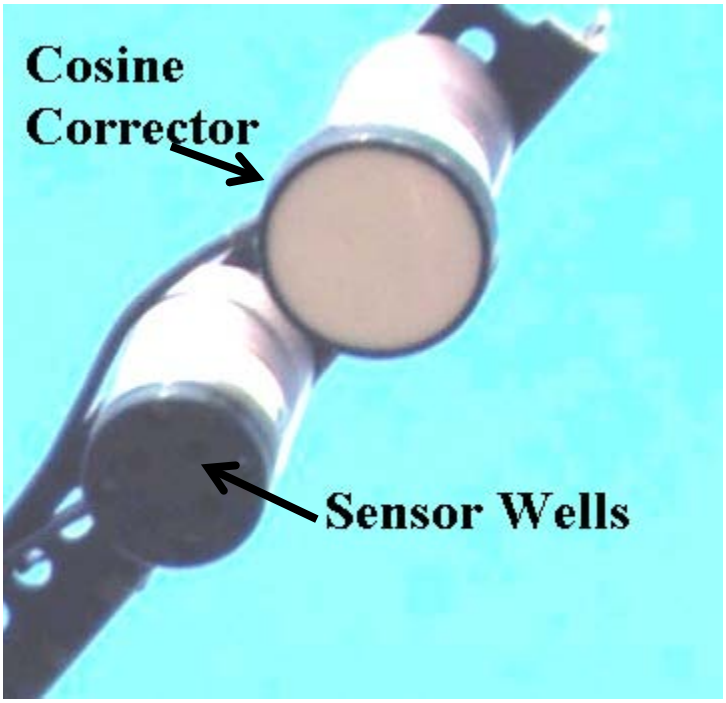

Figure 2.5: Close-up of SKYE instruments to indicate how the sensors wells are more likely to be impacted by insects and spiders crawling inside. Instruments fitted with the cosine corrector were protected from insects and spiders.

The 30-minute averaged reflectance of spectral band "i" (ρ_i) was determined as the ratio of the 30-minute average upwelling radiance ($R_{UW(\lambda)}$) and 30-minute average downwelling irradiance ($I_{DW(\lambda)}$). Depending on the calibration procedure, the calibration coefficient (CC) was applied either to the instrument pair ($CC_{UW(\lambda)-DW(\lambda)}$; eq. 2.3) or individual instruments ($CC_{UW(\lambda)}$, $CC_{DW(\lambda)}$; eq. 2.4):

$$\rho_i = R_{UW(\lambda)} * I_{DW(\lambda)}^{-1} * CC_{UW(\lambda)-DW(\lambda)} \quad (2.3)$$

$$\rho_i = (R_{UW(\lambda)} * CC_{UW(\lambda)}) * (I_{DW(\lambda)} * CC_{DW(\lambda)})^{-1} \quad (2.4)$$

Regardless of the calibration procedure used, the median of the 30 minute average reflectances between 10.5 and 15.5 h were used as the midday reflectance measurement in order to avoid skewing the data towards the minimum/maximum values of that day caused by drastic changes in the light conditions (overcast to sunny conditions) and to avoid bidirectional reflectance caused by low solar elevations. This resulted in 2632 spectra collected for maize (427 in 2003, 146 in 2004, 412 in 2005, 441 in 2009, 285 in 2010, 554 in 2011, and 367 in 2012) and 616 spectra for soybean (286 in 2004, 142 in 2010, and 188 in 2012).

2.4.4 Satellite Imagery

The satellite imagery examined in this research was from the MODerate Imaging Spectroradiometer (MODIS). The 250 m 8-day products from both Aqua (MYD09Q1) and Terra (MOD09Q1) sensors were utilized. The MODIS 8-day products were atmospherically corrected and the optimal surface reflectance pixel within each eight-day

window was identified using a constrained view-angle maximum value composite method (Huete et al., 2002). The date of pixel acquisition was used rather than the start date of the 8-day composite. The 250 m products contain only the red (620-670 nm) and NIR (841-876 nm) bands, thus the number of VIs examined using MODIS was limited (Chapter 6). The study area was within tile h10v04 and each field was comprised of 9 pixels. To avoid mixed pixels the central pixel from each field was selected.

2.4.5 Vegetation Indices (VIs)

Vegetation indices are the spectral combination of different wavebands. While the VIs examined between chapters does vary, all of the VIs examined in this research are located in Table 2.3. The only unique VI formulation presented in this research is the Green WDRVI, which is based on a previously published wide dynamic range vegetation index (WDRVI). The only difference is that the red band was replaced with green. The logic behind this approach is to have an index that is not dominated by high NIR reflectance values paired with a visible reflectance band that is still sensitive to changes of green LAI at high values (see Chapter 1 for details).

As indicated in 2.3.1 Hyperspectral reflectance, MODIS and MERIS bands were used in the hyperspectral data set. MODIS bands were used unless a red edge band was required for the VI, then MERIS bands were utilized.

2.4.6 Percentage of potential photosynthetically active radiation

The potential PARin values (Figure 2.6) for each day (mol m^{-2} day^{-1}; PARpotential) were determined using the method outlined in Weiss and Norman (1985).

Table 2.3: List of vegetation indices. The subscript indicates the satellite (M: MODIS, S: MERIS/Sentinel-2) and band utilized.

Index	Equation	Reference
Simple Ratio (SR)	$NIR_{M2} * Red_{M1}^{-1}$	(Jordan, 1969)
Normalized Difference Vegetation Index (NDVI)	$(NIR_{M2} - Red_{M1}) * (NIR_{M2} + Red_{M2})^{-1}$	(Rouse et al., 1974)
Red Edge Inflection Point (REIP)	$Red\ Edge_{S9} + 45 * \{[(Red_{S7}+NIR_{S12}) * 2^{-1}) – Red\ Edge_{S9}] * (NIR_{S10} – Red\ Edge_{S9})^{-1}\}$	(Clevers et al., 2000; Guyot & Baret, 1988)
Green NDVI (Green NDVI)	$(NIR_{M2} - Green_{M4}) * (NIR_{M2} + Green_{M4})^{-1}$	(Gitelson & Merzlyak, 1994)
Red Edge NDVI (Red edge NDVI)	$(NIR_{S12} - Red\ Edge_{S9}) * (NIR_{S12} + Red\ Edge_{S9})^{-1}$	(Gitelson & Merzlyak, 1994)
Optimized Soil-Adjusted Vegetation Index (OSAVI)	$(1+1.16)*(NIR_{M2} – Red_{M1}) * (Red_{M1} + NIR_{M2} + 0.16)^{-1}$	(Rondeaux et al., 1996)
Green Chlorophyll Index (CI_{green})	$(NIR_{M2} * Green_{M4}^{-1}) - 1$	(Gitelson et al., 1996)
Red Edge Chlorophyll Index ($CI_{red\ edge}$)	$(NIR_{S12} * Red\ Edge_{S9}^{-1}) - 1$	(Gitelson et al., 1996)
Triangular Vegetation Index (TVI)	$0.5 * [120 * (NIR_{M2} – Green_{M4}) - 200 * (Red_{M} – Green_{M})]$	(Broge & Leblanc, 2001)
MERIS Terrestrial Chlorophyll Index (MTCI)	$(NIR_{S12} – Red\ Edge_{S9}) * (Red\ Edge_{S9} – Red_{S7})^{-1}$	(Dash & Curran, 2004)
Wide Dynamic Range Vegetation Index (WDRVI)	$(\alpha * NIR_{M2} - Red_{M1}) * (\alpha * NIR_{M2} + Red_{M1})^{-1} + (1 – \alpha) * (1 + \alpha)^{-1}$	(Gitelson, 2004; Peng & Gitelson, 2011)
Modified TVI 2 (MTVI2)	$1.5 * [1.2 * (NIR_{M2} – Green_{M4}) - 2.5 * (Red_{M1} - Green_{M4})] * < sqrt\{(2 * NIR_{M2} + 1)\text{^}2 – [6 * NIR_{M2} - 5 * sqrt(Red_{M1})] - 0.5\}>^{-1}$	(Haboudane et al., 2004)
Enhanced Vegetation Index 2 (EVI2)	$2.5 * (NIR_{M2} - Red_{M1}) * (NIR_{M2} + 2.4* Red_{M1} + 1)^{-1}$	(Jiang et al., 2008; H. Q. Liu & Huete, 1995)
Green Wide Dynamic Range Vegetation Index (Green WDRVI)	$(\alpha * NIR_{M2} – Green_{M4}) * (\alpha * NIR_{M2} + Green_{M4})^{-1} + (1 – \alpha) * (1 + \alpha)^{-1}$	(Gitelson, 2004; Peng & Gitelson, 2011)

PARpotential can be separated into its direct (i.e. from the sun) and diffuse components (eq. 2.5). The direct beam component on a horizontal surface can be estimated using Beer's Law (eq. 2.6) where the direct component is corrected for solar zenith angle, θ, at half hour measurements in correspondence to instrument readings. The average PARin atthe top of the atmosphere is 600 W m^{-2}. The extinction coefficient of light traveling through the atmosphere is 0.185. The average pressure at the three sites, 97.3 kPa (Standard Deviation: 0.77), was used in determining the ratio of actual pressure to pressure at sea level (101.325 kPa), $P * P_0^{-1}$. The optical air mass, *m*, was estimated using the solar zenith, θ (eq. 2.7). For the diffuse component ($PARpotential_{(diffuse)}$), 0.4 is the fraction of the direct component that is scattered after average PARin at the top of the atmosphere is corrected for the solar zenith angle (eq. 2.8). Deviations of PARin from PARpotential are expressed as a percentage of PARpotential (%PARpotential, eq. 2.9). The %PARpotential was greater than 70% and 50% in more than 69% and 81% of the daily measurements respectively (Figure 2.6).

$$PARpotential = PARpotential_{(direct)} + PARpotential_{(diffuse)} \quad (2.5)$$

$$PARpotential_{(direct)} = 600 \exp[-0.185 (P * P_0^{-1}) m] \cos\theta \quad (2.6)$$

$$m = (\cos\theta)^{-1} \quad (2.7)$$

$$PARpotential_{(diffuse)} = 0.4(600*\cos\theta - PARpotential_{(direct)}) \quad (2.8)$$

$$\%PARpotential = 100\% - (PARpotential - PARin) * PARpotential^{-1} *100\% \quad (2.9)$$

2.4.7 Statistical analysis

The statistical package R (V. 2.12.2) (R Development Core Team, 2010), Matlab (V. 7.9.0.529, The MathWorks, Massachusetts, USA), and Excel 2010 (V. 14.0,

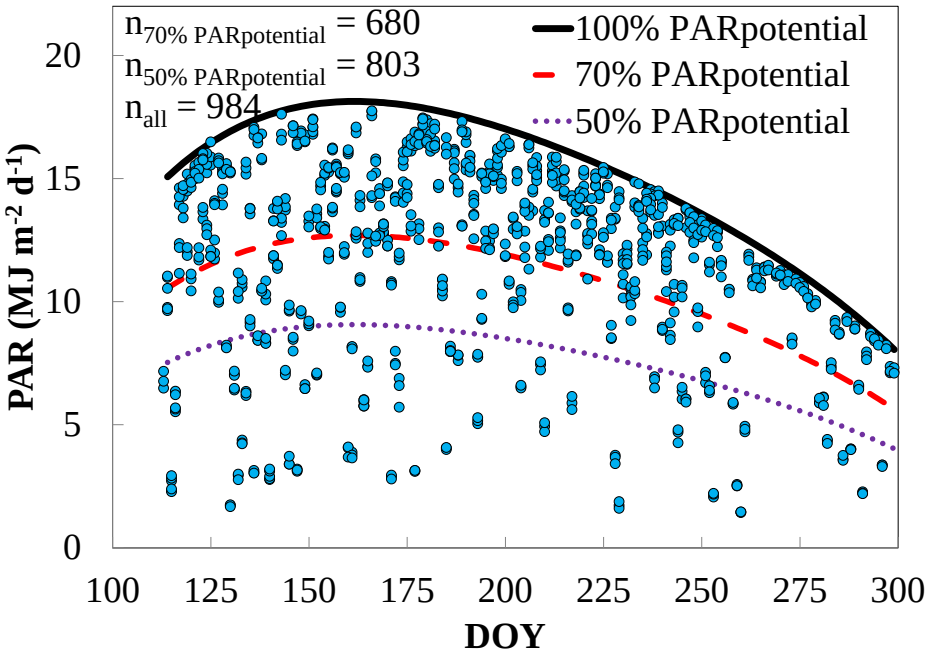

Figure 2.6: Daily PAR_{in} where 100%, 70%, and 50% of $PAR_{potential}$ are indicated

Microsoft Corp.) were used in statistical analyses including the best-fit functions, coefficients of determination (R^2), standard error (SE), root mean square error (RMSE), coefficients of variation (CV), standard deviation (σ), percent change, and interpolations (both linear and spline).

The algorithm search engine Eureqa Formulize (v. 0.97 Beta) was utilized to identify and rank potential regression models that best correspond to the input data (Schmidt & Lipson, 2009). Users input the desired relationship, e.g. VI = f(green LAI), along with potential operations (e.g. addition, subtraction, exponential, power, etc.) and an error metric (e.g. minimize absolute error, R^2, etc.). For this research, the fitness metric used to rank the best-fit functions constituted the minimization of the root mean square error (RMSE). The inverse of these relationships (i.e., green LAI vs. VI) was utilized for green LAI estimation using VIs and the summary statistics presented are

based on this relationship. This is preferable to using the VI vs. green LAI relationships since users are interested in estimating green LAI using VI values.

One calibration/validation procedure utilized herein (Chapter 4) to determine the estimates of model coefficients, R^2, SE, and CV was the *k*-fold (*k* = 10) cross-validation procedure (Kohavi, 1995). CV is the standard deviation of the green LAI vs. VI relationship divided by mean value of green LAI. The data or subgroups (i.e., different crops - maize or soybean) were randomly divided into ten sets using a random sequence generator (random.org), nine of which were used iteratively for calibration and the remaining set for validation. This approach is also known as the leave-one-out cross validation (LOO-CV) approach if *k* equals the sample size of the data set. LOO-CV was utilized for developing the green LAI products (Chapter 6) from the close-range sensors.

It is important to note that the R^2 values, as well as SE and CV of green LAI estimation, represent the dispersion of the points from the best-fit regression lines. They constitute measures of how good the regression model (best-fit function) is in capturing the relationship between green LAI and VI. However, when the best-fit function is nonlinear, the R^2 as well as the SE values may be misleading. To determine the accuracy of green LAI estimation in Chapter 4 and Chapter 5, we employed the noise equivalent (NE) of green LAI (Govaerts et al., 1999; Viña & Gitelson, 2005) that was calculated as:

$$NE\Delta\text{green LAI} = \text{RMSE(VI vs. green LAI)} * [d(\text{VI}) * d(\text{green LAI})^{-1}]^{-1} \quad (2.10)$$

Where $d(\text{VI}) * (\text{green LAI})^{-1}$ is the first derivative of VI with respect to green LAI and RMSE(VI vs. LAI) is the root mean square error of the VI vs. green LAI relationship.

The NEΔgreen LAI provides a measure of how well the VI responds to green LAI across its entire range of variation. NEΔgreen LAI takes into account not only the RMSE of green LAI estimation but also accounts for the sensitivity of the VI to green LAI, thus providing a metric accounting for both scattering of the points from the best fit function and the slope of the best fit function.

To test the applicability of VIs to estimate the green LAI of different crops with no algorithm re-parameterization, we performed an analysis of variance (ANOVA) between the coefficients of the best-fit function for both species (maize and soybean) combined, versus the coefficients obtained for each individual crop (Ritz & Streibig, 2008).

Chapter 3 : Using a simple radiometer to identify crop stage of development in maize and soybean

3.1 Objectives

The objectives of this research were to (1) determine temporal, diurnal and seasonal, behavior of reflectance in two contrasting (leaf structure and canopy architecture) crops, maize (*Zea mays*) and soybean (*Glycine max*) and (2) to remotely estimate stage of development in crops, as defined by the USA phenological Network and SpecNet, utilizing spectral spaces and VIs.

3.2 Results and discussion

3.2.1 Issues associated with long-term data collection

The SKYE radiometers were calibrated by the manufacturer using pairs of sensors. The calibration recommended in this study does not require sensor pairs but instead provided an independent calibration of each sensor band. If one instrument and/or sensor band in an upwelling/downwelling pair were to fail prior to the post-season calibration, data from the one functioning unit is still valuable and another calibrated sensor can be used as a replacement for the malfunctioning unit.

A summary of the changes in the calibration between the start and the end of the growing season ("dirty") and between the start of the growing season and after cleaning the instruments ("clean") is presented in Table 2.2. Overall the sensors deviated well below 20% (with only few exceptions) between the calibrations collected prior to and after the growing season in their "dirty" state. The differences were reduced to 9% or less once the sensors were cleaned. Differences between the "dirty" and "clean" conditions

were usually less in the downwelling sensors since the cosine collector prevented dust and insects from collecting in the sensor wells (Table 2.2). A deviation of 42% may be of concern if only one calibration coefficient was applied to the data; however, the application of a second calibration coefficient bypasses the error commonly caused by a rapid contamination of the sensor wells. As indicated for many of the bands in this study, the sensors are quite stable except when insects and/or spiders intruded into the sensor channels. For example, after cleaning only 7% of the visible sensor bands differed more than 5% from the pre-season calibration. The NIR band was the most variable where 33% of the bands varied more than 5%. However, none of the bands varied more than 9%.

3.2.2 Diurnal reflectance

Canopy reflectances in all four bands were higher at solar zenith angles exceeding 70° (e.g. just after sunrise and just before sunset). Because specular reflectance was higher at these solar zenith angles, this impacted the bidirectional reflectance factor (Norman et al., 1985; Ranson et al., 1985). However, diurnal canopy reflectances varied little during periods of smaller (< 70°) solar zenith angles (between 10.5 and 15.5 h CDT and mostly clear skies for both maize (Figure 3.1A) and soybean (Figure 3.1B) when the canopy was at full cover (LAI above 3.0 m^2 m^{-2}). The minimal solar zenith angle for each day during the study ranged between 17.7° (DOY ~172) and 54.1° (DOY ~300). Even at DOY 300, the reflectance was relatively stable during this period (Figure 3.1C). During cloudy conditions the reflectance was also relatively stable (Figure 3.1D-E). Thus, the median reflectance ±2.5h from solar noon was representative of midday reflectance that is minimally sensitive to short-term instant reflectance variability and effect of solar

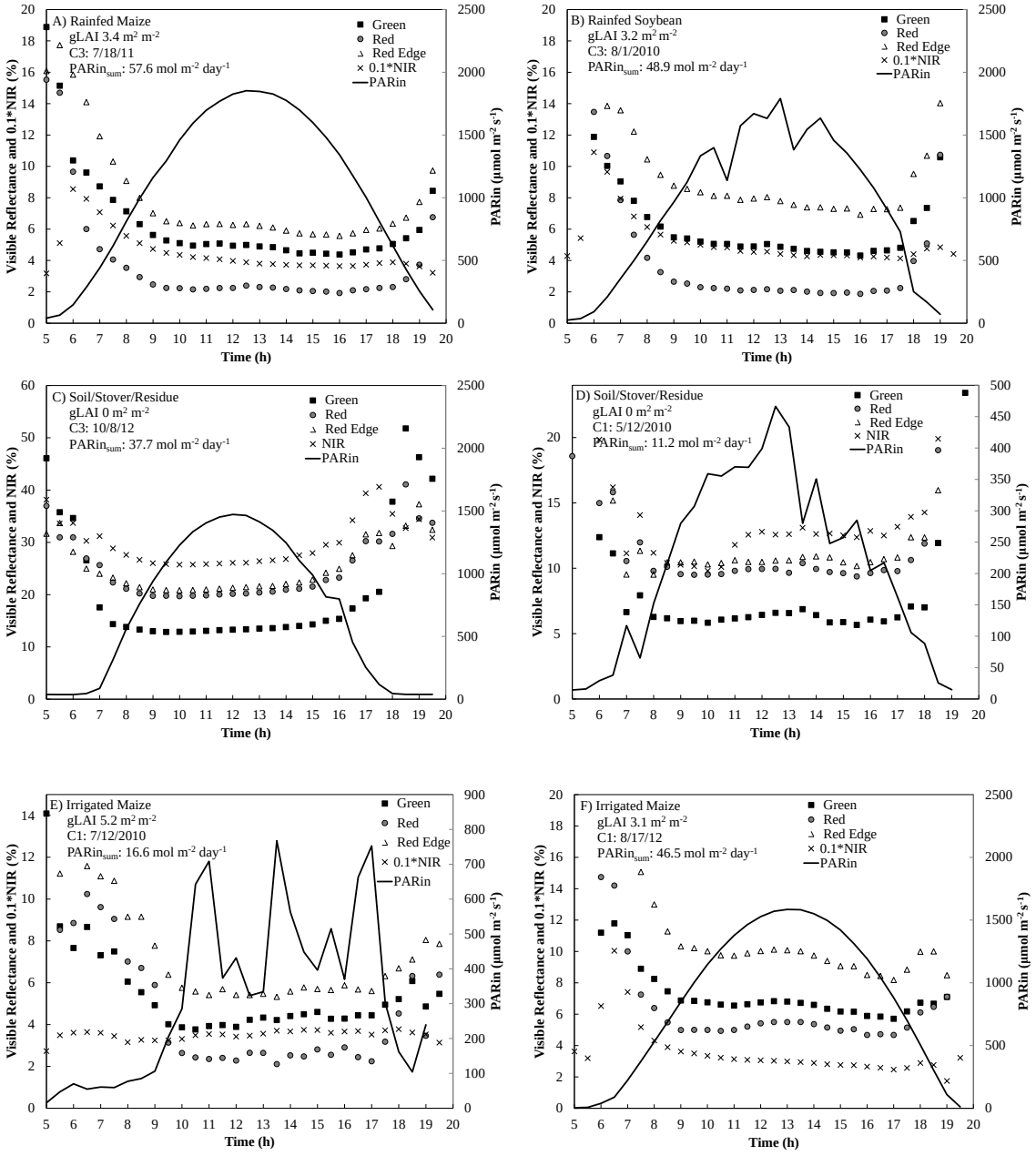

Figure 3.1: Diurnal behavior of SKYE reflectance during mostly cloud-free conditions for (A) maize, (B) soybean, and (C) the non-growing season. Diurnal behavior of SKYE reflectance during cloudy days for (D) maize and (E) soybean. Diurnal behavior of SKYE reflectance during periods of hotter, drier days for (F) maize, (G) soybean, and (H) the non-growing season.

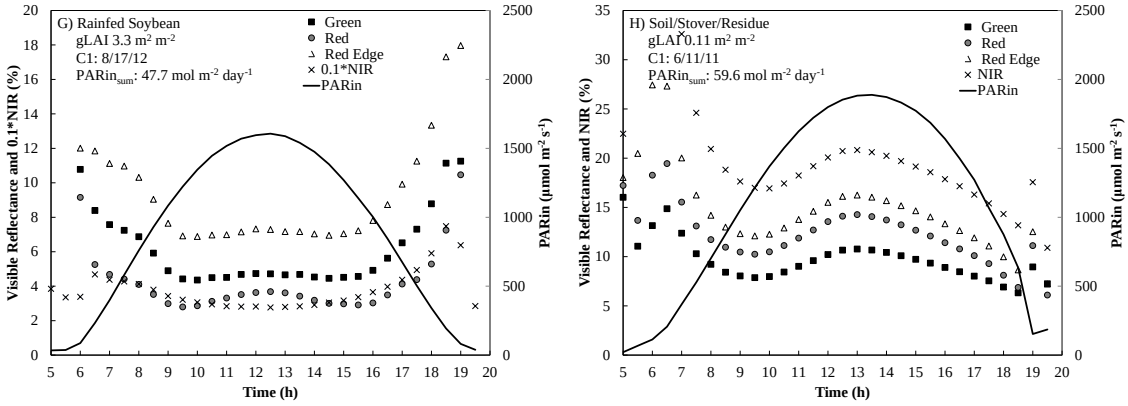

Figure 3.1 (continued): Diurnal behavior of SKYE reflectance during mostly cloud-free conditions for (A) maize, (B) soybean, and (C) the non-growing season. Diurnal behavior of SKYE reflectance during cloudy days for (D) maize and (E) soybean. Diurnal behavior of SKYE reflectance during periods of hotter, drier days for (F) maize, (G) soybean, and (H) the non-growing season.

zenith angle variability. Therefore, the median value of reflectances collected between 10.5 and 15.5h was used as the midday reflectance.

On some occasions, the visible reflectance increased at solar noon compared to the reflectance collected 2.5 h before or after solar noon (Figure 3.1F-H). Of the 1537 midday reflectance measurements collected from all three fields in 2010 through 2012, 243 midday reflectance measurements (15.8%) display a peak of 5% or greater. Of the measurements that contain the peaks, the average peak was 9.1% and the maximum peak was 23% greater at solar noon compared to the 2.5 h before or after.

Similar trends in diurnal reflectance have been reported before and it was attributed to the variations to specular reflectance from plant, residue and soil, given the row structure and illumination angles (Ranson et al., 1985) or reduced shadowing when

the sun is highest for the day so that the canopy appears 'brighter' (Kimes, 1983). In addition, plant light protection mechanisms (photoprotection) may play a role, where absorption decreases as plants minimize excessive light striking the chloroplasts through leaf curling/folding and/or chloroplast avoidance movement (Zygielbaum et al., 2009, 2012). However, this hypothesis would require that plants are able to recover after the peak at solar noon. These slight increases of reflectance occur more often when conditions are hot and dry and require further study to understand the reason behind this behavior in the diurnal reflectance. Since the solar noon peak is uncommon (occurrence in 15.8% of samples), it is a rather minor component of the variation in the data set.

There is minimal variation between the spectral reflectance measurements from two downward facing sensors placed 30 cm apart (either directly over or between the

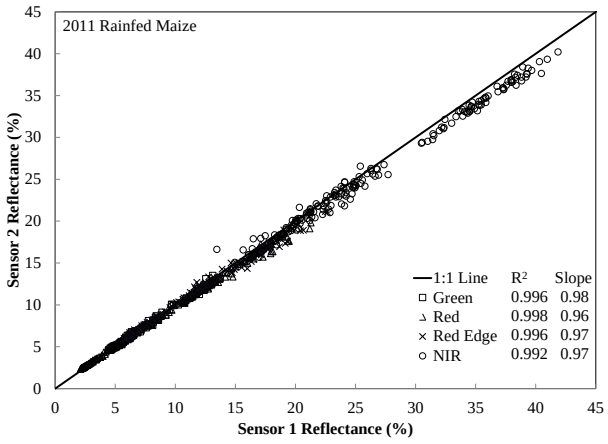

Figure 3.2: The relationship between the maize reflectance determined from two upwelling radiance sensors in 2011. One sensor was placed over the row and another one between the rows. Both were paired with the same downwelling irradiance sensor and reflectance was calculated as a ratio of upwelling radiance to downwelling irradiance. The slope of each line was determined with intercept set to zero.

planting rows) on a rainfed maize dataset collected in 2011 for the entire growing season (Figure 3.2). The slopes of the relationship indicate that there are some differences between the two sensors at higher reflectance values. This was likely due to the placement of the sensor either over or between the rows. The signal from the sensor that was placed between rows was likely influenced by the soil component in the field of view, resulting in higher canopy reflectance values, than the signal from the sensor positioned over the crop row. The difference in reflectances was minimized when the vegetation fraction was above 60%. Regardless, the differences between the two sensors are rather minimal due to their placement 6 m above the canopy. At this height, the field of view contains multiple rows, thus both row and in-between row structure.

3.2.3 Temporal behavior of reflectance during the growing season

Temporal behavior of the midday reflectances during the growing season was in accord with that reported in previous studies of maize and soybean (Foerster et al., 2012; Kollenkark et al., 1982; Song, 1999; Verhulst et al., 2011). As the plants developed and LAI increased, green, red, and red edge reflectances decreased due to an increase in pigment absorption, while NIR reflectance increased due to leaf scattering (Figure 3.3). Of all the visible wavebands investigated, the red reflectance showed the greatest variation over the range of green LAI values; however, it saturated at LAIs greater than 3 m^2 m^{-2} (Figure 3.3). As LAI increased, NIR reflectance peaked and was the most variable around the time of tasseling in maize and maximal green LAI in soybean. In maize, when LAI decreased, the NIR reflectance gradually decreased during the early reproductive stages and then dropped rapidly during senescence. For soybean, the NIR reflectance

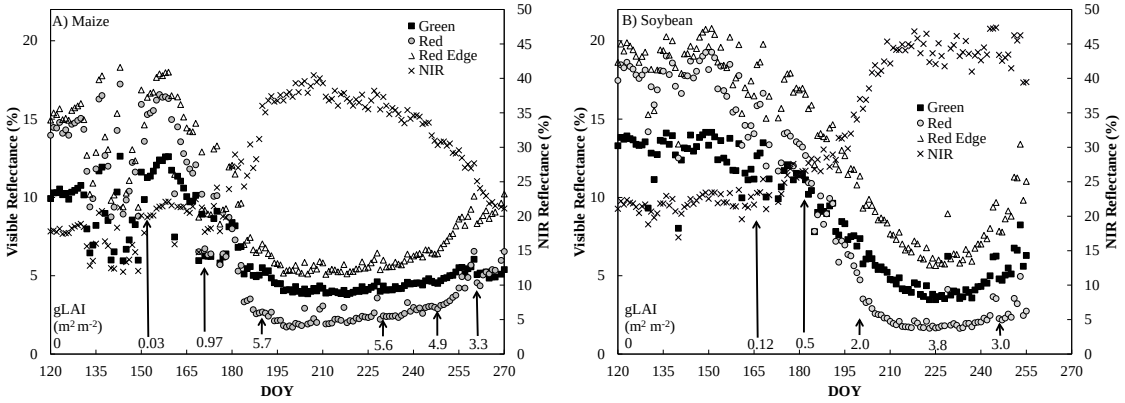

Figure 3.3: Temporal behavior of median reflectance collected between 10:30 and15:30 CDT for A) maize and B) soybean during a year with typical weather conditions. Crop green leaf area index (green LAI) is indicated.

remained almost invariant at the top of season (DOY ~225) when green LAI was around 3 m^2 m^{-2}, and began to decrease near the time of instrument failure on DOY 255. For maize, grain maturity occurred around DOY 270 when green LAI was below 2 m^2 m^{-2}. At this time, the green, red, and red edge reflectances increased rapidly.

While the midday reflectance at each day of year (DOY) removed most of the variation within a specific date, it does not remove all possible variation. Plants at the same development stage with the same LAI may have different reflectance due to different weather conditions affecting the light climate inside the canopy deviating from the general trend in the temporal behavior (Figure 3.4). During periods of predominantly diffuse PAR (cloudy days), the light penetrates somewhat uniformly into the canopy from all directions. Self-shadowing decreases and therefore, a larger fraction of the upwelling radiation is from “illuminated” vegetation and soil rather than from shaded components of the vegetation and soil when the direct beam dominates. Thus, a relative increase in

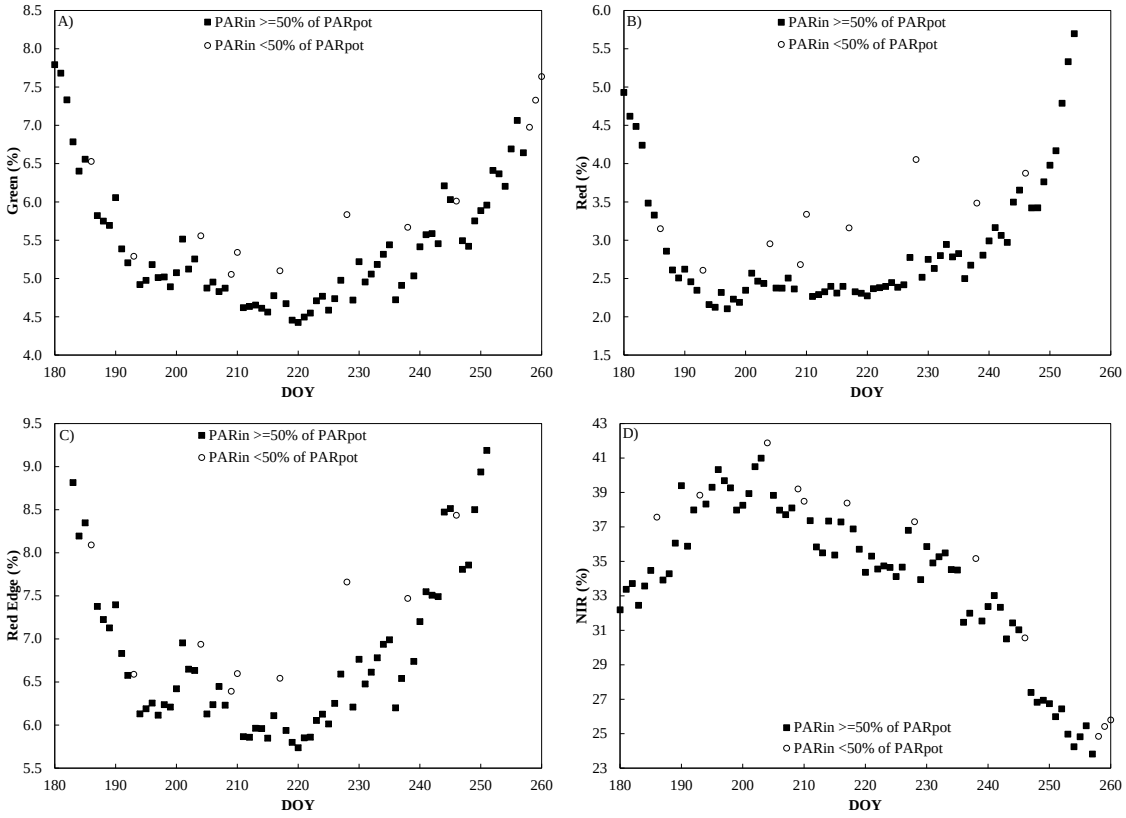

Figure 3.4: Median daily maize reflectance, collected at rainfed site in 2011, plotted vs. day of year (DOY) for incident irradiance either greater or below 50% of PAR potential. Decrease in incident irradiance and its subsequent decrease in direct component leads to an increase in reflectance in all spectral bands studied.

crop canopy reflectance occurs during cloudy conditions (Deering & Eck, 1987; Gitelson, 2003; Schaaf & Strahler, 1993). These points can easily be removed from a data set using %PARpotential to identify predominantly cloudy days.

Sensors set up for diurnal monitoring can capture reflectance on days of cloud cover when satellite- and airborne-based sensors cannot; however, the increase in reflectance due to increase of the ratio of diffuse to direct light can result in an underestimation of a biophysical property when used in a model calibrated with

reflectances collected under sunny conditions. Fortunately, these low light levels can be easily identified. While we excluded these data in this study, one could use incoming radiation as a parameter in developing these relationships as was done for gross primary production estimation (Peng & Gitelson, 2011).

3.2.4 Two-dimensional spectral spaces

While the daily temporal behavior indicated similar patterns between reflectance bands in the visible spectral range, important additional information can be extracted when examining spectral spaces. Spectral spaces are relationships between reflectances in different spectral bands. Thus, this approach capitalized on the different band information content and provided additional information regarding vegetation physiological and stage of development. Gitelson et al. (2002) demonstrated that spectral spaces in visible ranges are useful in estimating vegetation fraction when using a data set of multiple crops with various soil backgrounds. However, when using a high temporal resolution data set, such as provided by SKYE, one can also monitor stage of development of a crop remotely.

Up to five distinct vegetative growth stages were clearly identifiable using reflectances in the red vs. green spectral space: soil/residue, green-up, peak vegetative, senescence, and soil/stover/residue stages (Figure 3.5A, Figure 3.6). The soil/residue lines were similar for both crops since the soil type and land management practices were similar. While most of the variation in reflectances for the soil/residue line was likely due to changes in soil moisture (Lobell & Asner, 2002), reflectance varied minimally during this stage.

Both crops had a similar green-up stage where both red and green reflectance rapidly synchronously decreased. The red reflectance changed 1.9 times faster than green

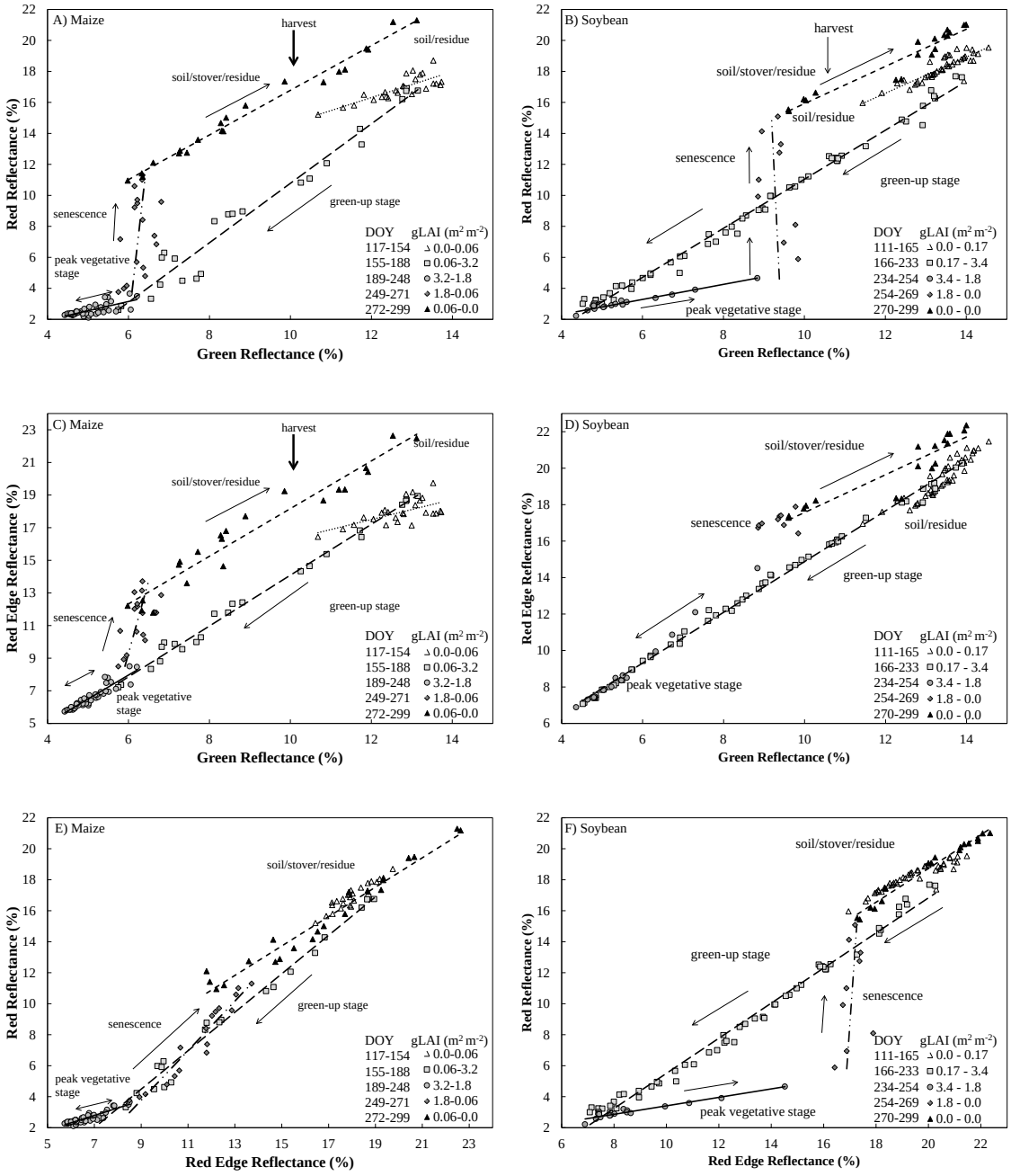

Figure 3.5: Two dimensional spectral spaces formed by median midday rainfed A-B) maize or C-D) soybean reflectances when PAR_{in} was > 70% of PAR potential collected in 2011 or 2012 respectively. Ranges of green leaf area index (green LAI) are shown. Maximal green LAI for maize (3.49 m^2 m^{-2}) was reached on DOY 216 and for soybean (3.31 m^2 m^{-2}) on DOY 230.

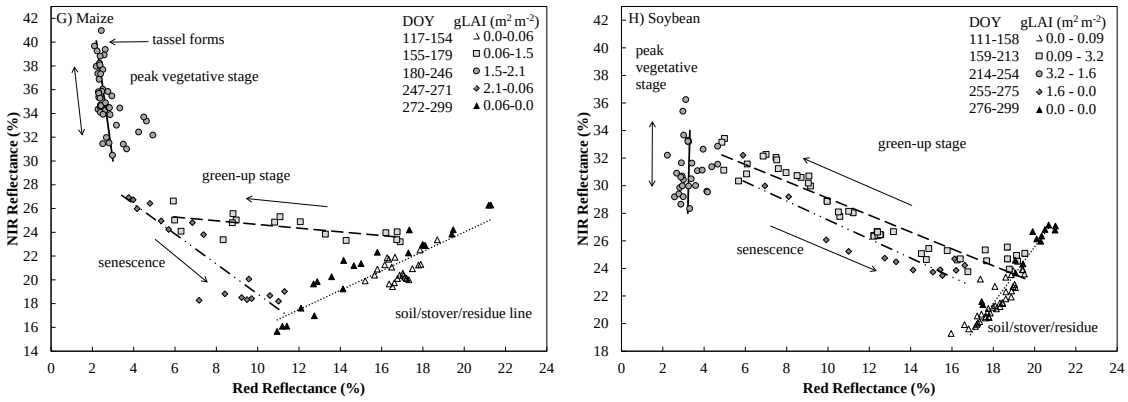

Figure 3.5 (continued): Two dimensional spectral spaces formed by median midday rainfed A-B) maize or C-D) soybean reflectances when PAR_{in} was > 70% of PAR potential collected in 2011 or 2012 respectively. Ranges of green leaf area index (green LAI) are shown. Maximal green LAI for maize (3.49 m^2 m^{-2}) was reached on DOY 216 and for soybean (3.31 m^2 m^{-2}) on DOY 230.

reflectance in maize and 1.6 times faster in soybean. When vegetation fraction exceeds 70%, slope of the relationship red reflectance vs. green reflectance decreased. The red reflectance was nearly invariant while green reflectance still changed for both maize and soybean. Thus, both crops had a distinct “vegetation line” (Gitelson et al., 2002).

A major change in the red vs. green reflectance behavior occurred at the onset of senescence: the green reflectance remained relatively low (~6% in maize and ~9% in soybean) and virtually invariant, while red reflectance increased drastically (from 3% to 12% in maize and to 15% in soybean). Thus, this plant stage of development can be clearly identified. Both crops had a similar soil/stover/residue line that was offset from the soil/residue line at the start of the growing season. In minimum-till management systems, fresh stover and residue have a distinctly different spectral characteristic from

pre-planting conditions. Fresh stover and residue is usually brighter than the background soil. After harvest the remaining residue will begin to decompose and become incorporated into the soil, thus reducing its reflectance (Streck et al., 2002). That was why the soil/stover/residue line appeared higher and longer than soil/residue line. By the beginning of the next growing season, the reflectances will overlay onto the soil/residue line of the previous year with some variation due to different decay rates, crop type from previous year, etc.

The shape of the red edge vs. green relationship was nearly identical to the red vs. green relationship in maize (Figure 3.5C). In soybean, there was no difference between the green-up and peak vegetative stage (Figure 3.5D), thus this relationship is not as useful as the red vs. green relationship. Likewise, the red vs. red edge relationship has overlaps between stages in maize (Figure 3.5E). However, the red vs. red edge relationship in soybean has a more distinct separation such that the overlap of the green-up and senescence stages is minimized (Figure 3.5FC). Therefore, for soybean the red vs. red edge reflectance relationship would be more beneficial than the other spectral spaces examined for identifying developmental stage without ancillary data (see 3.2.6 Using spectral spaces to identify).

NIR vs. red relationships have been widely used in previous studies (Ayyangar et al., 1980; Broge & Leblanc, 2001; Gobron et al., 1999). For this relationship, four distinct classes were identified for maize (Figure 3.5G) and three for soybean (Figure 3.5H). Stover did not influence the NIR vs. red relationship in contrast to the red vs. green reflectance relationship. This was because the leaves scatter more light in the NIR region than do soil and brown leaves. Once the crop fully senesced or was harvested and the

leaves are redistributed, the NIR reflectance reached its minimum. While soil moisture had an impact on the soil/stover/residue line (decreasing visible reflectance), the remaining chlorophyll in the residue leaf material also impacted the reflectance. Thus, red

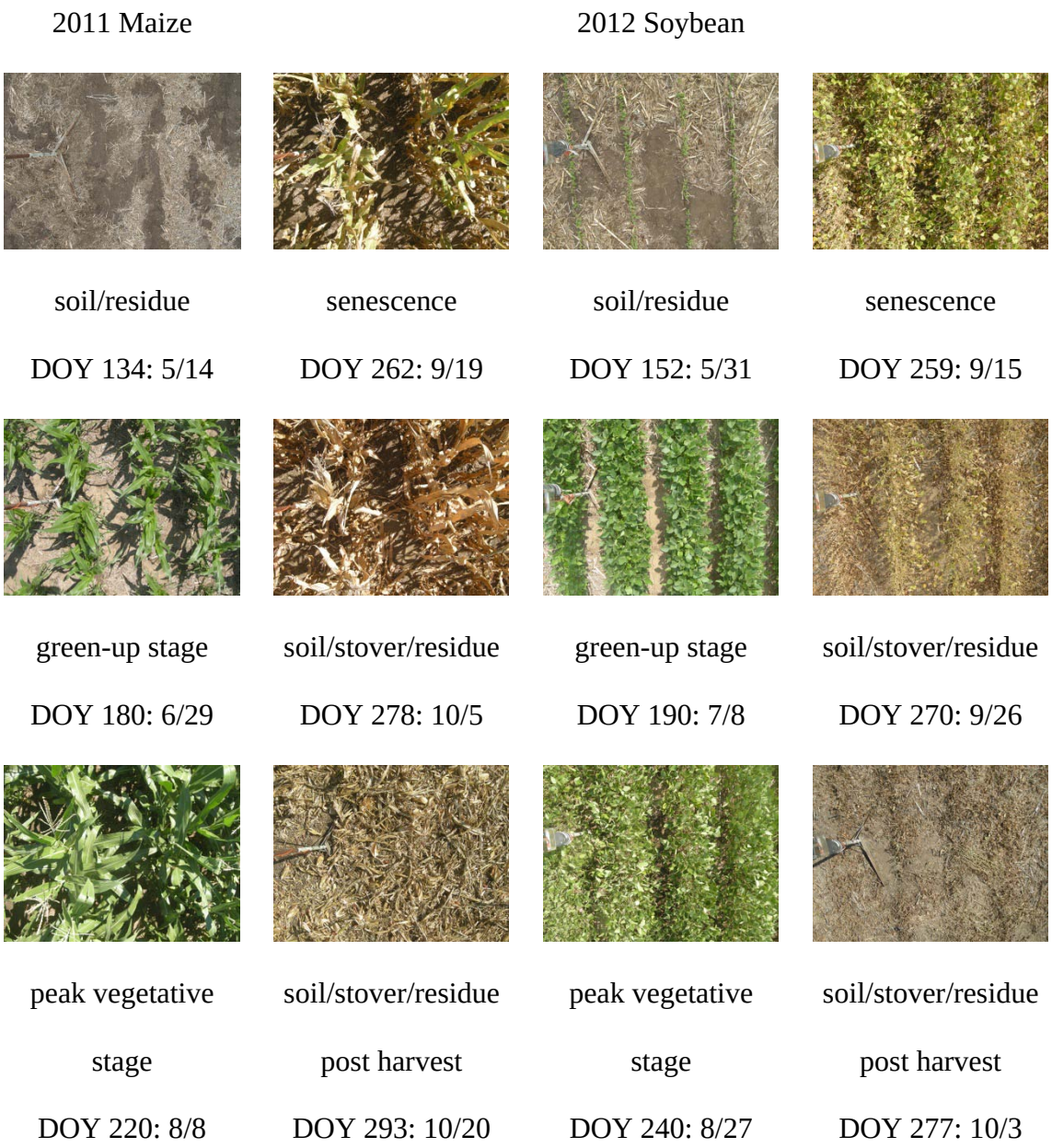

Figure 3.6: Images acquired from the rainfed fields for both maize and soybean. Images selected represent crop developmental stages identified in the spectral space.

reflectance still varied and this was why the range of the soil/stover/residue line of maize was larger than the soil/residue line of soybean.

Another and major difference between maize and soybean occurred during the transition stages of green-up and senescence. For soybean, red reflectance changed at a rate approximately 1.6 times faster than NIR reflectance during green-up and nearly the same rate of change (1.4 times) during senescence. However, in maize this rate during the green-up stage was 6.4 times faster. In the senescence stage, NIR reflectances changed faster (1.3 times) than red reflectance, indicating that leaf architecture was changing faster than chlorophyll degradation.

Differences between maize and soybean in the NIR vs. red reflectance relationships can be explained by the different developmental patterns of these crops. During the green-up stage, maize primarily grows vertically, thus the scattering of NIR reflectance by maize leaves is minimized until the leaves fully mature in the peak vegetative stage when green LAI is greater than 3 m^2 m^{-2} (Figure 3.6). Soybean expands both vertically and horizontally (Figure 3.6) and, thus, scattering in the NIR, occurs simultaneously with the absorption of red light by chlorophyll. For more examples of spectral spaces see Appendix B: Additional data for determining stage of development.

3.2.5 Vegetation Indices

VIs were designed to capture the variation of reflectance in several spectral bands and reduce this information into a number that can be related to a property of the vegetation. The various VIs investigated had distinct temporal behavior (Figure 5). However, while soil/residue and green up stages were distinguishable in maize, only the

soil/residue stage was recognizable in soybean. It was quite difficult to identify the end of peak vegetative stage in maize (Figure 3.7A), as well as beginning and end of this stage in soybean (Figure 3.7B). In addition, soil/stover/residue stage is easily recognizable in soybean, it is not in maize. For more examples see Appendix B: Additional data for determining .

The NDVI and EVI2 were unable to separate the soil background with or without fresh stover without reference to the day of year; however, for VARI, fresh stover caused values to drop below -0.2 (Figure 3.7). Therefore VARI may be useful in separating these classes. Unfortunately, this drop in values is rather short-lived in soybean. The residue for soybean is decomposes faster than maize. The soybean residue is also lighter and is easily redistributed by rain and wind. Thus, soil is quickly exposed and VARI values return pre-season levels quickly.

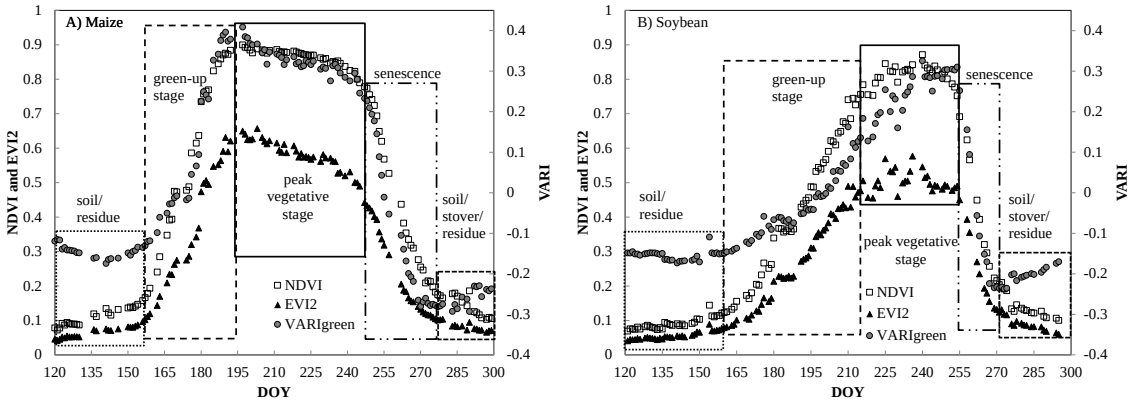

Figure 3.7: Temporal behavior of three vegetation indices for a A) maize site in 2011 and a B) soybean site in 2012. Crop developmental stages identified in green vs. red reflectance relationships (Figure 3.5) are labeled in each panel.

An additional issue was that many VIs were also sensitive to plant stress. This was not surprising since the original purpose of many VIs was to monitor plant health. During periods of stress, the variation in the VIs adds 'noise' in the VI vs. DOY relationship. This made it more difficult to distinguish developmental stages. For example, the rainfed soybean field in 2012 experienced drought (Figure 3.7B) and the peak vegetative stage was not as clearly defined as it was in the maize data (Figure 3.7A). For an example of a clearly defined peak vegetative stage for soybean see Figure B.5C in Appendix B: Additional data for determining . When examining spectral spaces, this noise was not incorporated into the red vs. green reflectance relationship and the peak vegetative stage was clearly defined (Figure 3.5B).

3.2.6 Using spectral spaces to identify crop developmental stage

While this study has already identified crop developmental stages using spectral spaces, it is also possible to identify these stages without any ancillary data (e.g. day after planting) or context (e.g. reflectance values collected recently before or after point of interest). It was possible to identify the peak vegetative stage using VIs (see 3.2.5 Vegetation Indices); however, it was impossible to differentiate between the green-up and senescence since they have similar VI values. Using the spectral spaces identified in 3.2.4 Two-dimensional spectral spaces, we selected two spectral space diagrams (red vs. green reflectance and NIR vs. red reflectance) capable of distinguishing the green-up and senescence stage for maize (Figure 3.8A-B) and one (red vs. red edge) for soybean (Figure 3.8C). As identified in each of the figures, the NDVI values were approximately

0.45 or roughly half of the maximum NDVI values found at peak vegetative stage for both the green-up and senescence stages.

For the red vs. green reflectance relationship in maize, the red and green reflectance was nearly equal for the green-up stage and red reflectance was higher for senescence. For the NIR vs. red reflectance relationship in maize, the green-up stage had higher NIR reflectance comparatively to the senescence stage for the same red reflectance. The difference between the two stages in maize for both relationships was most pronounced during normal growing conditions. When stressed (2012 was extremely dry even in irrigated fields), the differences between the green-up and senescence stages

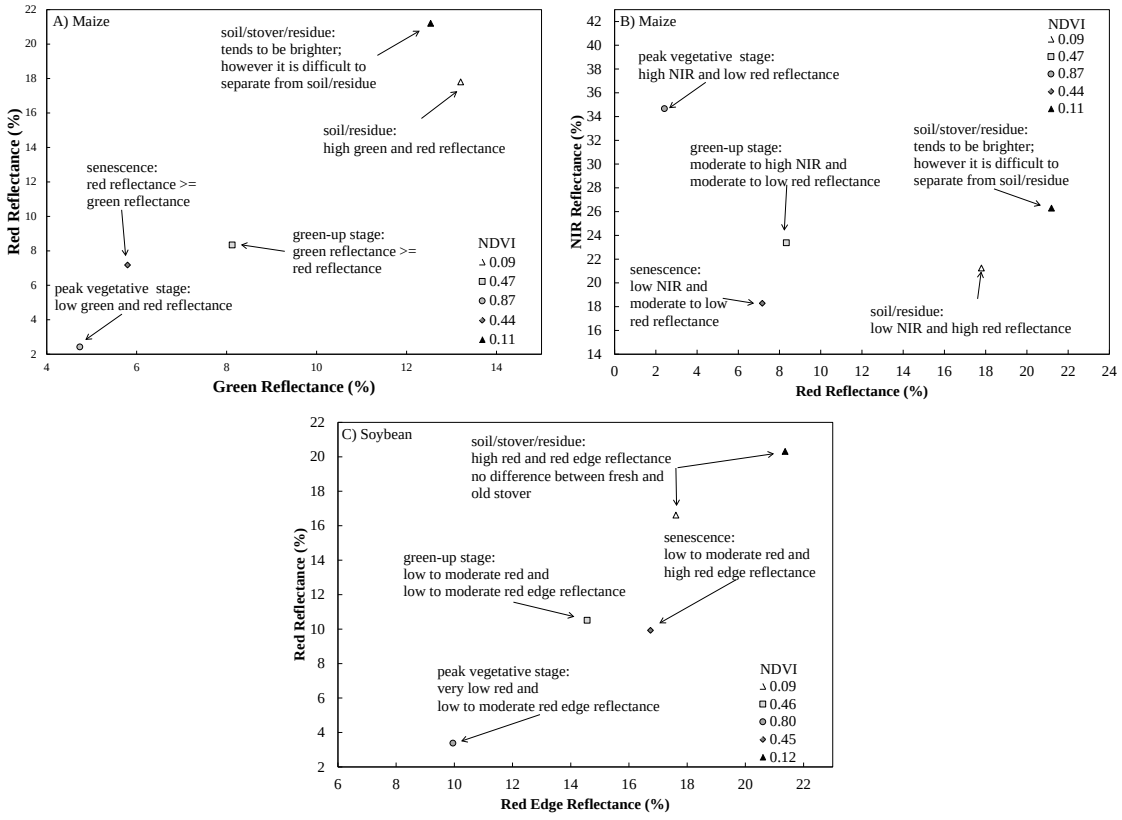

Figure 3.8: Spectral spaces useful for identifying crop stage of development independently of ancillary data for maize (top row) and soybean (bottom row)

decreased and became nearly indistinguishable (Figure B.1F-G, Figure B.4F-G).

While it may be possible to separate the green-up and senescence stages without any context (e.g. day of planting) using spectral spaces, it is still necessary to know the crop planted since this approach is species-specific. Thus, using spectral spaces for identifying the plant stage of development would be best suited for data sets using high temporal sensors or where some additional information (e.g. day of planting) was known. However, in areas of multiple cropping systems of the same crop, this approach may provide useful information to end users. For example, users who apply algorithms developed for specific growth stage needs to be able to accurately identify the crop stage of development before applying the algorithm. An examination of the reflectances in spectral space can provide this information.

3.3 Conclusions

This study determined that it is possible to deploy 4-band radiometers for accurate real-time monitoring of crop stage development and physiological status throughout the growing season. The calibration procedure using a calibrated light source was an effective method to determine calibration coefficients. This study also found that the median midday reflectance was a reasonable measure of reflectance for maize and soybean under varying weather conditions.

The two-dimensional spectral spaces (e.g. relationships between reflectances in green and red spectral bands) were explored for detecting crop developmental stages in maize and soybean. Using the changes in sensitivity of each individual spectral band to crop status, five distinct vegetative growth stages were identified in both maize and

soybean. The behavior of these spectral spaces did vary between the two crops. Thus, they were species-specific. The red vs. green reflectance relationship separated the green-up and senescence stages for maize and the red vs. red edge reflectance relationship separated the two stages for soybean. Future studies should be directed towards determining whether or not these stages can be discerned in other species or crop types and if the patterns identified are similar to those found in this study. It was shown that two-dimensional spectral spaces bring additional information to that of VIs and further studies should focus on understanding of value of information that spectral spaces bring.

Chapter 4 : Combining vegetation indices to achieve maximal sensitivity

This chapter is based on the published paper:

Nguy-Robertson, A.L. A.A. Gitelson, Y. Peng, A. Viña, T. Arkebauer, and D. Rundquist (2012) Green leaf area index estimation in maize and soybean: Combining vegetation indices to achieve maximal sensitivity. Agronomy Journal, 104(5): 1336-1347.

4.1 Objectives

The objectives of this study were to: (1) test the performance of twelve VIs for estimating green LAI in maize (*Zea may*s) and soybean (*Glycine max*); (2) identify an algorithm that does not require re-parameterization for estimating green LAI in both maize and soybean (C3 vs. C4 crops); and (3) devise a "combined vegetation index" that is maximally sensitive to green LAI along its entire range of variability (i.e. 0 to more than 6 $m^2 m^{-2}$), and is applicable to current operational satellite-based sensors such as the Moderate Resolution Imaging Spectroradiometer (MODIS) on board the National Aeronautics and Space Administration (NASA) Terra and Aqua satellites, or the European Space Agency (ESA) Medium Resolution Imaging Spectroradiometer (MERIS).

4.2 Results and discussion

4.2.1 Temporal behavior of green leaf area index

While both maize and soybean undergo three major stages of development (green-up, reproductive, and senescence), the temporal dynamics of their green LAI are very different (Figure 4.1). In maize, the green-up period was longer (~20 days) than in soybean. Maize remained in the vegetative stage as green LAI increased until it reached the maximum green LAI, which occurred when silking began. There was a decrease in green LAI of about 1 $m^2 m^{-2}$ during the kernel development. Then, during the final stage before maturity (dent), green LAI dropped to nearly 0 $m^2 m^{-2}$ (Figure 4.1A). In contrast, soybean flowered before maximum green LAI was reached, which occurred during pod and seed development, and decreased once the plant reached full seed (Figure 4.1B). The ranges of maize and soybean green LAI variability were also different. In irrigated maize, the maximum green LAI reached 6.5 $m^2 m^{-2}$ while in soybean it did not exceed 5.5 $m^2 m^{-2}$. For both crops, green LAI maxima in rainfed fields were typically lower than in irrigated fields (Figure 4.1, Table 2.1). Thus, the maximum green LAI differed on per crop (i.e., maize vs. soybean) and water status (i.e. irrigated vs. rainfed) bases.

4.2.2 Sensitivity analysis of the VI vs. green LAI relationships

All best-fit functions established between green LAI and VI for either maize (Table 4.1) or soybean (Table 4.2) were non-linear, and the shapes of the relationships VI vs. green LAI differed among VIs (Figure 4.2). For example, NDVI reached an asymptote at around 0.7 when green LAI was between 2 and 3 $m^2 m^{-2}$, and became almost invariant for green LAI > 4$m^2 m^{-2}$ in both maize and soybean (Figure 4.2B). This saturation of the NDVI (Figure 4.2B) reduces its functionality for green LAI estimation at moderate-to-high green LAI values, since it generates large uncertainty in model

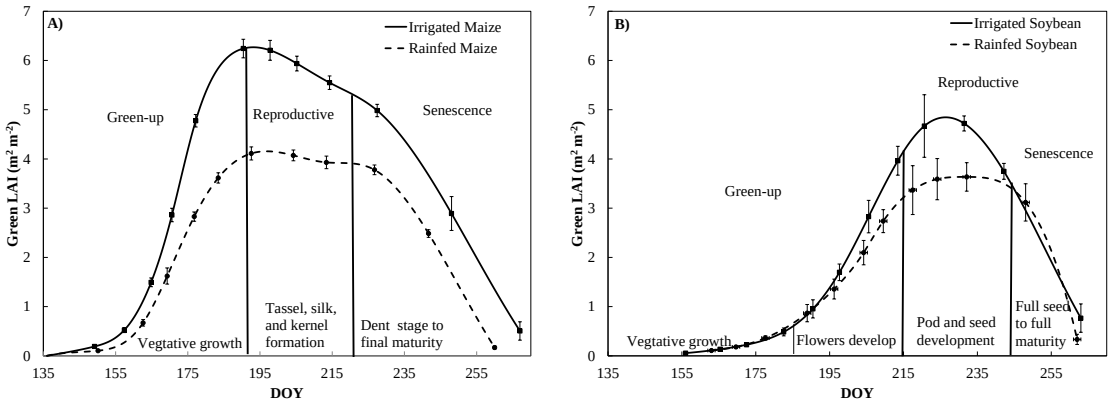

Figure 4.1: Temporal dynamics of green LAI in (A) maize in 2007 and (B) soybean in 2008, in both irrigated (solid line) and rainfed (dashed line) fields. Major crop growth stages (vegetative, reproductive, and senescence) are indicated. Bars represent one standard error of destructive green LAI determination at six intensive measurement zones in each field.

inversions: almost the same value of VI corresponds to green LAI ranging from 4 to more than 6 $m^2 m^{-2}$. Several other normalized difference indices (green NDVI, red edge NDVI, EVI2, and WDRVI with $\alpha = 0.2$), TVI and MTVI2 also showed different degrees of decreased sensitivity at moderate-to-high green LAI values (Figure 4.2C, D, E, H, J, K, L). SR had an exponential relationship with lower sensitivity to green LAI < 1 $m^2 m^{-2}$ than to higher green LAI values (Figure 4.2A). For green LAI > 1 $m^2 m^{-2}$, the relationship between SR and green LAI was nearly linear. The relationships for CIs and the MTCI exhibited a similar shape, with an increase in slope at moderate to high green LAI (Figure 4.2F, G, I).

In this study, we found that among the twelve VIs examined, only the red edge NDVI (ANOVA: $p = 0.36$, $n = 423$, $F = 1.09$) and the $CI_{red\ edge}$ (ANOVA: $p = 0.11$, $n =$

423, $F = 1.65$) can be applied for maize and soybean with no re-parameterization of the model. Best-fit functions of the relationships green LAI vs. red edge NDVI and $CI_{red\ edge}$ for both maize and soybean are presented in Table 5. All other VIs were crop-specific (ANOVA: $p < 0.001$, $n = 423$, $F > 4.5$).

As noted in the Materials and Methods (Section 2.4.7 Statistical analysis), R^2 and SE may be misleading when comparing non-linear and linear relationships. For example, although the relationship NDVI vs. green LAI resulted in high R^2 values, the slope of the relationship decreased as green LAI exceeded 3 $m^2\ m^{-2}$ and became close to zero at green LAI values above 3.5 $m^2\ m^{-2}$ for soybean and above 4 $m^2\ m^{-2}$ for maize (Figure 4.2B). With the decrease in sensitivity of VIs to green LAI (i.e., when green LAI exceeds 3 $m^2\ m^{-2}$), the scattering of the points from the best-fit functions drops, as can be seen for NDVI, green NDVI, red edge NDVI and OSAVI (Figure 4.2B, C, D, E). Thus, most of the VIs had similar R^2 and SE (Table 4.1 and Table 4.2) but very different shapes of the relationships VI vs. green LAI (e.g., increasing exponential decay in NDVI vs. exponential growth in SR). Therefore, a different accuracy metric, specifically the NE Δgreen LAI, was needed to compare the performance of VIs in estimating green LAI along its entire range of variation.

Figure 4.3 displays values of NE Δgreen LAI for normalized difference VIs, MTCI and ratio indices (SR, CIs). TVI and MTVI2 were not included in this analysis because their NE Δgreen LAI values were always greater than those of normalized difference indices at low to moderate green LAI, and also were always greater than those of SR, CIs and MTCI at moderate to high green LAI. Therefore, TVI and MTVI2 did not

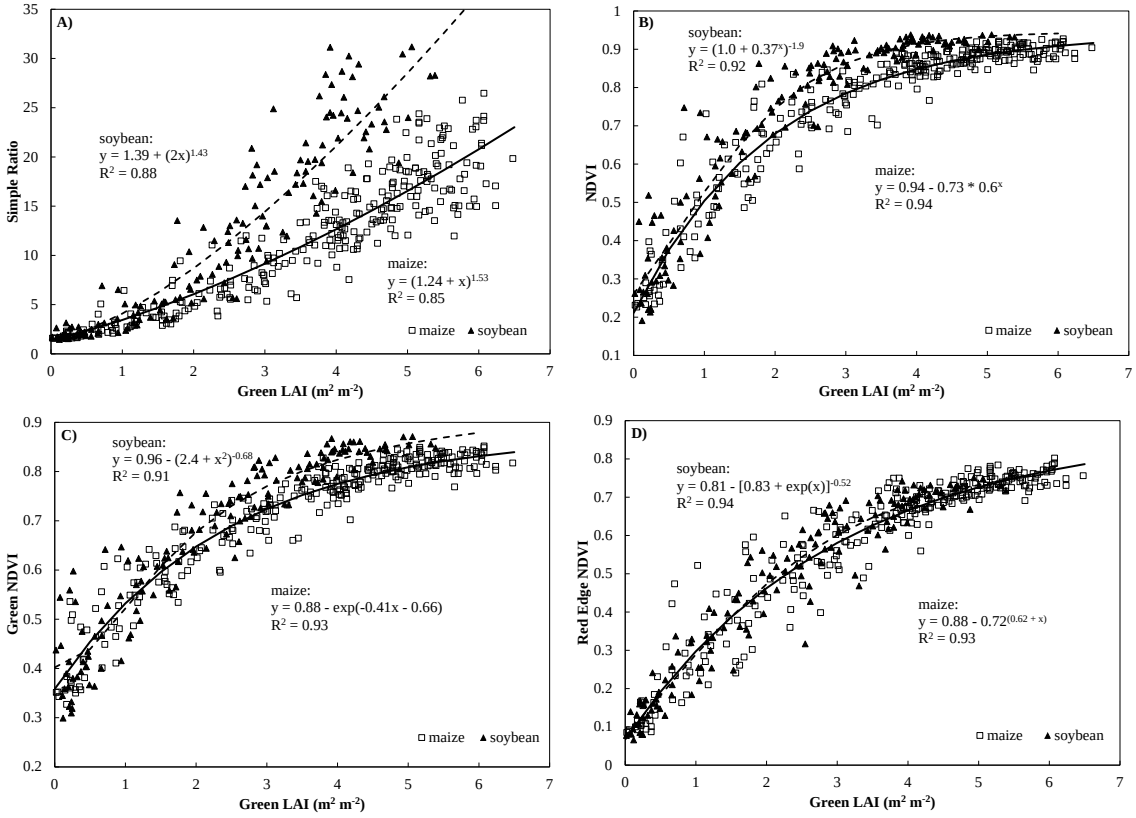

Figure 4.2: Vegetation indices plotted versus green leaf area index, green LAI: (A) Simple Ratio, (B) Normalized Difference Vegetation Index (NDVI), (C) green NDVI, (D) red edge NDVI, (E) Optimized Soil-Adjusted Vegetation Index (OSAVI), (F) Chlorophyll Index Green (CI_{green}), (G) $CI_{red\ edge}$, (H) Triangular Vegetation Index (TVI), (I) MERIS Terrestrial Chlorophyll Index (MTCI), (J) Wide Dynamic Range Vegetation Index (WDRVI) α=0.2, (K) Modified TVI 2 (MTVI2), and (L) Enhanced Vegetation Index 2 (EVI2). In all panels – maize: open squares, solid line is best-fit function; soybean: closed triangles, dashed line is best fit function. The inverse of these relationships green LAI vs. VIs along with their summary statistics are shown in Tables 3 and 4.

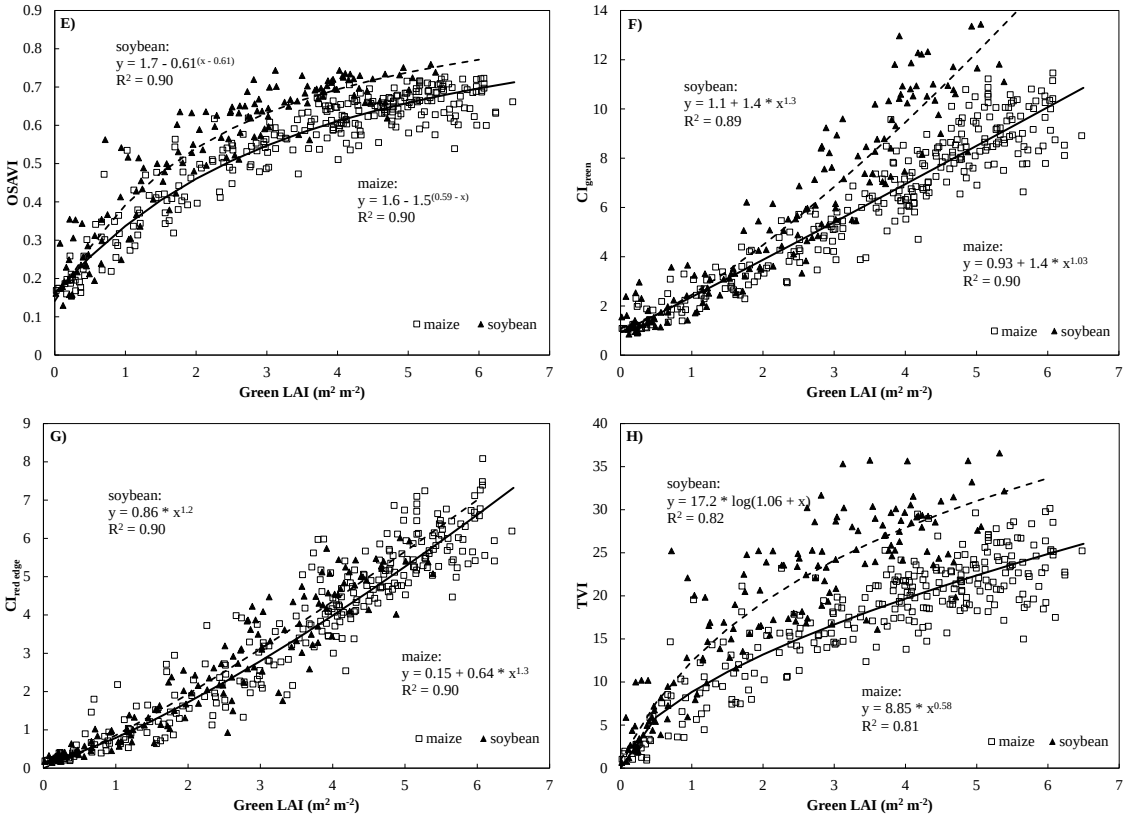

Figure 4.2 (continued): Vegetation indices plotted versus green leaf area index, green LAI: (A) Simple Ratio, (B) Normalized Difference Vegetation Index (NDVI), (C) green NDVI, (D) red edge NDVI, (E) Optimized Soil-Adjusted Vegetation Index (OSAVI), (F) Chlorophyll Index Green (CI_{green}), (G) $CI_{red\ edge}$, (H) Triangular Vegetation Index (TVI), (I) MERIS Terrestrial Chlorophyll Index (MTCI), (J) Wide Dynamic Range Vegetation Index (WDRVI) α=0.2, (K) Modified TVI 2 (MTVI2), and (L) Enhanced Vegetation Index 2 (EVI2). In all panels – maize: open squares, solid line is best-fit function; soybean: closed triangles, dashed line is best fit function. The inverse of these relationships green LAI vs. VIs along with their summary statistics are shown in Tables 3 and 4.

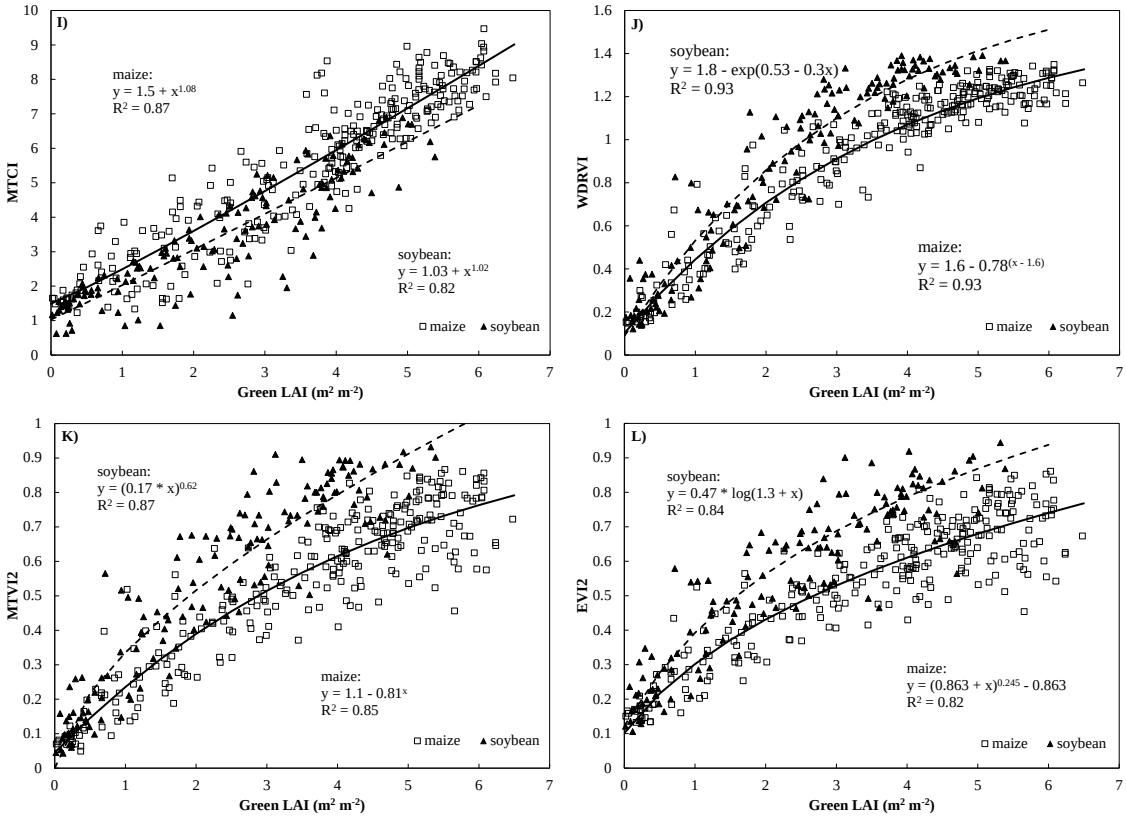

Figure 4.2 (continued): Vegetation indices plotted versus green leaf area index, green LAI: (A) Simple Ratio, (B) Normalized Difference Vegetation Index (NDVI), (C) green NDVI, (D) red edge NDVI, (E) Optimized Soil-Adjusted Vegetation Index (OSAVI), (F) Chlorophyll Index Green (CI_{green}), (G) $CI_{red\ edge}$, (H) Triangular Vegetation Index (TVI), (I) MERIS Terrestrial Chlorophyll Index (MTCI), (J) Wide Dynamic Range Vegetation Index (WDRVI) α=0.2, (K) Modified TVI 2 (MTVI2), and (L) Enhanced Vegetation Index 2 (EVI2). In all panels – maize: open squares, solid line is best-fit function; soybean: closed triangles, dashed line is best fit function. The inverse of these relationships green LAI vs. VIs along with their summary statistics are shown in Tables 3 and 4.

Table 4.1: Best-fit functions of the relationships between green leaf area index (green LAI) and vegetation indices (VI) obtained using a cross-validation procedure for maize; x = VI, y = green LAI, R^2 is the coefficient of determination, and the SE is the standard error of the green LAI estimation, in $m^2 m^{-2}$.

Index	Equation green LAI vs. VI	R^2	SE
SR	$y = x^{0.654} - 1.24$	0.86	0.66
NDVI	$y = \log_{0.6}[-1.37 * (x - 0.943)]$	0.87	0.64
Green NDVI	$y = -\{2.44 * [\ln(0.876 - x) + 0.66]\}$	0.87	0.63
Red edge NDVI	$y = \log_{0.716}(0.88 - x) - 0.623$	0.90	0.54
OSAVI	$y = -[1.49 * \ln(x) + 2.71] * \ln(x)^{-1}$	0.81	0.78
CI_{green}	$y = [0.694 * (x - 0.931)]^{0.971}$	0.89	0.59
$CI_{red\ edge}$	$y = [1.56 * (x - 0.15)]^{0.775}$	0.90	0.55
TVI	$y = (0.113 * x)^{1.73}$	0.65	1.05
MTCI	$y = (x - 1.49)^{0.926}$	0.85	0.69
WDRVI α=0.2	$y = \log_{0.775}(1.61 - x) + 1.61$	0.88	0.60
MTVI2	$y = \log_{0.81}(1.05 - x)$	0.67	1.01
EVI2	$y = (x + 0.863)^{4.08} - 0.863$	0.63	1.07

Table 4.2: Best-fit functions of the relationships between green leaf area index (green LAI) and vegetation indices (VI) obtained using a cross-validation procedure for soybean; x = VI, y = green LAI, R^2 is the coefficient of determination, and the SE is the standard error of green LAI estimation, in $m^2 m^{-2}$.

Index	Equation green LAI vs. VI	R^2	SE
SR	$y = 0.5 * [(x - 1.39)^{0.698}]$	0.89	0.51
NDVI	$y = \log_{0.37}[x^{-0.526} - 1.03]$	0.90	0.48
Green NDVI	$y = \text{sqrt}[(0.964 - x)^{-1.48} - 2.35]$	0.89	0.51
Red edge NDVI	$y = \ln[(0.805 - x)^{(1.92)} - 0.82]$	0.91	0.46
OSAVI	$y = -[0.916 * \ln(x^{-1}) - 1.79] * \ln(x^{-1})^{-1}$	0.84	0.60
CI_{green}	$y = [0.725 * (x - 1.08)]^{0.767}$	0.90	0.49
$CI_{red\ edge}$	$y = (1.16x)^{0.854}$	0.91	0.46
TVI	$y = \exp(0.0581x) - 1.06$	0.60	0.95
MTCI	$y = (x - 1.03)^{0.981}$	0.80	0.67
WDRVI α=0.2	$y = -\{3.33 * [\ln(1.79 - x) - 0.532]\}$	0.90	0.47
MTVI2	$y = 5.81x^{1.61}$	0.82	0.64
EVI2	$y = \exp(2.12x) - 1.3$	0.76	0.75

meet the criteria for determining the best indices either for low-to-moderate, for moderate-to-high, or for the entire range of green LAI.

The normalized difference VIs had asymptotic relationships with green LAI (Figure 4.2B, C, D, H, L); thus, the NE Δgreen LAI was lowest at green LAI below 2.5 $m^2 m^{-2}$ for maize and below 2 $m^2 m^{-2}$ for soybean (Figure 4.3). SR and CIs had exponential relationships with green LAI (Figure 4.2A F, G); thus, the lowest values of NE Δgreen LAI were at green LAI exceeding 3 $m^2 m^{-2}$ (Figure 4.3). Therefore, the normalized difference VIs were more accurate in estimating low-to-moderate green LAI while the ratio indices, SR and CIs, were more accurate in estimating moderate-to-high green LAI.

While the relationship of MTCI with green LAI was asymptotic, the slope of the relationship was almost constant in a wide range of green LAI variation (Figure 4.2I). Therefore, for MTCI, NE Δgreen LAI varied little throughout the entire range of green LAI (Figure 4.3). In the range of green LAI below 2.5 $m^2 m^{-2}$, the MTCI had lower accuracy than normalized difference VIs and almost the same accuracy as SR and CI indices. However, in the range of green LAI > 2.5 $m^2 m^{-2}$, it had lower accuracy than SR and CIs. Thus, it did not outperform normalized difference VIs or SR and CI indices in their respective regions of highest sensitivity to changes in green LAI.

At moderate to high green LAI, the noise equivalents of normalized difference indices in soybean were higher than those in maize. This may be explained by the very different canopy architectures and leaf structures of these crops. For the same amount of foliar chlorophyll content, the chlorophyll density on the adaxial side of soybean leaves is higher than that in maize leaves, causing a higher absorption in the red range and thus

lower reflectance of soybean canopies: 2% for leaf chlorophyll above 500 mg m^{-2} (Gitelson et al., 2005) compared to 3-5% of maize leaves. In addition, for the same green LAI, canopy reflectance of soybean in the NIR region was higher than that of maize: for green LAI around 5 m^2 m^{-2}, NIR reflectance was 60% in soybean vs. 40% in maize (Peng & Gitelson, 2011). Thus, for the same green LAI, especially within the moderate-to-high range, the NIR to red reflectance ratio is higher in soybean than in maize. Therefore, the value of green LAI above which the normalized difference indices became insensitive to green LAI was lower in soybean than in maize.

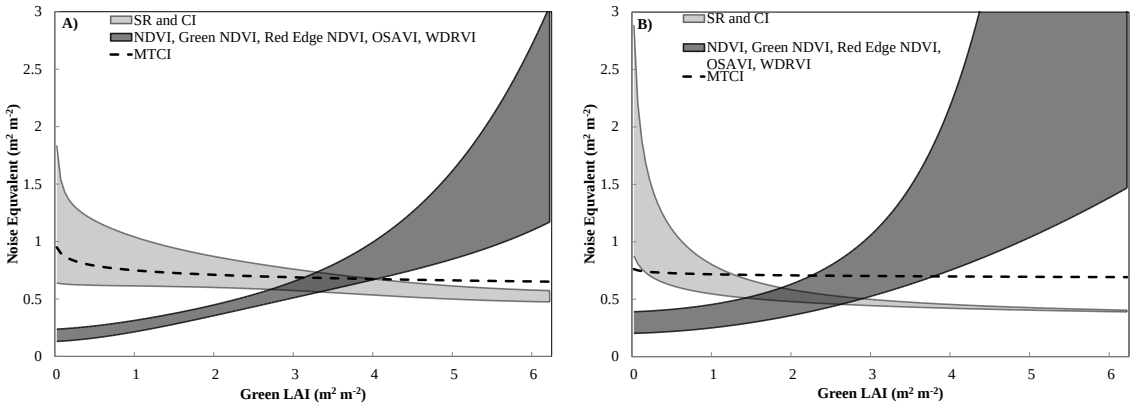

Figure 4.3: Minimal and maximal values of the noise equivalent NE Δgreen LAI for (A) maize and (B) soybean for groupings of vegetation indices demonstrating increase of NE (decrease in accuracy) at moderate-to-high green LAI (NDVI, green NDVI, red edge NDVI, OSAVI, and WDRVI), high NE at low-to-moderate green LAI (SR, CI_{green} and $CI_{red\ edge}$) and almost invariant NE throughout the entire dynamic range (MTCI).

Analysis of the NE Δgreen LAI of VIs (Figure 4.3) showed that for green LAI below 2.5 m^2 m^{-2}, normalized difference VIs had the lowest NE Δgreen LAI, and thus highest accuracy of green LAI estimation, while SR and CIs had the highest accuracy for

green LAI > 3 m^2 m^{-2} and were the best suited for estimation of moderate-to-high green LAI. Therefore, there was no single index that had the lowest uncertainties of green LAI estimation along the entire range of green LAI variation. In order to obtain the highest possible accuracy (i.e., lowest NE Δgreen LAI) across the entire range of green LAI, we suggest using more than one VI in combination, i.e., a combined vegetation index (CVI).

4.2.3 Combined vegetation index

The CVI is comprised of two VIs that are the most accurate in green LAI estimation at different ranges of green LAI: the first index for low-to-moderate green LAI (below 2.5 m^2 m^{-2}) and the second index for moderate-to-high green LAI (above 2.5 m^2 m^{-2}). While it is possible to scale the VIs in CVI to create a linear relationship, any scaled

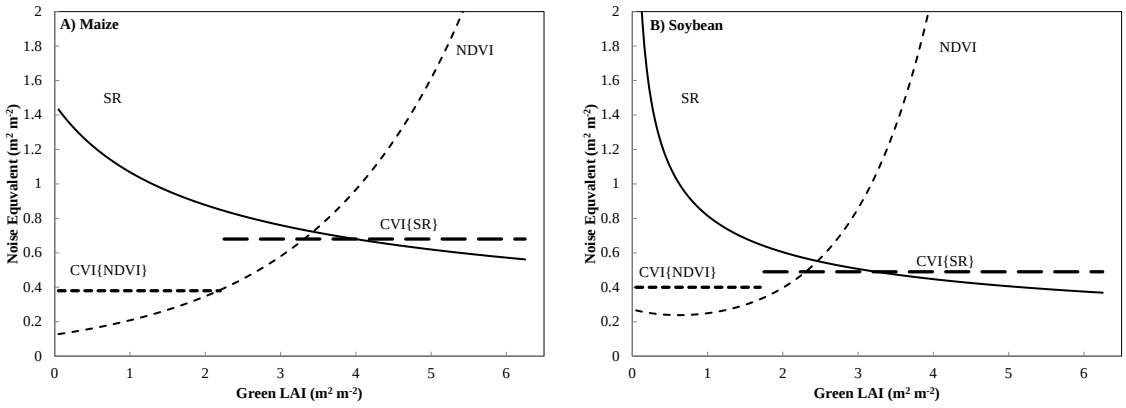

Figure 4.4: Noise equivalent NE Δgreen LAI of NDVI, SR and suggested combined vegetation index CVI{NDVI, SR} for (a) maize and (b) soybean. NDVI < 0.7 is the first index and SR is the second index.

algorithm will be data-set dependent and may result in a decrease in the sensitivity of the VI to green LAI. For both MODIS and MERIS data, containing the red and NIR bands,

we suggest using NDVI as the first index and SR as the second index - CVI{NDVI, SR}. An NDVI value around 0.7 has been previously reported as a typical point where the NDVI vs. green LAI relationship becomes saturated (Gitelson et al., 2003b; Myneni et al., 1995). Therefore, we selected NDVI = 0.7 as a threshold for both maize and soybeans. In the range of NDVI from 0 to 0.7, the best fit functions of NDVI vs. green LAI for both crops were linear and, thus, NE Δgreen LAI was constant and as low as 0.38 $m^2 m^{-2}$ for maize (Figure 4.4A) and 0.4 $m^2 m^{-2}$ for soybean (Figure 4.4B).

As green LAI exceeded 2.5 $m^2 m^{-2}$, the NE Δgreen LAI of SR decreased and the accuracy of green LAI estimation increased for both species (Figure 4.4). When SR was above 5.7 (corresponding to NDVI =0.7), the best-fit function of SR vs. green LAI was linear and, thus, NE Δgreen LAI was constant and equal to 0.68 $m^2 m^{-2}$ for maize (Figure 4.4A) and 0.49 $m^2 m^{-2}$ for soybean (Figure 4.4B). A CVI comprised of two indices (NDVI and SR and, thus, using only red and NIR bands), was able to estimate green LAI ranging from 0 to more than 6 $m^2 m^{-2}$ with a RMSE below 0.72 $m^2 m^{-2}$ and a CV of 20% for maize, and a RMSE below 0.54 $m^2 m^{-2}$ and a CV of 23% for soybean. However, the

Table 4.3: Best-fit functions of the relationships between green leaf area index (green LAI) and vegetation indices (VI) for both maize and soybean combined; x = VI, y = green LAI, R^2 is the coefficient of determination, and the SE is the standard error of the green LAI estimation, in $m^2 m^{-2}$.

Index	Equation green LAI vs. VI	R^2	SE
Red Edge NDVI	$y = (0.155x^{-1} - 0.173)^{-0.542} - 0.739$	0.90	0.56
$CI_{red\ edge}$	$y = 1.11x^{0.898}$	0.91	0.54

algorithms relating green LAI and CVI{NDVI, SR} for maize and soybean required different coefficients (Table 4.3) and, thus, were crop specific.

Alternatively, we suggest using the red edge NDVI as the first CVI index and the $CI_{red\ edge}$ as the second CVI index – i.e., CVI{red edge NDVI, $CI_{red\ edge}$} (Figure 4.5) for data acquired by sensor systems containing red edge and NIR bands (e.g., MERIS, HYPERION). This combined index was not crop-specific, at least for the species evaluated (i.e., maize and soybean), which have quite contrasting leaf and canopy structures. Therefore, this CVI does not require re-parameterization, since the same algorithm coefficients can be applied to estimate green LAI in both crops (Table 4.4). Based on the NE Δgreen LAI results, presented in Figure 4.5, we suggest using a threshold of red edge NDVI equal to 0.6. For the range of red edge NDVI of 0 to 0.6, the NE Δgreen LAI was 0.46 $m^2\ m^{-2}$ and for $CI_{red\ edge}$ above 3 (corresponding to the red edge NDVI value of 0.6) the NE Δgreen LAI was 0.55 $m^2\ m^{-2}$ (Figure 4.5). For both species,

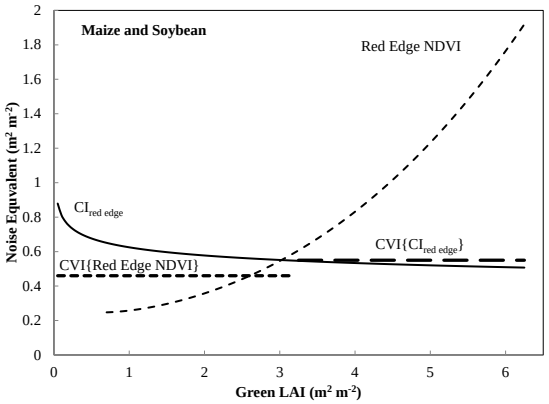

Figure 4.5: Noise equivalent NE Δgreen LAI of red edge NDVI, CIred edge and suggested combined vegetation index CVI{red edge NDVI, CIred edge} for maize and soybean combined. Red edge NDVI < 0.6 is the first index and CIred edge is the second index.

Table 4.4: Best-fit functions for combined vegetation indices (CVI) as used to estimate green LAI. CVI represents the combination of two vegetation indices where the first index (i.e., NDVI or red edge NDVI) are most sensitive to low-to-moderate green LAI and the second index (i.e., SR or $CI_{red\ edge}$) are most sensitive to moderate-to-high green LAI. The threshold for NDVI was set at 0.7 and for red edge NDVI at 0.6. CV is coefficient of variation.

Index	Crop	First index below threshold	Second index above threshold	CV (%)
CVI{NDVI, SR}	Maize	5.55 * (NDVI - 0.28)	0.286 * (SR + 1.0)	20
CVI{NDVI, SR}	Soybean	4.55 * (NDVI - 0.27)	0.161 * (SR + 3.2)	23
CVI{Red Edge NDVI, $CI_{red\ edge}$}	Maize and Soybean	7.14 * (red edge NDVI – 0.13)	1.05 * ($CI_{red\ edge}$ – 0.63)	20

CVI{red edge NDVI, $CI_{red\ edge}$} was able to estimate green LAI along its entire range of variation (i.e., 0 to > 6 $m^2\ m^{-2}$), with a RMSE below 0.60 $m^2\ m^{-2}$ and a CV of 19%.

In applications where prior knowledge about crop type is available, using sensor systems containing red and NIR bands with spatial resolutions high enough to reduce the effects of mixed pixels, the CVI{NDVI,SR} is adequate. However, in many cases, there is uncertainty about the crop type present within a pixel (e.g., coarse spatial resolutions, mixed pixels, areas of crop rotation without prior knowledge of planted crops). Thus, the CVI{red edge NDVI, $CI_{red\ edge}$}, having a unified algorithm for crops with different leaf and canopy structures (e.g., maize and soybean), brings an objective estimation of total green LAI, even in the case of mixed pixels and crops at different growth stages.

We acknowledge that further research is needed to evaluate the CVI{red edge NDVI, $CI_{red\ edge}$} in other crops. However, since in this study it was tested in crops that are very different (maize and soybean), it will likely be insensitive to leaf and canopy

structure of crops that are not as different. It is also important to investigate the reliability of the CVIs developed when applied to estimating green LAI in other vegetation types, such as grasslands and forests. Additionally, the calibration equations for the CVIs built with simulated MODIS and MERIS bands obtained from close-range hyperspectral data should be tested against actual MODIS and MERIS data. However, it is likely that these equations are reliable since it has been shown that the coefficients of the relationships between green LAI and WDRVI, when taken at close-range, remained the same as those applied to MODIS 250 m data, due to accurate atmospheric correction of the MODIS 250 m surface reflectance product (Gitelson et al., 2007; Guindin-Garcia et al., 2012).

The approach presented in this study is not limited to green LAI, as it may also be used for the remote estimation of other biophysical characteristics, such as vegetation cover, fraction of absorbed photosynthetically active radiation and gross primary production. Nevertheless, the CVIs presented in this study may not constitute the best vegetation index combinations for measuring these other vegetation characteristics. Therefore, future studies are needed to investigate which VI combinations are the most appropriate for assessing other biophysical characteristics of vegetation.

4.3 Conclusions

Twelve vegetation indices, calculated from simulated spectral bands of MODIS and MERIS satellite sensors, were evaluated for remotely assessing green LAI in two crop species with contrasting leaf structures and canopy architectures, maize and soybeans. All VIs investigated had essentially non-linear relationships with green LAI, although with different sensitivities along the range of green LAI variability evaluated.

On this basis, we suggested combining vegetation indices that exhibit high sensitivity to changes in green LAI at particular ranges (i.e., low-to-moderate and moderate-to-high). When combined, these indices constitute suitable and accurate remotely sensed surrogates of green LAI along its entire range of variability. Specifically, we suggested combining the NDVI and the SR, CVI{NDVI, SR} to be used in the case of sensors with spectral bands in the red and NIR (e.g., MODIS 250 m, Landsat TM and ETM+), although this combined index is crop-specific and requires re-parameterization of the algorithm for each crop. Alternatively, if a band in the red-edge region is available (e.g., MERIS, HYPERION), we suggested combining the red edge NDVI and the $CI_{red\ edge}$, CVI{red edge NDVI, $CI_{red\ edge}$}. Since it was not crop-specific, this combined index was capable of estimating green LAI with high accuracy, thus providing a suitable procedure for remotely estimating green LAI of crops with contrasting canopy architectures and leaf structures.

Chapter 5 : Examination of vegetation indices for the remote estimation of green LAI in maize, potato, soybean, and wheat

5.1 Objectives

The objectives of this investigation were to: (1) test the performance of VIs in green LAI estimation in four different crop types: maize (*Zea mays*), potato (*Solanum tuberosum*), soybean (*Glycine max*), and wheat (*Triticum* sp.); and (2) determine potential VIs that can be used in a unified algorithm for green LAI estimation for the whole growing season with no re-parameterization for different crop developmental stages. We examined the relationships between VI and green LAI, published previously, for potato and wheat (Herrmann et al., 2011) and maize and soybean (Gitelson et al., 2003; Viña et al., 2011; Nguy-Robertson et al., 2012) as compared to the other respective crops using reflectance simulated in the spectral bands of the MODIS and MERIS/Sentinel-2 satellite-based sensor systems. Then, we determined accuracy of the algorithms that were found to be the best for potato and wheat when applied to maize and soybean, and vice versa. Thus, we presented a suite of algorithms that can be used for four unrelated crops with very different leaf structures and canopy architectures. We also explored how the behavior of the VI vs. green LAI relationship varied between the green up and reproductive stages.

5.2 Results and discussion

5.2.1 Relationships between VIs and green LAI for potato and wheat

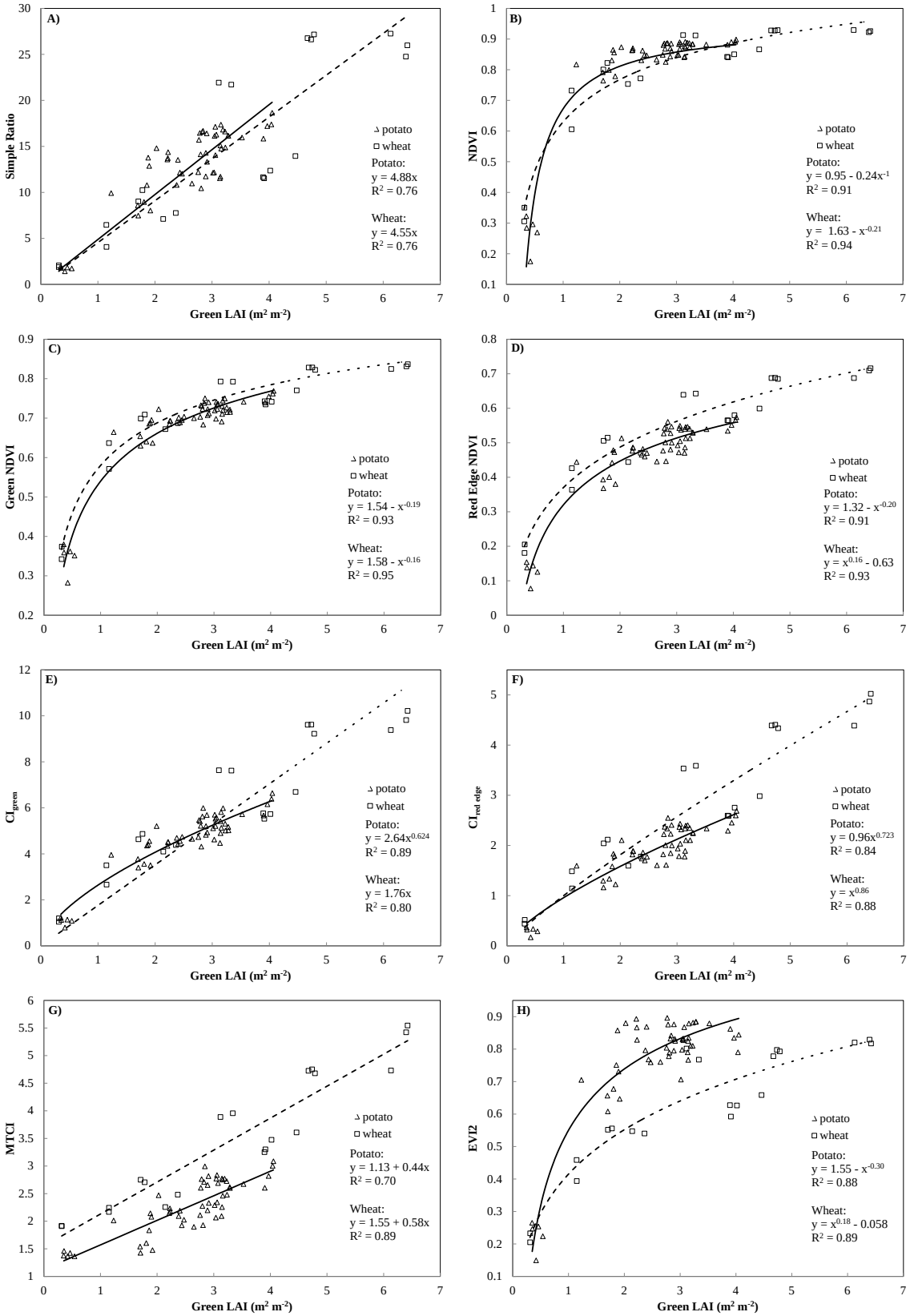

Figure 5.1: Vegetation indices vs. green LAI for potato and wheat in green up stage.

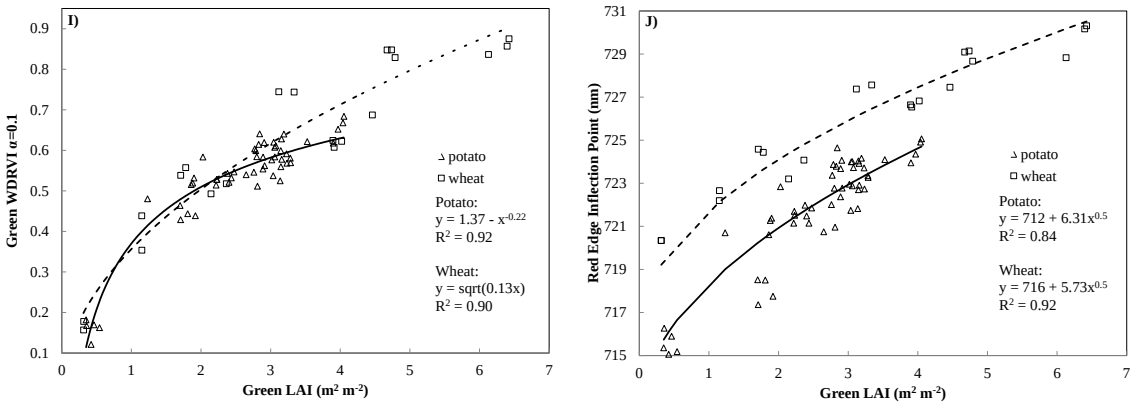

Figure 5.1 (continued): Vegetation indices vs. green LAI for potato and wheat in green up stage.

Firstly, relationships between VIs, which were accurate in estimating green LAI in maize and soybean (Nguy-Robertson et al., 2012; Viña et al., 2011), were developed for potato and wheat (Figure 5.1). Importantly, these relationships were established for the green-up stage only when green LAI equals total LAI. All indices tested in this study, related to green LAI quite closely with R^2 above 0.76. For potato and wheat, relationships between normalized difference VIs (NDVI, EVI2, green NDVI, red-edge NDVI, green WDRVI) and the green LAI showed a moderate to strong decrease in sensitivity when green LAI was greater than 2 $m^2 m^{-2}$ (Figure 5.1B-D, H, I). It was more pronounced for potato than for wheat. Among these VIs, green WDRVI and EVI2, decreased the least in sensitivity to moderate to high green LAI. The SR and MTCI had linear relationships with green LAI for both crops; however, the scattering of points from the best-fit function was quite wide for SR in both potato and wheat and for MTCI in potato (Figure 5.1A,G). The chlorophyll indices CI_{green}, and $CI_{red\text{-}edge}$ had linear relationships with green LAI in wheat and quite close to linear for potato (Figure 5.1E, F). The relationships REIP vs. green LAI were non-linear for both species (Figure 5.1J). However, the decrease in

sensitivity to moderate to high green LAI was less pronounced for REIP than for the normalized difference indices. Thus, the behavior of the relationships VI vs. green LAI for potato and wheat were consistent with previous studies in maize and soybean (Viña et al., 2011; Nguy-Robertson et al., 2012).

5.2.2 Green LAI estimation in potato, wheat, maize and soybean

One of the goals of this study was to determine if VIs found to be effective for estimating green LAI in maize and soybean (Viña et al., 2011; Nguy-Robertson et al., 2012) are effective in estimating green LAI in potato and wheat. Similarly we also wanted to examine whether the REIP, which was accurate in estimating green LAI in potato and wheat (Herrmann et al., 2011), is able to accurately estimate green LAI in maize and soybean. Figure 5.2 provides best-fit-functions VIs vs. green LAI for all four species studied *in the green up stage only* and Table 2 includes the equations of the best-fit functions for estimating green LAI using VIs. Notably, for different crops, grown in different environments, and treated differently, the best-fit functions were *similar* in shape for all VIs (six were presented in Figure 5.1). However, REIP and MTCI demonstrated strong deviation in slopes and intercepts for different species (Figure 5.2).

The relationships between green LAI and VIs had very different shapes (Figure 5.2) and may have similar determination coefficients, i.e., R^2 values (Table 5.1). Therefore, to assess the performance of different VIs, it is important to use other metrics besides R^2, such as the noise equivalent NEΔgreen LAI (see 2.4.7 Statistical analysis for details), as computed from the best-fit functions presented in Figure 5.2. This is essential when the relationship VI vs. green LAI is not linear. It allows the comparison of the

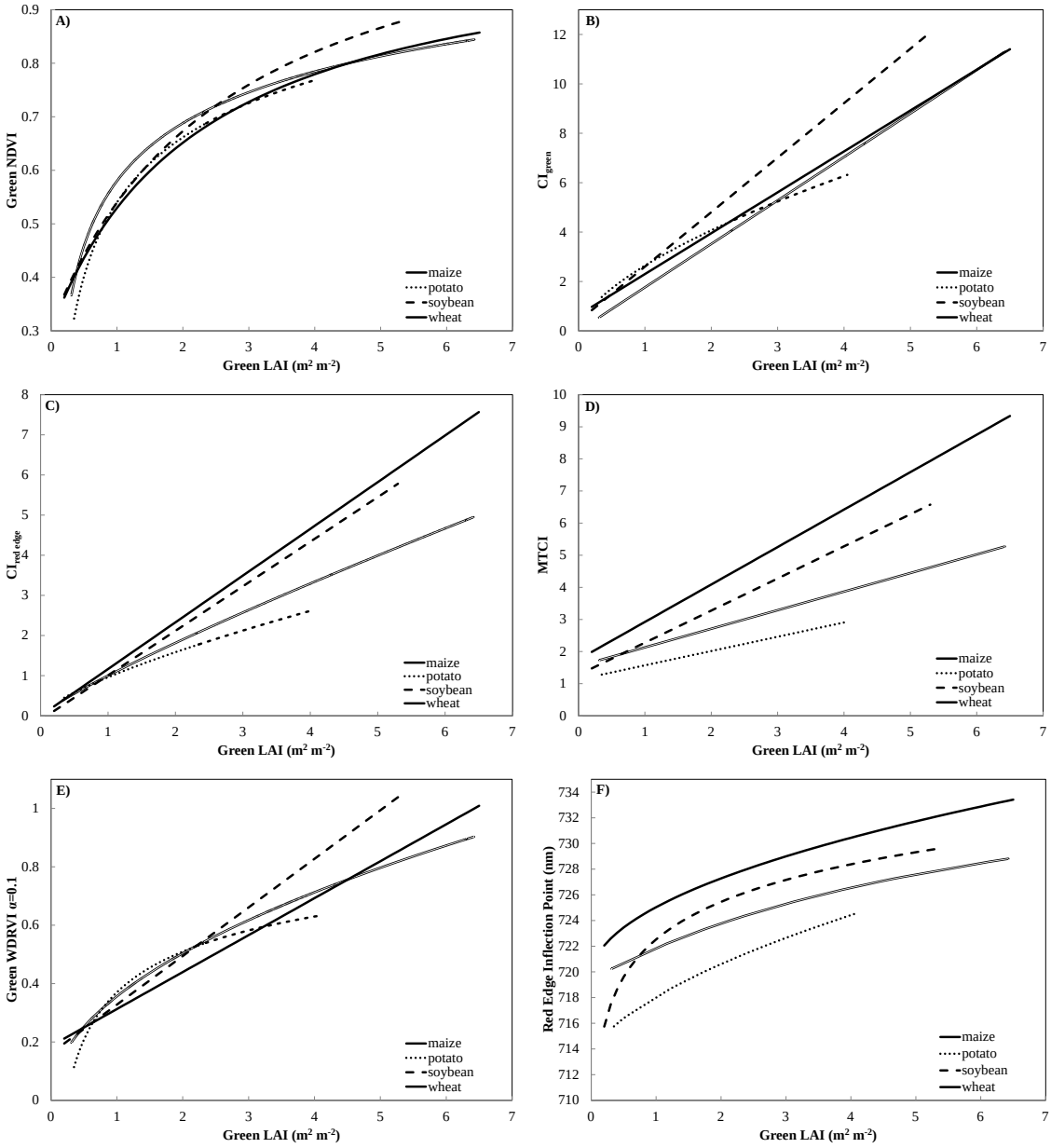

Figure 5.2: Best-fit functions of vegetation indices vs. green LAI relationships during the green-up stage for maize, potato, soybean, and wheat. Best-fit functions green LAI vs. VIs are presented in Table 5.1.

accuracy and the sensitivity of the VI to different green LAI values. For example, green NDVI has little dispersion from the best-fit function for all four crops (minimal R^2 was above 0.83, Table 5.1); however this VI, along with other normalized VIs (e.g. NDVI,

Table 5.1: Best-fit functions and determination coefficients, R^2, for the green LAI vs. vegetation indices, VI, relationship during the green-up stage.

Index	Crop	Equation green LAI vs. VI	R^2
SR	Maize	$y = [0.50 * (x - 1.31)]^{0.74}$	0.93
	Potato	$y = 0.20x$	0.77
	Soybean	$y = [0.33 * (x - 0.86)]^{0.73}$	0.89
	Wheat	$y = 0.22x$	0.69
NDVI	Maize	$y = -0.91x * (0.93x - 1)^{-1}$	0.93
	Potato	$y = -0.24 * (x - 0.95)^{-1}$	0.64
	Soybean	$y = -0.81x * (0.91x - 1)^{-1}$	0.88
	Wheat	$y = (1.63 - x)^{-4.67}$	0.79
REIP	Maize	$y = [0.19 * (719.6 - x)]^2$	0.88
	Potato	$y = [0.16 * (712.0 - x)]^2$	0.72
	Soybean	$y = \exp[0.24 * (x-722.5)]$	0.83
	Wheat	$y = [0.17 * (716.0 - x)]^2$	0.93
Green NDVI	Maize	$y = -(2.18x - 0.66) * (0.94x - 1)^{-1}$	0.94
	Potato	$y = (1.54 - x)^{-0.19}$	0.85
	Soybean	$y = -(3.17x - 0.98) * (1.16x - 1.36)^{-1}$	0.92
	Wheat	$y = (1.58 - x)^{-0.16}$	0.83
Red Edge NDVI	Maize	$y = -2.08x * (0.93x - 1)^{-1}$	0.94
	Potato	$y = (1.32 - x)^{-5.11}$	0.73
	Soybean	$y = -2.24x * (0.90x - 1)^{-1}$	0.94
	Wheat	$y = (0.63 + x)^{6.27}$	0.84
CI_{green}	Maize	$y = 0.60x - 0.39$	0.92
	Potato	$y = 0.44x^{1.30}$	0.85
	Soybean	$y = 0.45x - 0.18$	0.89
	Wheat	$y = 0.57x$	0.83
$CI_{red\ edge}$	Maize	$y = 0.86x$	0.94
	Potato	$y = 1.34x^{1.04}$	0.82
	Soybean	$y = 0.93x$	0.92
	Wheat	$y = x^{1.16}$	0.85
MTCI	Maize	$y = 0.85x - 1.50$	0.92
	Potato	$y = 2.27x - 2.57$	0.58
	Soybean	$y = x - 1.28$	0.90
	Wheat	$y = 1.72x - 2.67$	0.86
EVI2	Maize	$y = 9.65x^2$	0.82
	Potato	$y = (1.55 - x)^{-3.31}$	0.40
	Soybean	$y = 7.02x^2$	0.73
	Wheat	$y = (x + 0.58)^{5.42}$	0.67
Green WDRVI α=0.1	Maize	$y = 7.90x - 1.28$	0.93
	Potato	$y = (1.37 - x)^{-4.61}$	0.65
	Soybean	$y = 0.97x - 6.01$	0.91
	Wheat	$y = 7.89x^2$	0.84

Red-edge NDVI, EVI2) saturates at high green LAI (Figure 5.2A). The saturation reduces the sensitivity of the VIs to moderate to high green LAI values. It can be seen clearly in Figure 5.3 where NE is plotted versus green LAI. NEΔgreen LAI values were the highest for green NDVI as green LAI was above 2 m^2 m^{-2} for potato, maize, and soybean (Figure 5.3A, C, D). For wheat (Figure 5.3B), the green NDVI shows less sensitivity than MTCI and CI_{green} for green LAI above 3 m^2 m^{-2} and the REIP has the highest sensitivity to green LAI between 2.5 and 4 m^2 m^{-2}. Ratio VIs, such as CI_{green},

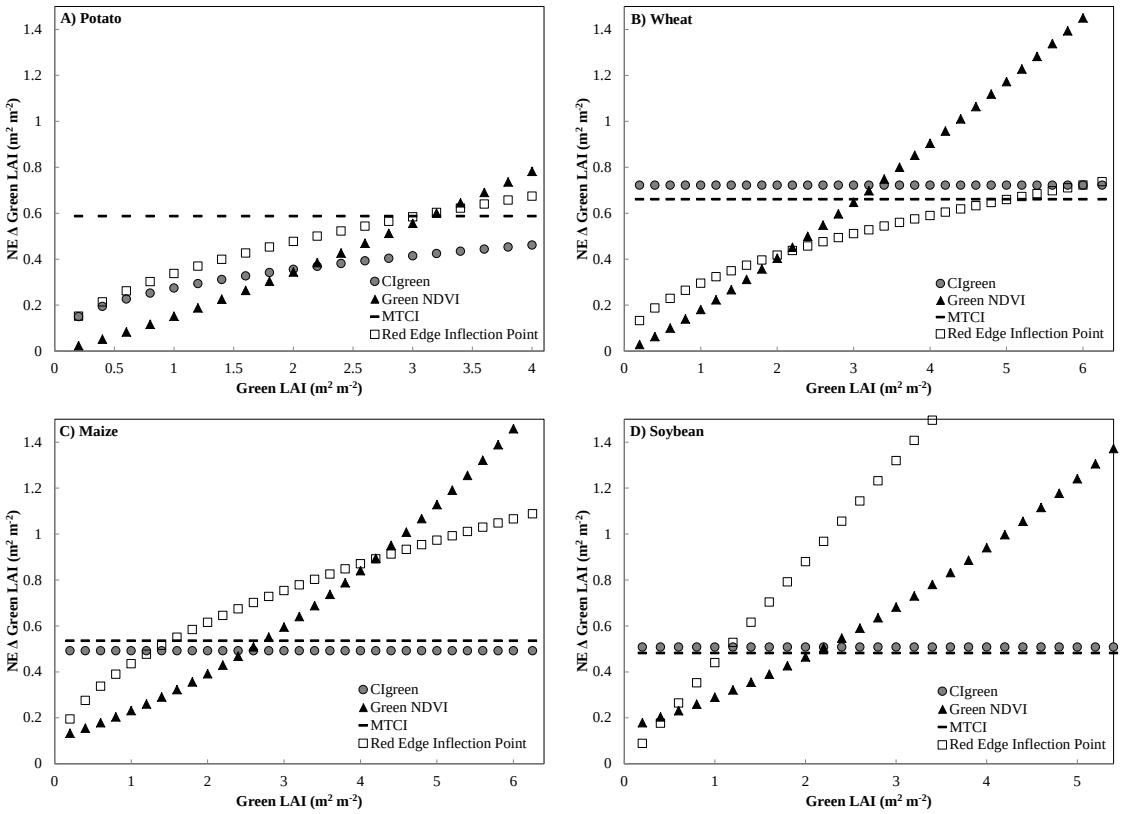

Figure 5.3: Noise Equivalent of green LAI estimation for four VIs: (a) potato, (b) wheat, (c) maize, and (d) soybean during the green-up stage only.

$CI_{red\text{-}edge}$, and SR were less sensitive at low green LAI compared to normalized difference VIs, but they were more sensitive to a higher values of green LAI (with lower NEΔgreen LAI) when green LAI exceeded 2-3 m^2 m^{-2} (Figure 5.3). MTCI remained sensitive to green LAI throughout the entire dynamic range (Figure 5.3). REIP was sensitive throughout the entire dynamic range of green LAI for potato and wheat (Figure 5.3A, B); however it was much less sensitive to maize and soybean green LAI (Figure 5.3C, D). This result is likely due to differences in sample collection with many more samples collected for maize and soybean (especially samples with high green LAI) than for potato and wheat.

While green LAI data were obtained very differently for species studied in Israel and in US (transmittance of canopy in Israel versus destructive green LAI measurements in US), as well as in very different climatic conditions and very different leaf structure and canopy architecture, for most VIs the relationships were quite similar for all four species. Differences between species (Figure 5.2 and Table 5.1) can be attributed to the differences in green LAI measurements and the temporal collection of measurements. While an algorithm for green LAI estimation in all four crops was developed, we did not present it in this study since the results may be misleading due to the differences in green LAI measurements and data collection. The algorithm is influenced predominantly by maize and soybean due to a sample size bias from the larger number of samples collected for these two crops. A more in-depth study using the same methodology of green LAI determination for all four species is needed to develop a unified algorithm that does not require re-parameterization for different species.

5.2.3 Hysteresis of VIs vs. green LAI relationships

Reflectance and green LAI data for maize and soybean were obtained for the whole season including both the green-up and reproductive stages. Figure 5.4 shows the relationships of VI vs. green LAI for maize and soybean during the whole growing season. It was found that in both maize and soybean, determination coefficient values, R^2, for the relationship REIP and MTCI vs. green LAI (Figure 5.4E-H) were lower than those for ratio VIs and normalized difference VIs, such as $CI_{red\ edge}$ (Figure 5.4A-B), and red edge NDVI (Figure 5.4C-D). With the same green LAI, REIP and MTCI were much lower in the reproductive stage than in green-up stage. It was especially pronounced when green LAI was below 3 $m^2\ m^{-2}$. To the best of our knowledge, the relationship of VI vs. green LAI in different growth stages of crops was not previously studied in detail and we tried to understand and explain the reasons behind the hysteresis of these relationships. At least two factors contribute to the behavior of relationships between VIs and green LAI.

5.2.4 Factor 1: Hysteresis of Chl content vs. green LAI relationship

The hysteresis of the total Chl content vs. green LAI relationship is caused by differences in the greenness/Chl content of the leaves, *with the same green LAI* during both the green up and reproductive stages. The metric used for determining green LAI by the conventional destructive technique is subjective. If leaves appear green, their areas are included in the green LAI determination regardless of their actual Chl content. A schematic representation of this factor is illustrated in Figure 5.5A. According to previous

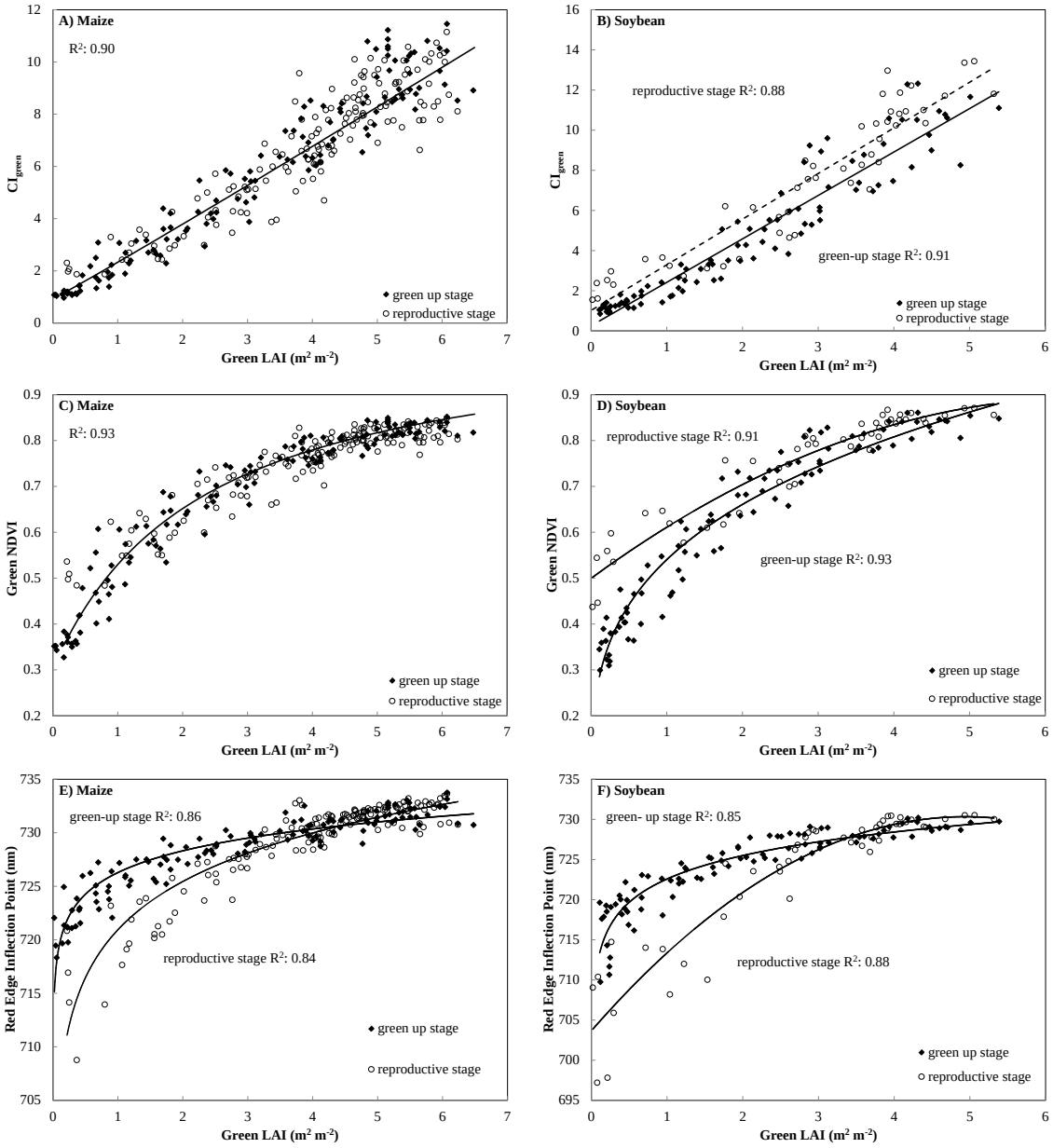

Figure 5.4: Vegetation indices plotted versus green LAI in maize (left column) and soybean (right column) with the best-fit functions for green up and reproductive stages.

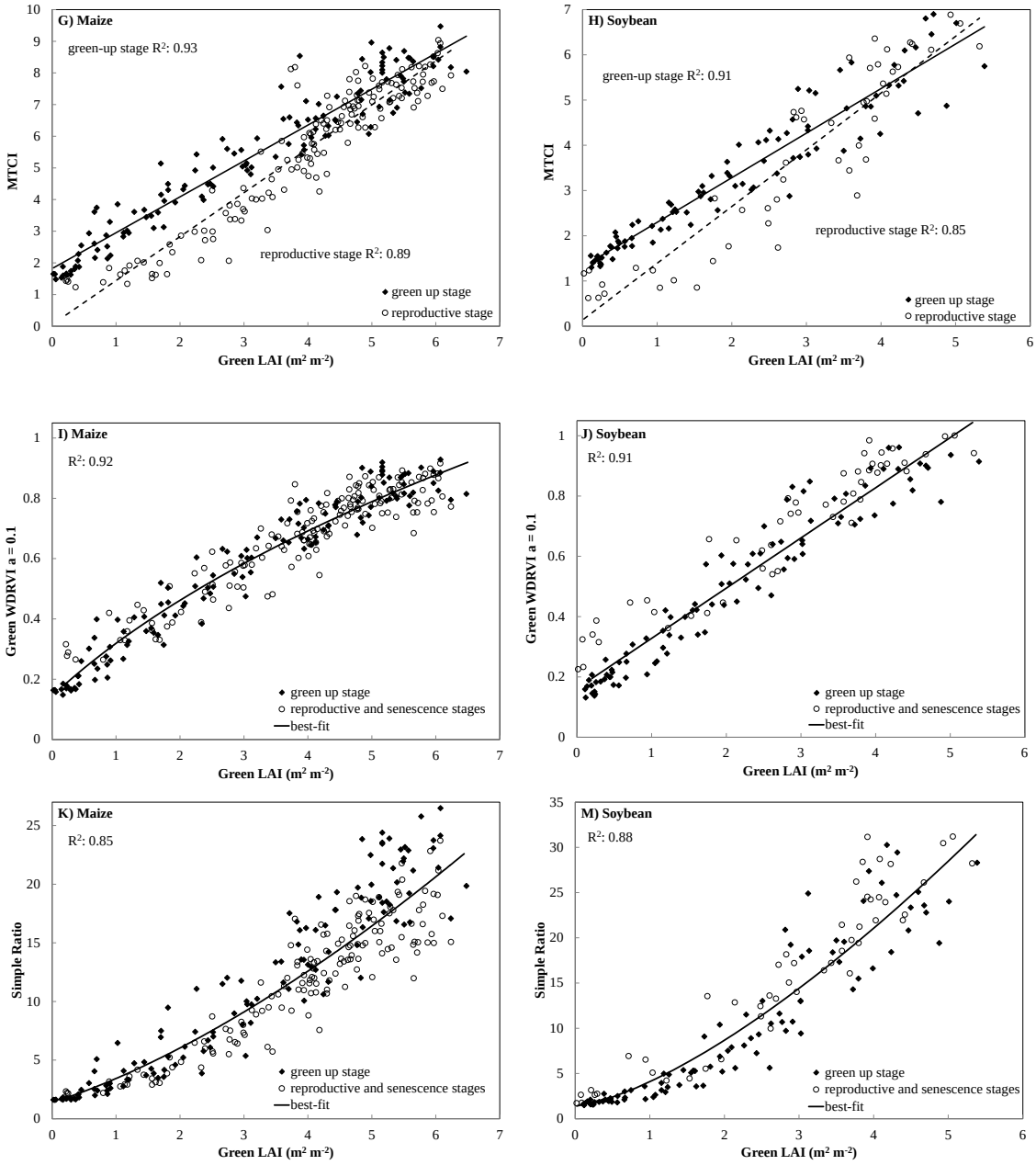

Figure 5.4 (continued): Vegetation indices plotted versus green LAI in maize (left column) and soybean (right column) with the best-fit functions for green up and reproductive stages.

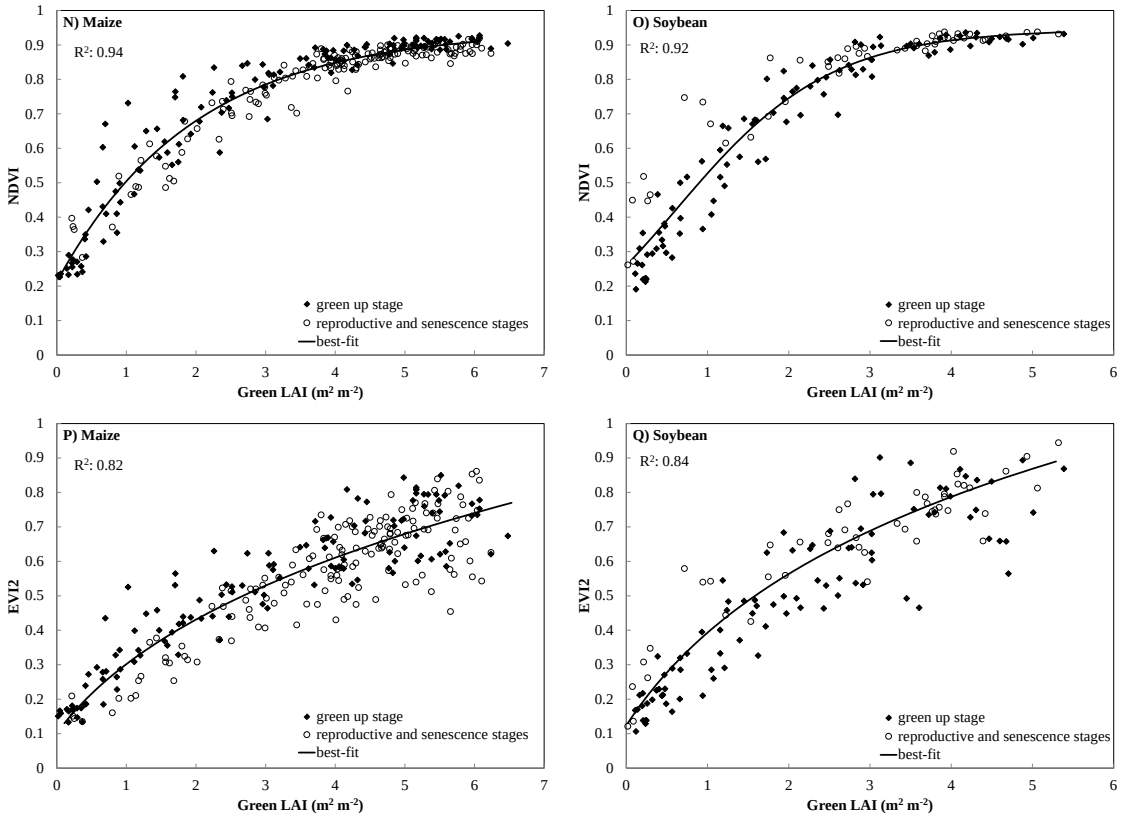

Figure 5.4 (continued): Vegetation indices plotted versus green LAI in maize (left column) and soybean (right column) with the best-fit functions for green up and reproductive stages.

studies (Ciganda et al., 2009; Peng et al., 2011), w*ith the same green LAI,* the Chl content in leaves in the green-up stage may be two fold higher than in the reproductive stage.

5.2.5 Factor 2: Hysteresis of VI vs. canopy Chl relationship

The hysteresis of the relationship VI vs. canopy total Chl content is caused by differences in the canopy architecture between the two developmental stages, green up and reproductive. *For the same total canopy Chl content*, total biomass is higher in the reproductive stage than in the green-up stage. Thus scattering in NIR region, mainly

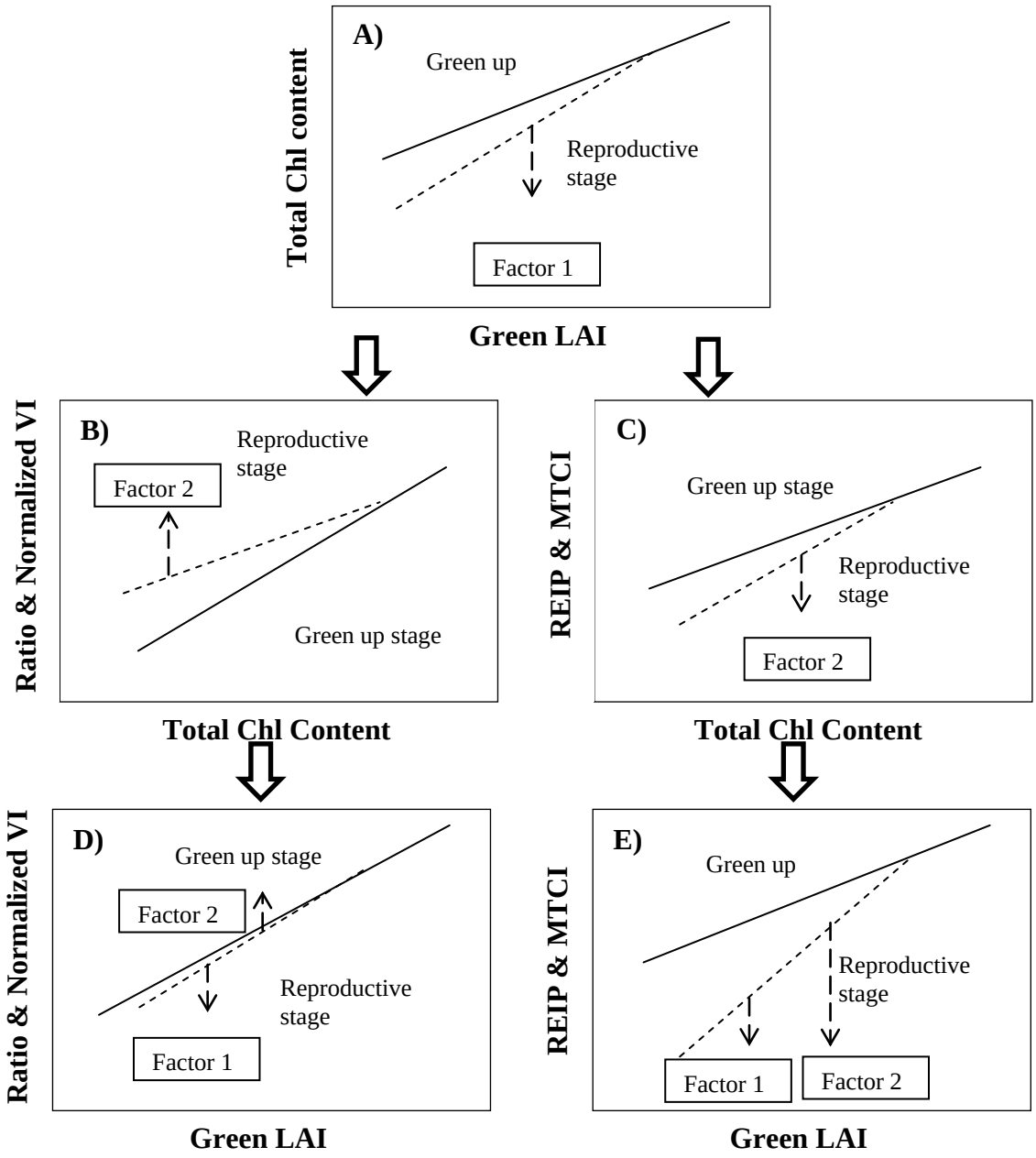

Figure 5.5: Relationship VI vs. green LAI is affected by two factors. A) Factor 1 is the hysteresis of the relationship total Chl content vs. green LAI caused by differences in the 'greenness' of the leaves between stages. Factor 2 is the direction of the hysteresis of the relationship VI vs. total Chl content caused by differences in the canopy architecture between these two stages which causes either (B) lower VI values during the green-up

stage or (C) higher VI values during the green-up stage. The result is either (D) a compensation of the two factors or (E) an exaggeration of the hysteresis.

affected by total biomass, is higher in the reproductive stage than in green up stage. While reflectance in the visible range is mainly affected by canopy absorption, for the same total Chl content it remains almost the same in green-up and reproductive stages. Therefore, this factor causes (i) higher normalized difference and ratio VIs values in the reproductive stage than in the green up stage (Figure 5.4B,D, Figure 5.5B), and (ii) smaller REIP and MTCI values in the reproductive stage than in the green-up stage (Figure 5.4E-H , Figure 5.5C). *With the same total Chl content*, the REIP is lower because higher NIR reflectance in the reproductive stage shifts the red-edge inflection point towards shorter wavelengths (Figure 5.4E-F). MTCI, as REIP, is also lower in the reproductive stage. NIR and red-edge reflectances, which both are affected by canopy scattering, are higher in the reproductive stage than in the green-up stage. The red reflectances, which are governed by Chl absorption, are quite similar in both the green-up and reproductive stages. Thus, in the two developmental stages, the numerator of MTCI, ρ_{NIR}-$\rho_{red\ edge}$, remains almost the same, while the denominator ($\rho_{red\text{-}edge}$-ρ_{red}) is higher in reproductive stage; thus, MTCI in the reproductive stage is smaller than in green up stage (Figure 5.4G-H).

5.2.6 Outcome of both Factors

The VIs, which are indicators of total Chl content, are affected by factor 1 in the same way. They are higher in green-up stage than in reproductive stage. Factor 2 affects

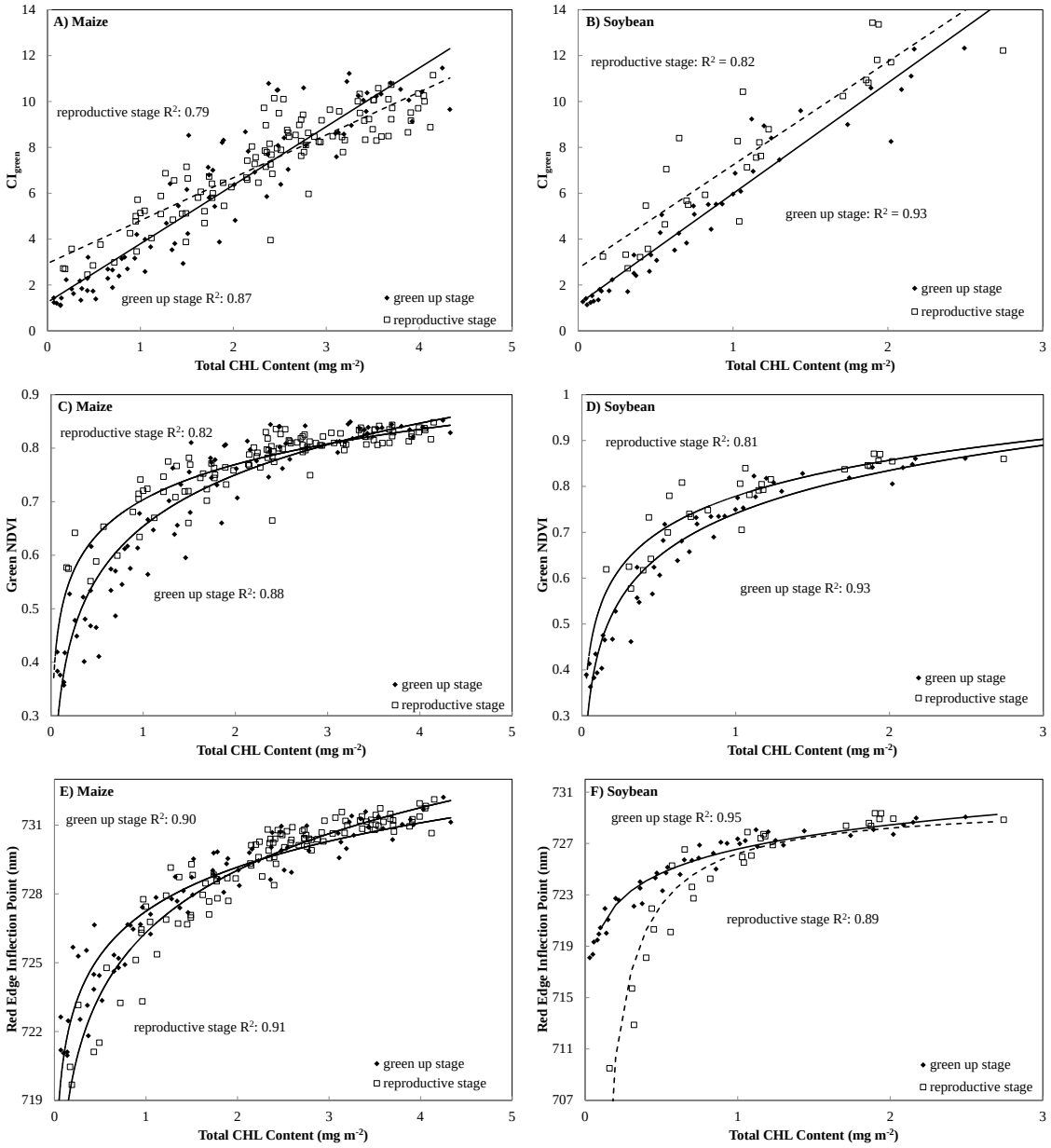

Figure 5.6: Vegetation indices plotted versus total canopy chlorophyll content in maize (left column) and soybean (right column) with the best-fit functions for green up and reproductive stages.

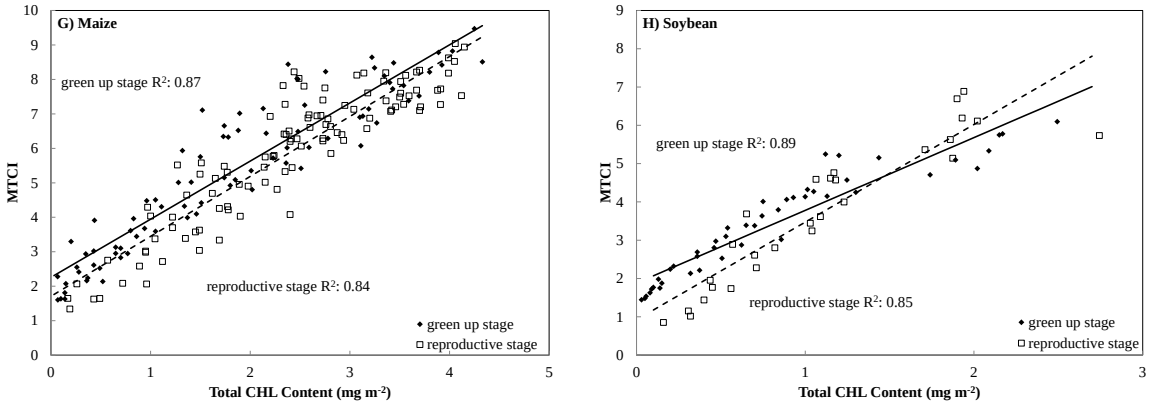

Figure 5.6 (continued): Vegetation indices plotted versus total canopy chlorophyll content in maize (left column) and soybean (right column) with the best-fit functions for green up and reproductive stages.

VIs differently - *for the same chlorophyll content / greenness*, normalized difference and ratio VIs are lower in the green- up stage than in the reproductive stage (Figure 5.6A-D, Figure 5.5B). In contrast, REIP and MTCI values in the green-up stage are higher compared to that in the reproductive stage (Figure 5.6E-H, Figure 5.5C). As a result, the effect of both factors on the VI vs. green LAI relationship leads to a *decrease* in the hysteresis between the green-up and reproductive stages for normalized difference and ratio VIs (Figure 5.5D) and an *increase* in this hysteresis for REIP and MTCI (Figure 5.5E).

5.3 Conclusions

VIs utilized in estimating green LAI for maize and soybeans were applicable and found to be quite accurate in estimating green LAI for potato and wheat. It was shown that VI responses to green LAI are similar for all four crops. The normalized difference indices were more sensitive to low green LAI, while ratio indices were more sensitive to

moderate to high green LAI. MTCI is sensitive throughout the entire range of green LAI, but generally less sensitive than the normalized difference or ratio VIs in the LAI region where they are the most sensitive to green LAI. Due to different methodologies in measuring “ground truth” green LAI, it was impossible to confirm whether established algorithms for maize and soybean can be applied with no re-parameterization to wheat and potato and vice versa.

The relationships green LAI vs. REIP and green LAI vs. MTCI are significantly different in green up and reproductive stages due to the influence of two factors that work in concert: differences in the 'greenness' of the subjective green LAI measurement and differences in the canopy structure. Thus, algorithms for green LAI estimation using REIP and MTCI are different between the green up and reproductive stages and need to be re-parameterized for each stage. For ratio and normalized difference VIs, the two factors work in opposition; thus, they may be used to accurately estimate green LAI with no re-parameterization between the two major developmental stages. For all four crops, green and red-edge chlorophyll indices appear to be the most accurate for green LAI estimation.

Chapter 6 : The use of close-range radiometers for MODIS product calibration

6.1 Objectives

The objectives of this study were to: (1) compare the reflectance and VI products collected from close-range- and satellite-based sensors collected over maize (*Zea mays*) and soybean (*Glycine max*); (2) develop linear thematic calibration algorithms for green LAI products designed for application in high spatial MODIS imagery from the close-range sensors; (3) validate the green LAI products using 8-day 250 m MODIS satellite data, and (4) develop green LAI products for additional satellite sensors that can be applied in future studies. Since the green band has a relatively coarse pixel size (500 m), this generally results in mixed pixels in typically sized agricultural fields in Nebraska for this band. Therefore only the red and NIR bands (250 m) were studied in depth in this study. Because red and NIR were the only two bands examined, the number of VIs investigated in detail were limited to those containing these bands (NDVI, WDRVI, and EVI2).

6.2 Results and discussion

6.2.1 Comparison of the close-range and satellite reflectance products

The temporal behavior of the reflectance products from all three sensors was similar for both maize and soybean (Figure 6.1). The satellite vs. close-range reflectance relationships indicated that both were similar for data collected from both the hyperspectral (OO: Figure 6.2), and multispectral sensors (SKYE: Figure 6.3). The

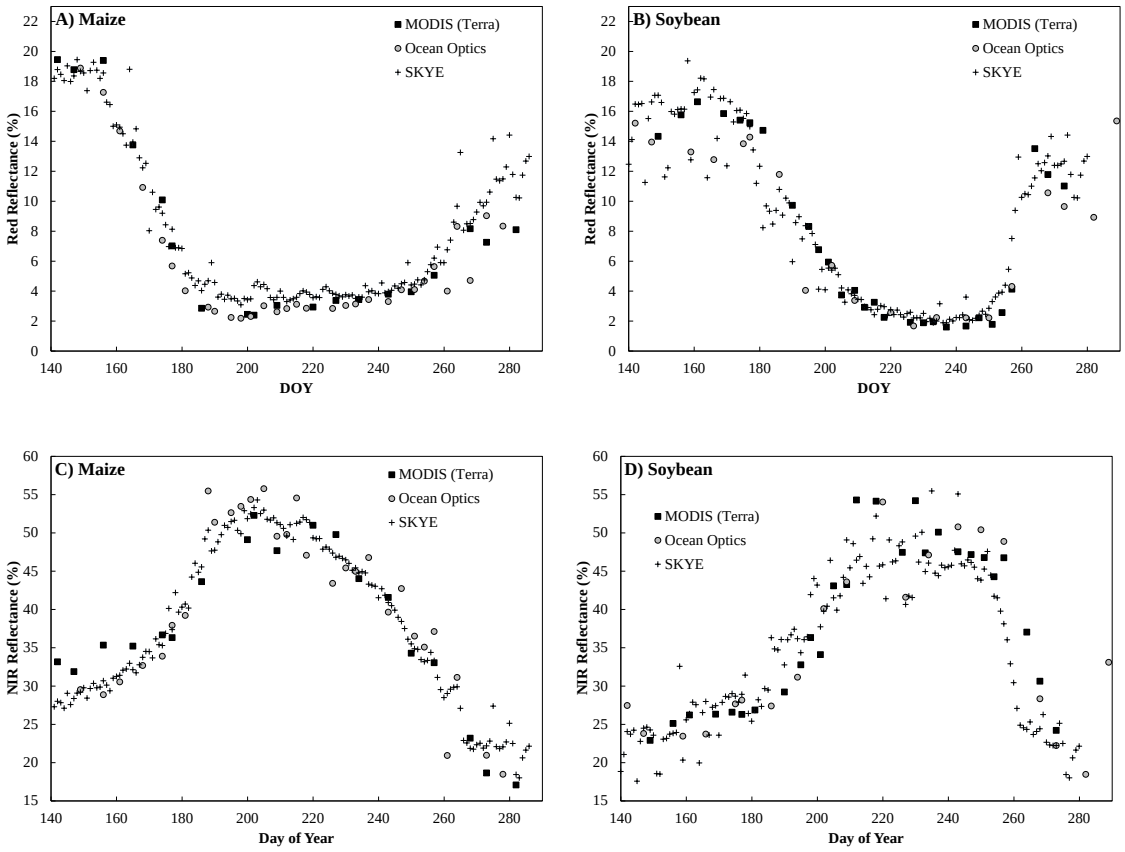

Figure 6.1: Temporal behavior of red (top row) and near infrared (NIR) (bottom row) reflectances (%) for satellite [MODIS (Terra)] and close-range [Ocean Optics, SKYE] sensors collected in 2004 over irrigated maize (left column) and rainfed soybean (right column)

MODIS reflectance was slightly higher than the close range reflectance measurements (offset > 0 in all cases). For the red reflectance, hyperspectral reflectance measurements had the lowest RMSE (< 1.5%) and CV (< 20%) (Figure 6.2A-B); however, the NIR reflectance collected using the multispectral sensors had lower RMSE (< 5%) and CV (< 15%) (Figure 6.3).

The high negative bias and high CV for the SKYE sensors in the red reflectance relationship was because of water infiltrating the downwelling sensors. This problem was

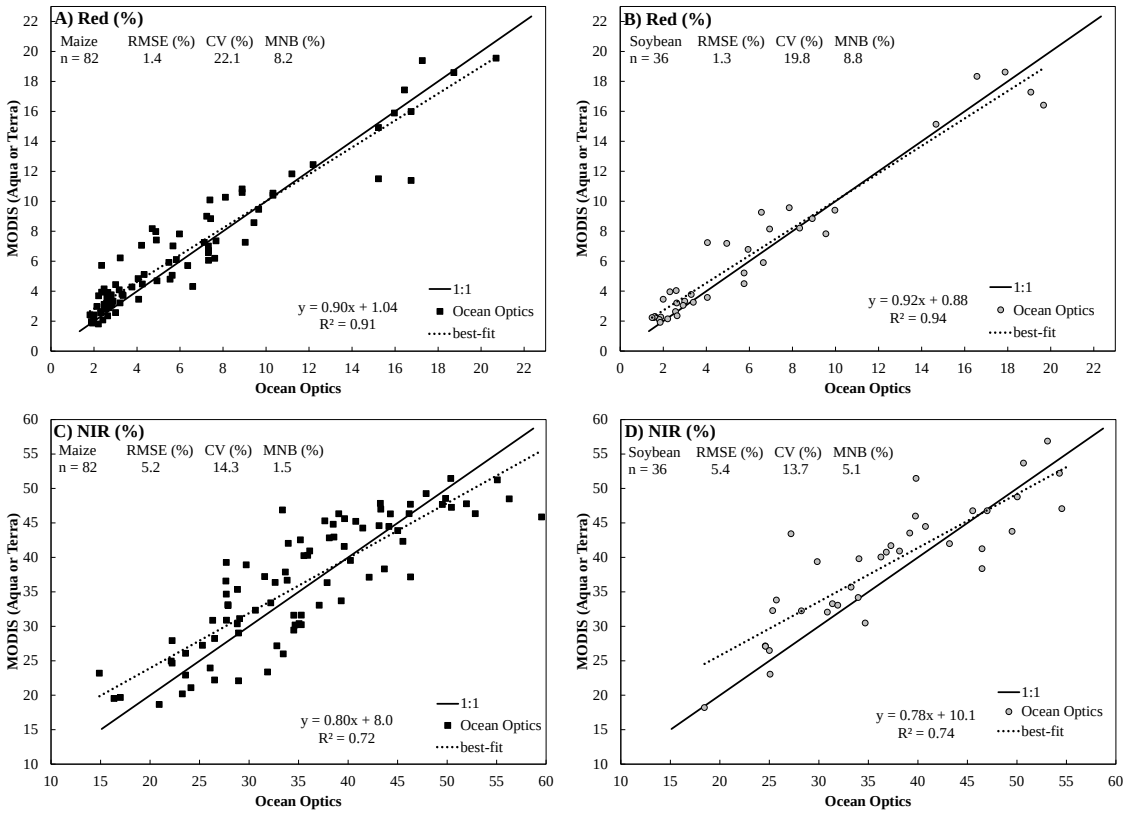

Figure 6.2: Satellite [MODIS (Aqua or Terra)] reflectance plotted versus close-range Ocean Optics reflectance collected over maize (left column) and soybean (right column) with the 1:1 line, best-fit line, and sample number. The coefficient of determination (R^2) was calculated from the best-fit line while the root mean square error (RMSE), coefficient of variation (CV) and mean normalized bias (MNB) was calculated from the 1:1 line.

identified in 2009 during the post-calibration process. During either irrigation or a rain event, water would penetrate the cosine corrector lowering the incoming light received. This increased the reflectance values during these periods since only the downwelling instruments were impacted. Over time the water evaporated and the measured reflectance returned to the 'expected' values. The presence of water did not impact the NIR

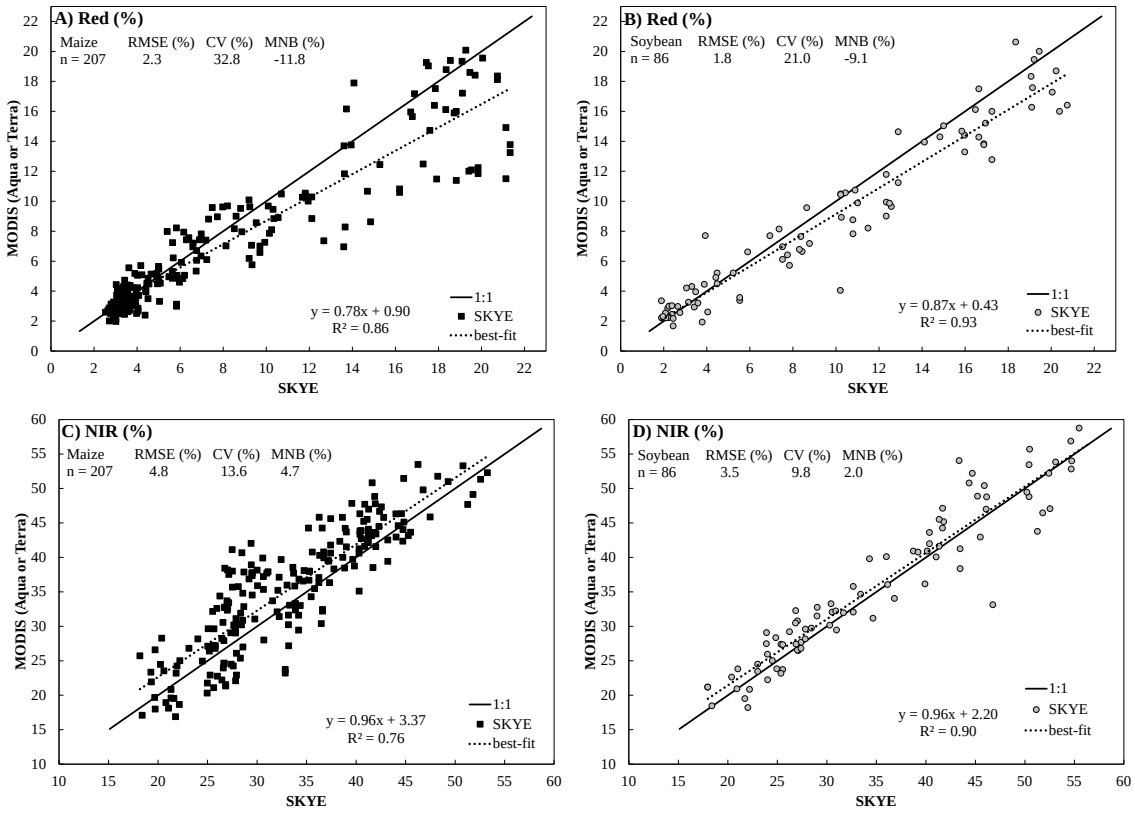

Figure 6.3: Satellite [MODIS (Aqua or Terra)] reflectance plotted versus close-range SKYE reflectance collected over maize (left column) and soybean (right column) with the 1:1 line, best-fit line, and sample number. The coefficient of determination (R^2) was calculated from the best-fit line while the root mean square error (RMSE), coefficient of variation (CV) and mean normalized bias (MNB) was calculated from the 1:1 line.

reflectance as strongly since the NIR reflectance values were much higher and the absorption by water was a small percentage of the total reflectance.

The NIR reflectance accuracy was likely higher for SKYE because each reflectance measurement is an average of approximately 1800 scans (about one scan per second collected over a 30 minute time period). The OO sensor averages only 8 scans in

less than 30 seconds. Thus, variation in the canopy architecture impacting NIR caused by wind (Kuusk, 1991) has been reduced in the SKYE measurements.

6.2.2 Comparison of the close-range and satellite vegetation index products

The three VIs investigated in this study in detail were the NDVI, WDRVI $\alpha = 0.1$, and EVI2 (see Table 2.3 for the formulations of these VIs). As was the case for the reflectance products, the temporal behavior of the VIs was similar for all sensors (Figure 6.4). The MODIS VI products were biased such that the MODIS VIs were higher than those determined using close-range multiband sensors (SKYE: Figure 6.6). This was likely due to bias in the red reflectance mentioned above. The bias was small to non-existent when MODIS VIs were compared to the close-range hyperspectral sensors (Ocean Optics: Figure 6.5). The NDVI values calculated using the Ocean Optics reflectance was the closest to those determined using the MODIS sensors (CV: Maize 7.8%, Soybean 9.4%; Figure 6.5A-B); however, this was likely due to the strong saturation of the VI to high biomass and fewer points collected over bare or near-bare soil. This caused a disproportional number of points from both the close-range and satellite sensors to be similar. Despite the bias between some of the MODIS VI products and the close-range sensors, the error was reasonable for all relationships examined (CV < 18%).

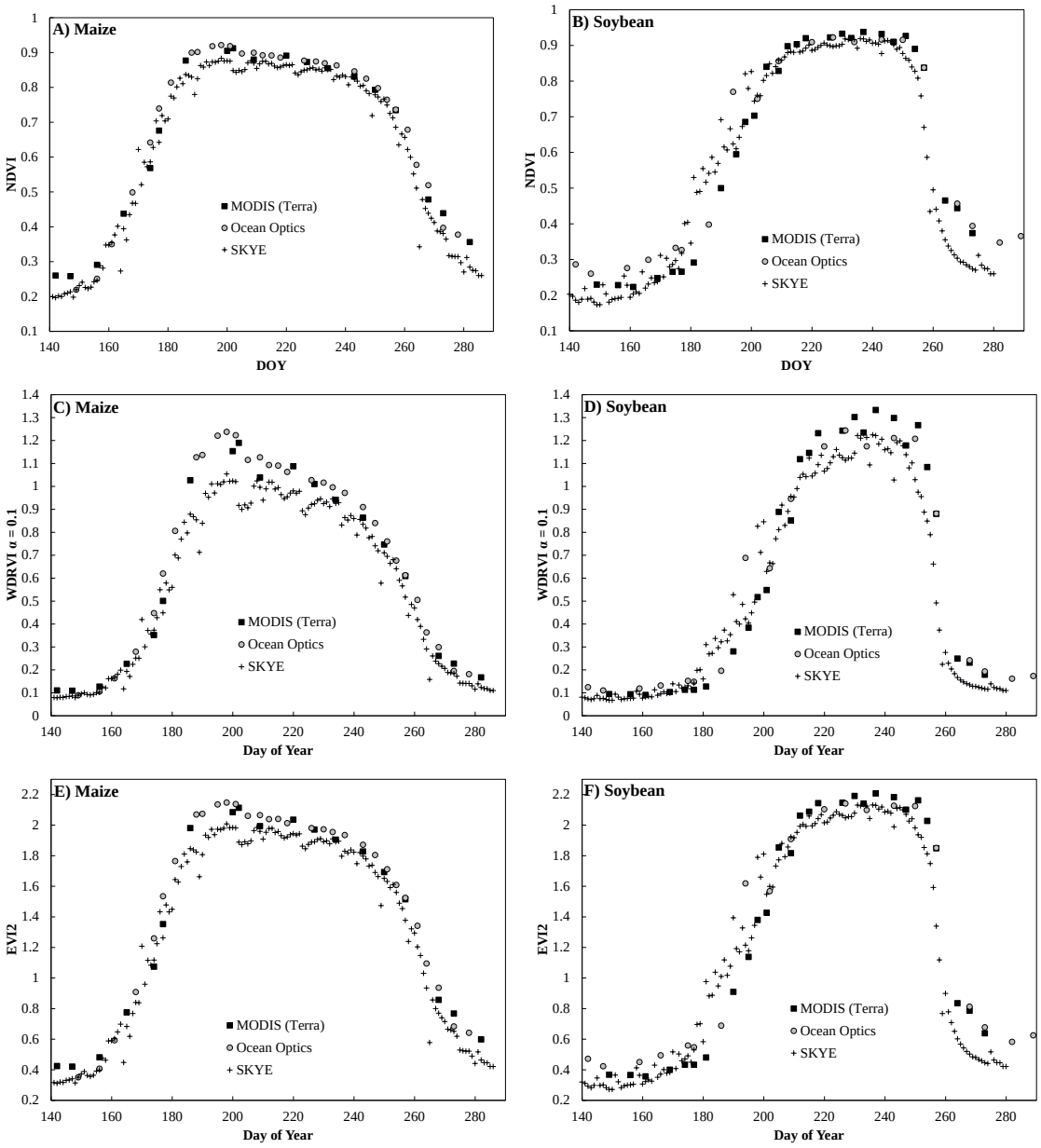

Figure 6.4: Temporal behavior of Normalized Difference Vegetation Index [NDVI] (top row), Wide Dynamic Range Vegetation Index [WDRVI α = 0.1] (middle row), and Enhanced Vegetation Index 2 [EVI2] (bottom row) for satellite [MODIS (Terra)] and close-range [Ocean Optics, SKYE] sensors collected in 2004 over irrigated maize (left column) and rainfed soybean (right column)

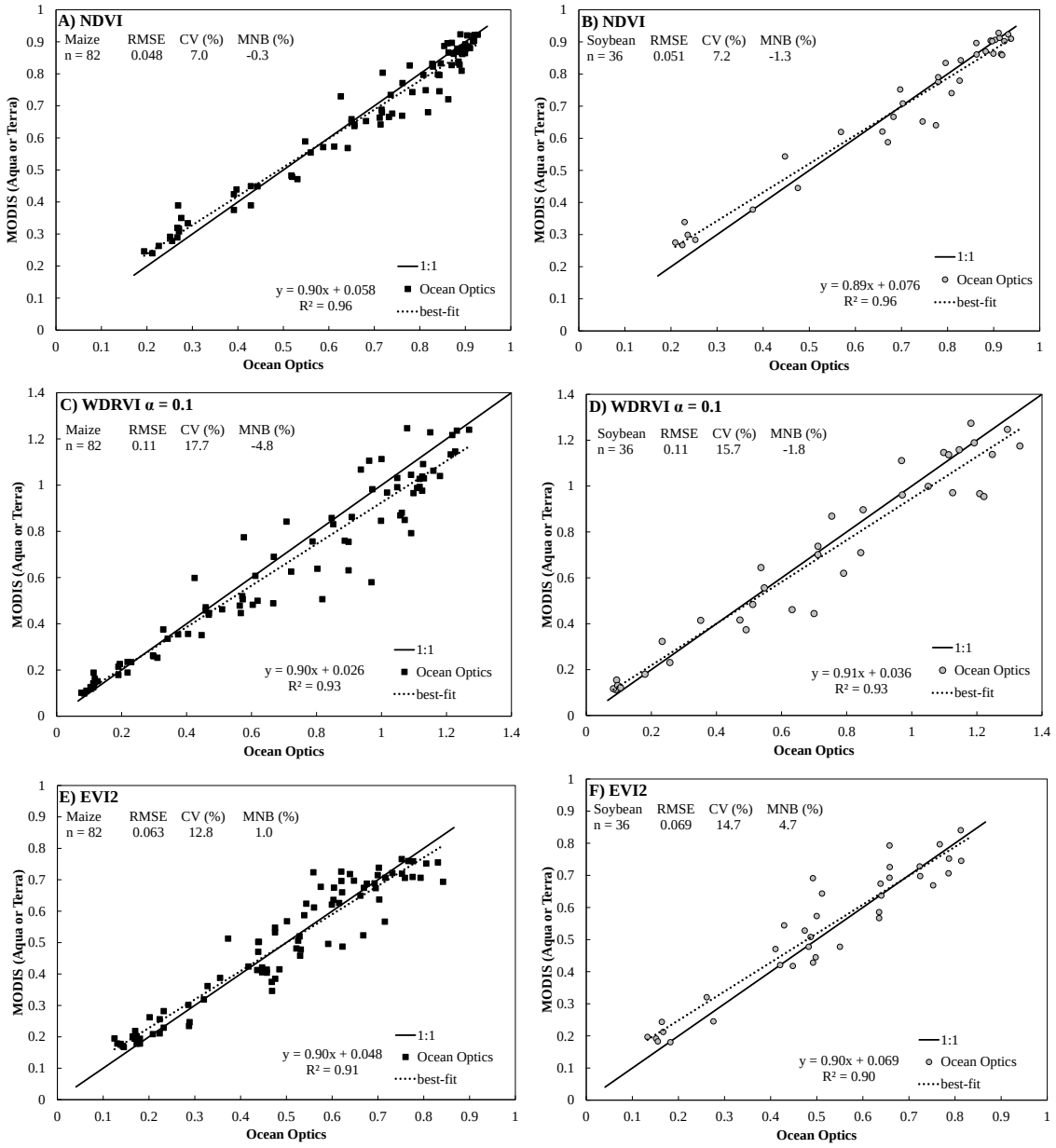

Figure 6.5: Satellite [MODIS (Aqua or Terra)] derived vegetation indices plotted versus close-range Ocean Optics derived vegetation indices collected over maize (left column) and soybean (right column) with the 1:1 line, best-fit line, and sample number. The coefficient of determination (R^2) was calculated from the best-fit line while the root mean square error (RMSE), coefficient of variation (CV) and mean normalized bias (MNB) was calculated from the 1:1 line.

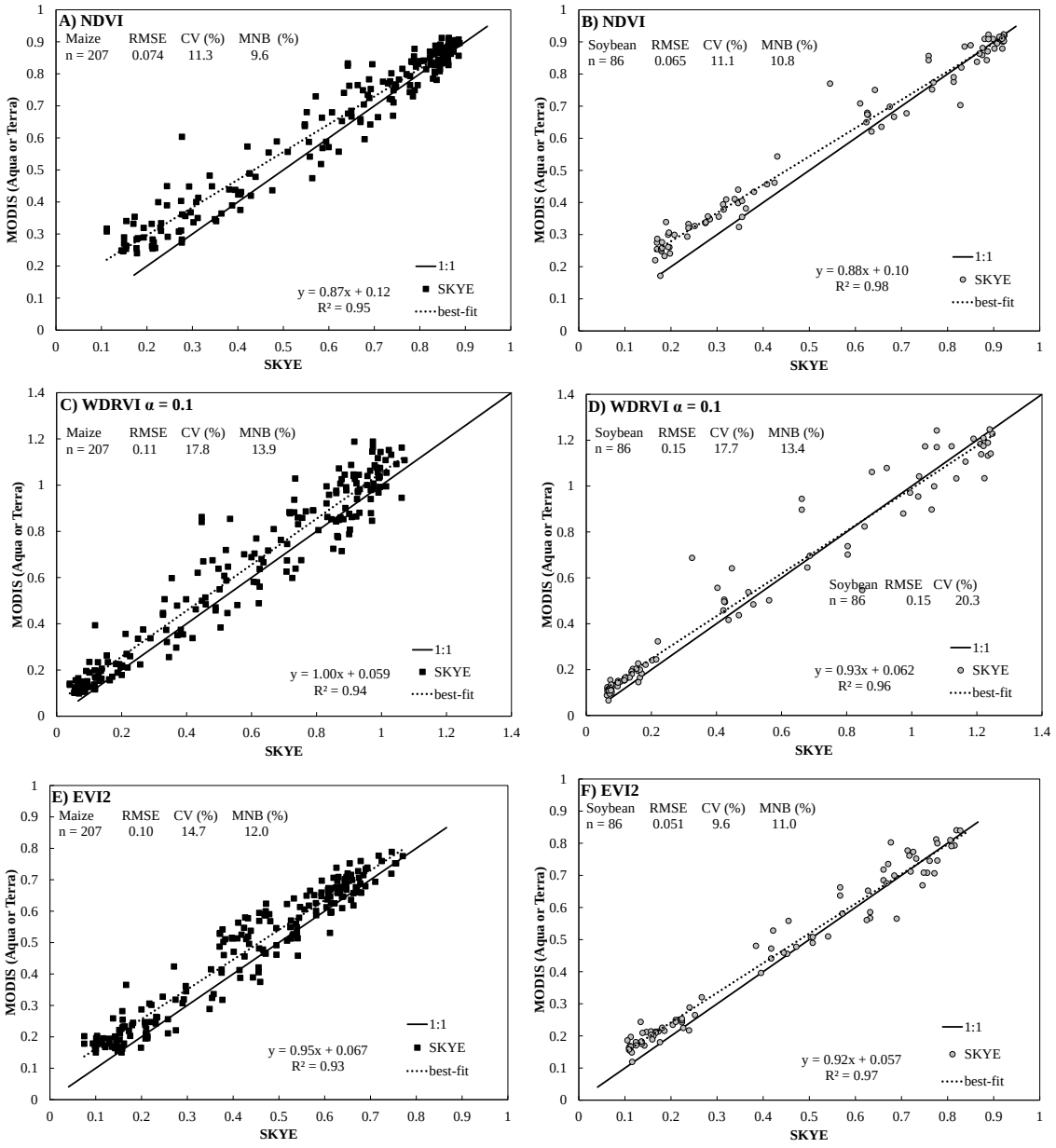

Figure 6.6: Satellite [MODIS (Aqua or Terra)] derived vegetation indices plotted versus close-range SKYE derived vegetation indices collected over maize (left column) and soybean (right column) with the 1:1 line, best-fit line, and sample number. The coefficient of determination (R^2) was calculated from the best-fit line while the root mean square error (RMSE), coefficient of variation (CV) and mean normalized bias (MNB) was calculated from the 1:1 line.

6.2.3 Close-range VI vs. green LAI relationships

Since we have already shown that non-linear models are not ideal due to issues regarding sensitivity (see section 4.2.2 Sensitivity analysis of the VI vs. green LAI relationships), the focus of this section will be on the linear models of the VIs vs. green LAI (Figure 6.7 and Figure 6.8). Rather than limit the calibrations, we will use all of the data we have available, even on dates when the MODIS imagery was not selected for the 8-day composite. For the SKYE product, due to an abundance of reflectance data, only dates where destructive sampling of green LAI was examined to avoid bias due to the interpolation process.

NDVI has an obvious non-linear behavior with green LAI (Figure 6.7A-B and Figure 6.8A-B). The green LAI vs. VI relationships for WDRVI and EVI2 were both reasonable (RMSE < 0.82 m^2 m^{-2}); however, these relationships were species-specific (ANOVA: *F*-value > 74, *p*-value < 0.001). Thus, we propose separate green LAI products for maize and soybean respectively. Despite the differences in the methodology for collecting the reflectance data (e.g. point measurements vs. measurements collected along the access road), band centers of the reflectances utilized (e.g. averaged to MODIS bands vs. fix SKYE bands), and differences in sample number in calibration of the algorithms, the green LAI products created from the two sensors examined were still quite similar. There was overlap of the first standard deviation of the green LAI products created with the different sensors (Figure 6.9).

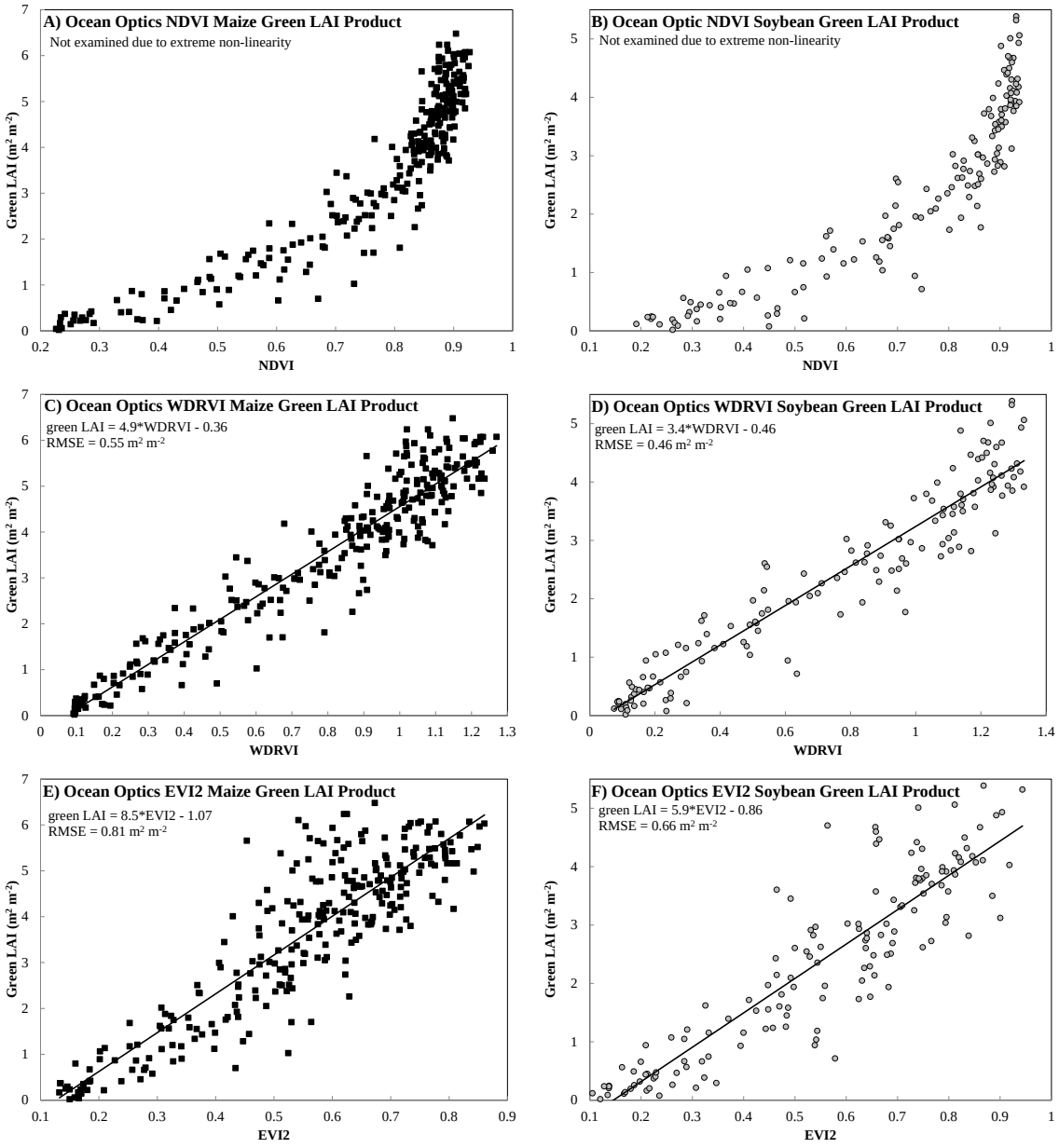

Figure 6.7: Vegetation index versus green LAI relationships developed using the close-range Ocean Optics sensor over maize (left column) and soybean (right column). The linear best-fit relationship is indicated.

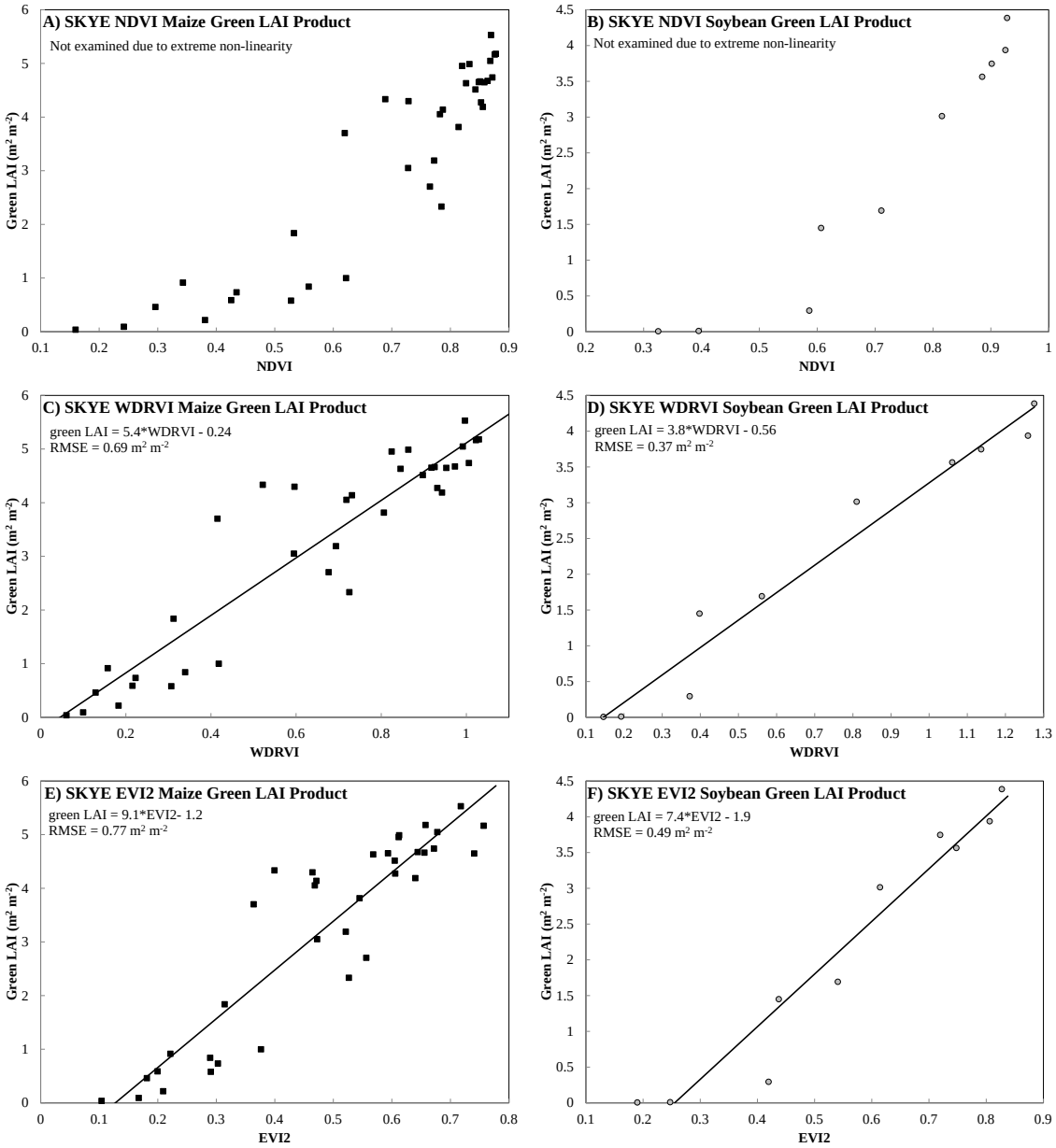

Figure 6.8: Vegetation index versus green LAI relationships developed using the close-range SKYE sensor over maize (left column) and soybean (right column). The linear best-fit relationship is indicated.

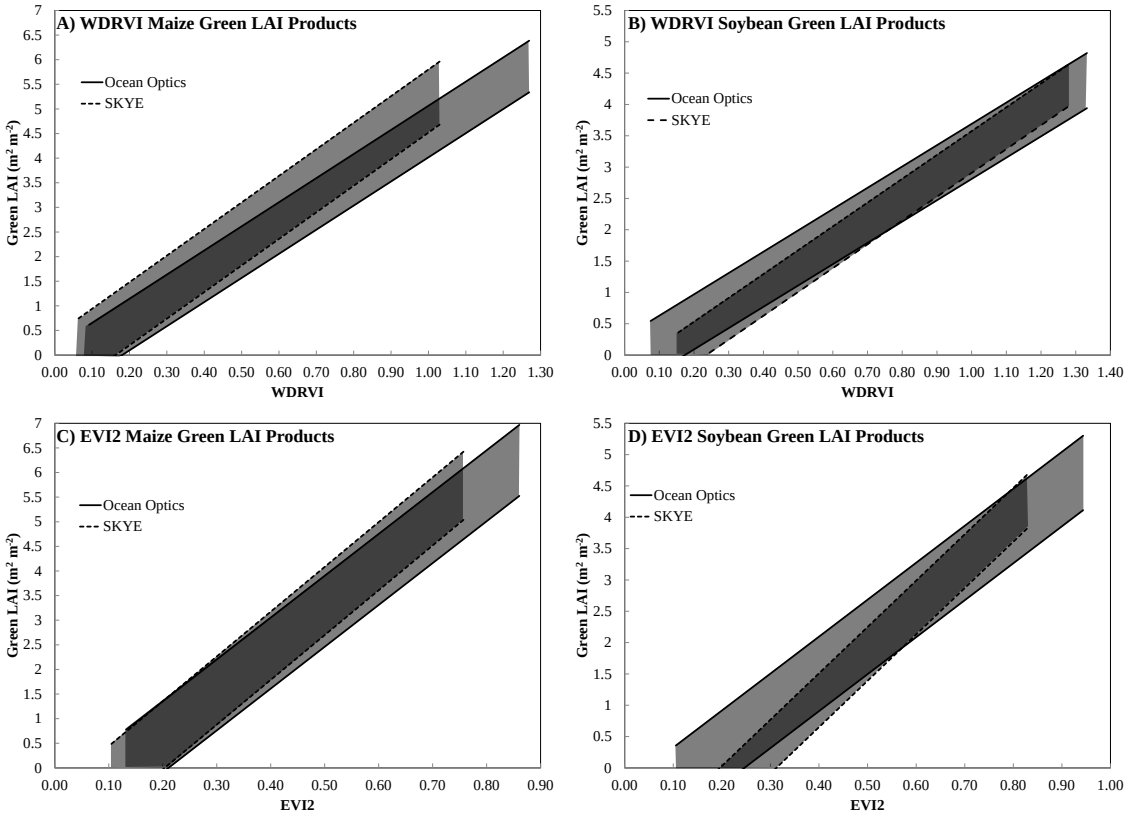

Figure 6.9: First standard deviations from the Vegetation index versus green LAI relationships developed using both close-range sensor Ocean Optics sensor over maize (left column) and soybean (right column). Darker areas indicate overlap between the products between sensors.

6.2.4 Application of the close-range relationships to satellite data

When the algorithms identified in above were applied to the MODIS VI products to estimate green LAI (Figure 6.10 and Figure 6.11), the results indicate a reasonable amount of error (CV < 34%). The results for estimating green LAI in maize using WDRVI $\alpha = 0.1$ green LAI product from the Ocean Optics (RMSE = 0.54 m^2 m^{-2}; CV = 16.8%) and SKYE (RMSE = 0.69 m^2 m^{-2}; CV = 21.5%) sensors calculated from the 250 m MODIS Terra reflectance product (MOD09Q1) were in accord with the Guindin-Garcia et al. (2012) study using only MODIS Terra data to develop and validate the green LAI vs. WDRVI $\alpha = 0.1$ relationship (RMSE = 0.59 m^2 m^{-2}; CV = 16%). The RMSE and CV was higher when the WDRVI green LAI products developed using the Ocean Optics (RMSE = 0.66 m^2 m^{-2}; CV = 21.7%) and SKYE (RMSE = 0.75 m^2 m^{-2}; CV = 24.5%) sensors were applied to the MODIS Aqua (MYD09Q1) reflectance. However, these values were still reasonable and fall within the range of error (CV: 14-52%) estimated previously when using the MODIS 1,000 m LAI product provided by the Land Processes Distributed Active Archive Center (Tian et al., 2002).

The estimation of green LAI using WDRVI $\alpha = 0.1$ had lower error compared to EVI2 primarily because the algorithms for WDRVI were more accurate at low green LAI (Figure 6.10 and Figure 6.11). The maize green LAI products algorithms were more accurate than the soybean green LAI products for both VIs. This was likely due to poor estimation of green LAI at higher values in soybean. Since the change from green-up to senescence was rapid in soybean (Figure 4.1), the spline interpolations of the destructive measurements of green LAI likely overestimated the green LAI during these periods.

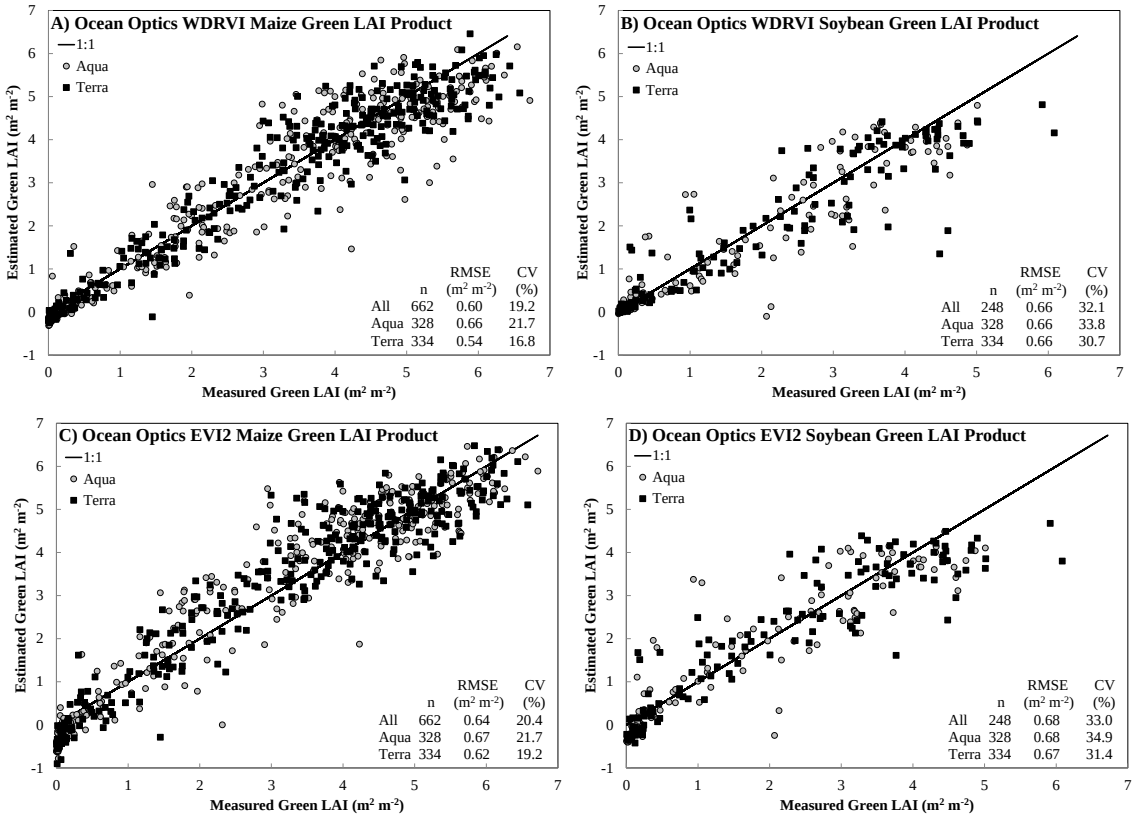

Figure 6.10: Green LAI estimated using MODIS reflectance and algorithms developed using close-range Ocean Optics sensor versus destructively measured green LAI. The 1:1 line, sample number, root mean square error (RMSE), and coefficient of variation (CV) is indicated.

Since this approach proved successful for MODIS satellite imagery, it is possible to apply this same approach to other satellite sensors. We suggest averaging the hyperspectral data to the specific sensor examined to produce satellite-specific products (Table 6.1); however, for multiband sensors this averaging is not possible and the number of green LAI products produced will be limited to the spectral ranges of the sensors used (Table 6.2). Fortunately, the green LAI products are similar between sensors (Table 6.1). For example the green LAI product using CI_{green} for both LandSat and MODIS was

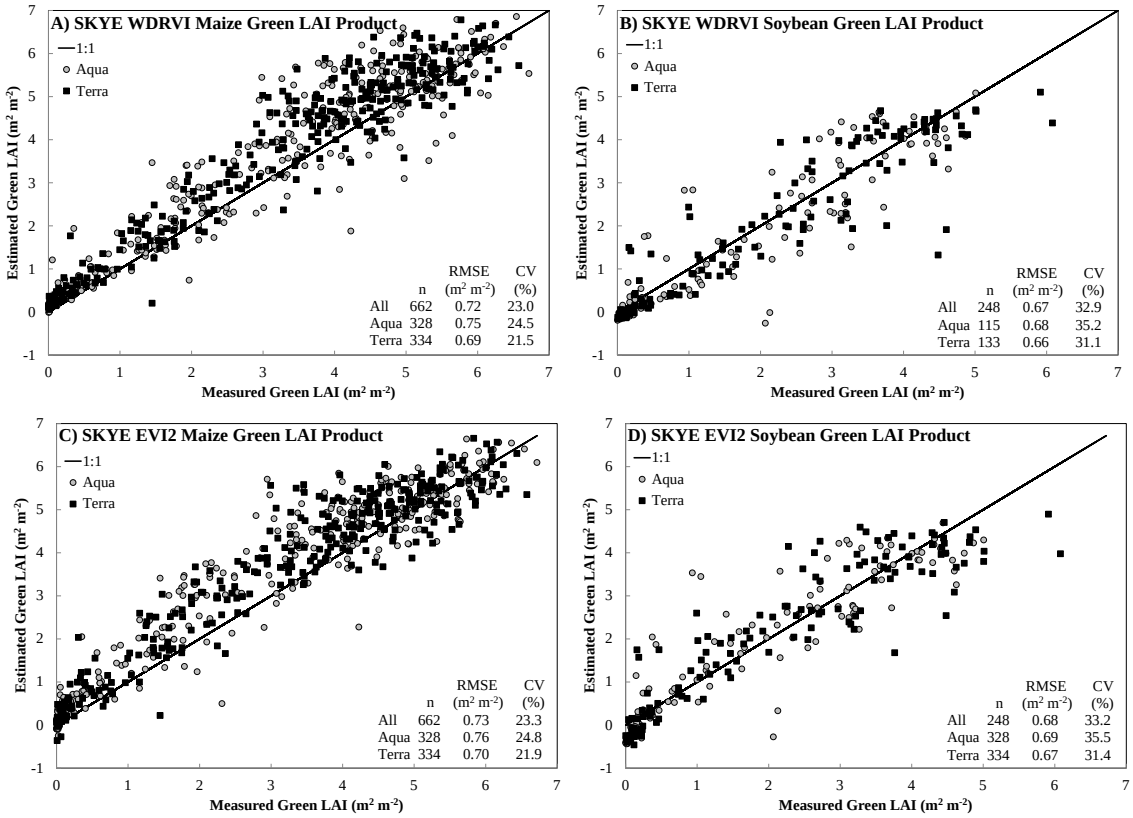

Figure 6.11: Green LAI estimated using MODIS reflectance and algorithms developed using close-range SKYE sensor versus destructively measured green LAI. The 1:1 line, sample number, root mean square error (RMSE), and coefficient of variation (CV) is indicated.

similar even though the band centers and band widths differ (LandSat: 560+/-17.5 nm; MODIS: 555+/-10 nm). However, in some cases these products were different. The products using $CI_{red\ edge}$ were similar between Sentinel-2 and Sentinel-3. However, for the sensor aboard Venμs, the slope, intercept, and RMSE were different. This was due to a shorter and wider red edge band in Venμs (702+/-12 nm) compared with Sentinel-2 (705+/-7.5 nm) and Sentinel-3 (708+/-5 nm). Since the red edge region represents a region of rapid change in reflectance (from chlorophyll absorption to canopy scattering),

Table 6.1: Green LAI products developed for application to various satellite sensors using the close-range reflectance data. Vegetation index formulations followed those presented in Table 2.3. The bands (e.g. green, red, red edge, NIR) utilized by each vegetation index were averaged from the hyperspectral data to simulate the bandwidth and spectral range of the specific satellite sensor indicated.

Applicable Satellite Sensor	Crop	Equation	RMSE (m^2 m^{-2})
MODIS	Maize	Green LAI = 4.9*WDRVI – 0.36	0.55
MODIS	Maize	Green LAI = 8.5*EVI2 – 1.07	0.81
MODIS	Maize	Green LAI = 0.58*CI_{green} – 0.09	0.57
LandSat	Maize	Green LAI = 0.48*CI_{green} + 0.14	0.57
Sentinel-2	Maize	Green LAI = 0.74*MTCI – 0.46	0.65
Sentinel-2	Maize	Green LAI = 0.65*$CI_{red\ edge}$ + 0.64	0.59
Sentinel-3	Maize	Green LAI = 0.82*$CI_{red\ edge}$ + 0.56	0.57
Venμs	Maize	Green LAI = 0.22*$CI_{red\ edge}$ + 1.07	0.72
MODIS	Soybean	Green LAI = 3.4*WDRVI – 0.15	0.46
MODIS	Soybean	Green LAI = 5.9*EVI2 – 0.86	0.66
MODIS	Soybean	Green LAI = 0.39*CI_{green} + 0.14	0.52
LandSat	Soybean	Green LAI = 0.31*CI_{green} + 0.28	0.51
Sentinel-2	Soybean	Green LAI = 0.79*MTCI – 0.38	0.65
Sentinel-2	Soybean	Green LAI = 0.61*$CI_{red\ edge}$ + 0.43	0.48
Sentinel-3	Soybean	Green LAI = 0.83*$CI_{red\ edge}$ + 0.37	0.48
Venμs	Soybean	Green LAI = 0.13*$CI_{red\ edge}$ + 0.72	0.57

Table 6.2: Green LAI products developed for application to various satellite sensors using the close-range reflectance data. Vegetation index formulations followed those presented in Table 2.3. Simulating band width and spectral range was not possible for the SKYE multi-spectral sensor.

Applicable Satellite Sensor(s)	Crop	Equation	RMSE (m^2 m^{-2})
LandSat/MODIS	Maize	Green LAI = 5.4*WDRVI – 0.24	0.69
LandSat/MODIS	Maize	Green LAI = 9.1*EVI2 – 1.16	0.77
LandSat/MODIS	Maize	Green LAI = 0.71*CI_{green} – 0.41	0.76
Sentinel-2/ Sentinel-3/ Venμs	Maize	Green LAI = 0.86*$CI_{red\ edge}$ + 0.33	0.76
LandSat/MODIS	Soybean	Green LAI = 3.8*WDRVI – 0.56	0.37
LandSat/MODIS	Soybean	Green LAI = 7.4*EVI2 – 1.88	0.49
LandSat/MODIS	Soybean	Green LAI = 0.40*CI_{green} – 0.17	0.94
Sentinel-2/ Sentinel-3/ Venμs	Soybean	Green LAI = 0.72*$CI_{red\ edge}$ + 0.13	0.83

shifts in band center and width will impact green LAI products based on the red edge band compared to similar products based on other visible/NIR spectral regions.

6.3 Conclusions

The results from this study indicated that reflectance and VI products collected from close-range sensors were related to products collected from satellites. The close relationship in reflectance and VIs allowed for the development of high spatial (250 m) MODIS green LAI products. Development was successful using models based on data taken by both multispectral and hyperspectral sensors oriented either as a point sensor or collected along a track respectively. This indicated that this method was not sensitive to different methodologies of close-range data collection.

However, the models using the red edge range of the spectrum were sensitive to the band centers and band width. This is due to the rapid change in reflectance in the red edge region. Thus, red edge range has a great potential for estimating vegetation biophysical characteristics. It may be tested further using data from near future satellite Sentinel-2 having two red edge bands. While we provided potential green LAI products applicable to various satellite sensors, future work is needed to verify these products in these sensors.

Chapter 7 : Summary and recommendations for future work

Close range remote sensing techniques have been shown to be effective for determining crop stage development and estimating green leaf area index (LAI). Both vegetation indices (VIs) and 2-dimensional spectral spaces were capable of identifying crop developmental stages.

A new approach was explored for maximizing the sensitivity of VIs to green LAI. Rather than use just one VI, we suggested using multiple VIs in different dynamic ranges. Thus, the sensitivity of the VI to the green LAI is preserved and simple linear models could be used instead of complex non-linear ones. Two versions of this combined vegetation index (CVI) were proposed. One used the commonly found bands red and NIR and the second used the red edge and NIR bands. A normalized difference index was suggested for the low-to-moderate range of green LAI and either the simple ratio or chlorophyll index was suggested for the moderate-to-high green LAI range.

The algorithms developed for estimating green LAI maize and soybeans were tested for LAI estimation in potato and wheat. The most promising VIs for developing a unified algorithm utilized either a green or red edge band. It was also noted that there is a hysteresis between green LAI and VIs based on both the differences in the greenness of leaves between the green-up and senescence stages and from canopy architecture. While this study did not examine the hysteresis in estimating other biophysical characteristics, the research does lend itself to suggest that other biophysical characteristics are likely impacted by the phenomena as well.

This study confirmed that reflectance and VI products collected from satellite sensors related closely to products developed at close-range. This allowed for the

development of green LAI products at close-range for the application to satellite imagery. The approach was verified using two different close-range sensors using different methodologies. The green LAI products developed herein but not tested in this study (e.g., Landsat, Sentinel-2 and -3) need to be thoroughly validated on data collected from these sensors. The results suggest that the approaches to estimate crop developmental stages and green LAI developed using close-range sensors presented in earlier chapters are applicable to satellite imagery.

The data sets herein have substantial potential for future work. A few recommendations include:

(1) Using the approaches herein, examine estimating additional biophysical characteristics (e.g. gross primary production, biomass, etc.)
(2) Examine spectral spaces with additional bands (e.g. blue, mid-IR, etc.)
(3) Determine if the approach using spectral spaces will work for other crops and vegetation types
(4) Examine the spectral spaces for camera-based values
(5) Determine if there is an 'ideal' waveband for an unified algorithm for all four crops
(6) Apply/validate the approach for developing green LAI products from close-range to satellite sensors to additional satellite sensors (e.g. Landsat, Wordview-2, etc.)
(7) Determine the spatial resolution necessary for using point sensors for accurate estimation of biophysical characteristics

(8) Use close-range reflectance and VI products for interpolating satellite products to produce high spatial and temporal data sets (e.g. data fusion)

(9) Quantify the difference in leaf greenness between the green-up and senescence stages

References

Abendroth, L. J., Elmore, R. W., Boyeer, M. J., & Marlay, S. K. (2011). *Corn growth and development* (p. 50).

Asrar, G. F., Kanemasu, M., ET Hatfield, J., Fuchs, M., Kanemasu, E. T., & Hatfield, J. L. (1984). Estimating absorbed photosynthetic radiation and leaf area index from spectral reflectance in wheat. *Agronomy Journal*, *76*(2), 300–306.

Ayyangar, R. S., Nagaeshwara Rao, P. P., & Rao, K. R. (1980). Crop cover and crop phenological information from red and infrared spectral responses. *Journal of the Indian Society of Photo-Interpretation and Remote Sensing*, *8*(1), 23–29.

Baghzouz, M., Devitt, D. a., Fenstermaker, L. F., & Young, M. H. (2010). Monitoring Vegetation Phenological Cycles in Two Different Semi-Arid Environmental Settings Using a Ground-Based NDVI System: A Potential Approach to Improve Satellite Data Interpretation. *Remote Sensing*, *2*(4), 990–1013.

Baret, F., & Guyot, G. (1991). Potentials and limits of vegetation indices for LAI and APAR assessment. *Remote Sensing of Environment*, *35*(2-3), 161–173.

Betancourt, J. L., Schwartz, M. D., Breshears, D. D., Cayan, D. R., Dettinger, M. D., Inouye, D. W., Post, E., & Reed, B. C. (2005). Implementing a U.S. National Phenology Network. *Eos, Transactions American Geophysical Union*, *86*(51), 539.

Bobée, C., Ottlé, C., Maignan, F., De Noblet-Ducoudré, N., Maugis, P., Lézine, a.-M., & Ndiaye, M. (2012). Analysis of vegetation seasonality in Sahelian environments using MODIS LAI, in association with land cover and rainfall. *Journal of Arid Environments*, *84*, 38–50.

Brantley, S. T., Zinnert, J. C., & Young, D. R. (2011). Application of hyperspectral vegetation indices to detect variations in high leaf area index temperate shrub thicket canopies. *Remote Sensing of Environment*, *115*(2), 514–523.

Broge, N. H., & Leblanc, E. (2001). Comparing prediction power and stability of broadband and hyperspectral vegetation indices for estimation of green leaf area index and canopy chlorophyll density. *Remote Sensing of Environment*, *76*(2000), 156–172.

Buermann, W., Dong, J., Zeng, X., Myneni, R. B., & Dickinson, R. E. (2001). Evaluation of the Utility of Satellite-Based Vegetation Leaf Area Index Data for Climate Simulations. *Journal of Climate*, *14*(17), 3536–3550.

Bulcock, H. H., & Jewitt, G. P. W. (2010). Spatial mapping of leaf area index using hyperspectral remote sensing for hydrological applications with a particular focus on canopy interception. *Hydrology and Earth System Sciences, 14*(2), 383–392.

Buschmann, C., & Nagel, E. (1993). In vivo spectroscopy and internal optics of leaves as basis for remote sensing of vegetation. *International Journal of Remote Sensing, 14*(4), 711–722.

Casa, R., Varella, H., Buis, S., Guérif, M., De Solan, B., & Baret, F. (2012). Forcing a wheat crop model with LAI data to access agronomic variables: Evaluation of the impact of model and LAI uncertainties and comparison with an empirical approach. *European Journal of Agronomy*, *37*(1), 1–10.

Ciganda, V., Gitelson, A. A., & Schepers, J. (2008). Vertical Profile and Temporal Variation of Chlorophyll in Maize Canopy: Quantitative "Crop Vigor" Indicator by Means of Reflectance-Based Techniques. *Agronomy Journal*, *100*(5), 1409.

Ciganda, V., Gitelson, A. A., & Schepers, J. (2009). Non-destructive determination of maize leaf and canopy chlorophyll content. *Journal of Plant Physiology*, *166*(2), 157–67.

Claverie, M., Demarez, V., Duchemin, B., Hagolle, O., Ducrot, D., Marais-Sicre, C., Dejoux, J.-F., Huc, M., Keravec, P., Béziat, P., Fieuzal, R., Ceschia, E., & Dedieu, G. (2012). Maize and sunflower biomass estimation in southwest France using high spatial and temporal resolution remote sensing data. *Remote Sensing of Environment*.

Clevers, J. G. P. ., De Jong, S. M., Epema, G. F., Addink, E. A., Van der Meer, F., Bakker, W. H., & Skidmore, A. K. (2000). MERIS and the red-edge index. *Second EARSeL Workshop on Imaging Spectroscopy, 2001*.

Cohen, Y., Alchanatis, V., Zusman, Y., Dar, Z., Bonfil, D. J., Karnieli, A., Zilberman, A., Moulin, A., Ostrovsky, V., Levi, A., Brikman, R., & Shenker, M. (2010). Leaf nitrogen estimation in potato based on spectral data and on simulated bands of the VENμS satellite. *Precision Agriculture*, *11*(5), 520–537.

Crist, E. P., & Cicone, R. C. (1984a). Application of the Tasseled Cap Concept to Simulated Thematic Mapper Data. *Photogrammetric Engineering and Remote Sensing*, *50*(3), 343–352.

Crist, E. P., & Cicone, R. C. (1984b). A Physically-Based Transformation of Thematic Mapper Data---The TM Tasseled Cap. *IEEE Transactions on Geoscience and Remote Sensing*, *GE-22*(3), 256–263.

Crist, E. P., & Kauth, R. J. (1986). The Tasseled Cap De-Mystified. *Photogrammetric Engineering and Remote Sensing*, *52*(1), 81–86.

Curran, P. J., & Milton, E. J. (1983). The relationships between the chlorophyll concentration, LAI and reflectance of a simple vegetation canopy. *International Journal of Remote Sensing*, *4*(2), 247–255.

Curran, P. J., & Steven, M. D. (1983). Multispectral Remote Sensing for the Estimation of Green Leaf Area Index [and Discussion]. *Philosophical Transactions of the Royal Society A: Mathematical, Physical and Engineering Sciences*, *309*(1508), 257–270.

Dash, J., & Curran, P. J. (2004). The MERIS terrestrial chlorophyll index. *International Journal of Remote Sensing*, *25*(23), 5403–5413.

Dash, J., & Curran, P. J. (2007). Evaluation of the MERIS terrestrial chlorophyll index (MTCI). *Advances in Space Research*, *39*(1), 100–104.

Daughtry, C. S. T., Gallo, K. P., Goward, S. N., Prince, S. D., & Kustas, W. P. (1992). Spectral estimates of absorbed radiation and phytomass production in corn and soybean canopies. *Remote Sensing of Environment*, *39*(2), 141–152.

Daughtry, C. S. T., Walthall, C. L., Kim, M. S., Brown de Colstoun, E., & McMurtrey III, J. E. (2000). Estimating Corn Leaf Chlorophyll Concentration from Leaf and Canopy Reflectance. *Remote Sensing of Environment*, *74*(2), 229–239.

De Wit, C. T. (1965). *Agricultural Research Reports no. 663: Photosynthesis of leaf canopies* (p. 57). Wageningen.

Deering, D. W., & Eck, T. F. (1987). Atmospheric optical depth effects on angular anisotropy of plant canopy reflectance. *International Journal of Remote Sensing*, *8*(6), 893–916.

Doraiswamy, P. C., Moulin, S., Cook, P. W., & Stern, A. (2003). Crop Yield Assessment from Remote Sensing. *Photogrammetric Engineering and Remote Sensing*, *69*(6), 665–674.

Ehleringer, J., & Forseth, I. (1980). Solar tracking by plants. *Science (New York, N.Y.)*, *210*(4474), 1094–8.

Eitel, J. U. H., Long, D. S., Gessler, P. E., & Hunt, E. R. (2008). Combined Spectral Index to Improve Ground-Based Estimates of Nitrogen Status in Dryland Wheat. *Agronomy Journal*, *100*(6), 1694.

Eitel, J. U. H., Long, D. S., Gessler, P. E., Hunt, E. R., & Brown, D. J. (2009). Sensitivity of Ground-Based Remote Sensing Estimates of Wheat Chlorophyll Content to Variation in Soil Reflectance. *Soil Science Society of America Journal*, *73*(5), 1715.

Eklundh, L., Jin, H., Schubert, P., Guzinski, R., & Heliasz, M. (2011). An optical sensor network for vegetation phenology monitoring and satellite data calibration. *Sensors (Basel, Switzerland)*, *11*(8), 7678–7709.

Elvidge, C. D., & Chen, Z. (1995). Comparison of broad-band and narrow-band red and near-infrared vegetation indices. *Remote Sensing of Environment*, *54*(1), 38–48.

Fang, H., Liang, S., & Hoogenboom, G. (2011). Integration of MODIS LAI and vegetation index products with the CSM-CERES-Maize model for corn yield estimation. *International Journal of Remote Sensing*, *32*(4), 1039–1065.

Foerster, S., Kaden, K., Foerster, M., & Itzerott, S. (2012). Crop type mapping using spectral–temporal profiles and phenological information. *Computers and Electronics in Agriculture*, *89*, 30–40.

Gamon, J. A., Rahman, a, Dungan, J., Schildhauer, M., & Huemmrich, K. F. (2006). Spectral Network (SpecNet)—What is it and why do we need it? *Remote Sensing of Environment*, *103*(3), 227–235.

Gao, X., Huete, A. R., Nif, W., & Miura, T. (2000). Optical–Biophysical Relationships of Vegetation Spectra without Background Contamination. *Remote Sensing of Environment*, *74*(3), 609–620.

Garbulsky, M. F., Peñuelas, J., Gamon, J. A., Inoue, Y., & Filella, I. (2011). The photochemical reflectance index (PRI) and the remote sensing of leaf, canopy and ecosystem radiation use efficiencies: A review and meta-analysis. *Remote Sensing of Environment*, *115*(2), 281–297.

Gitelson, A. A. (2003). Novel technique for remote estimation of CO 2 flux in maize. *Geophysical Research Letters*, *30*(9), 1486.

Gitelson, A. A. (2004). Wide Dynamic Range Vegetation Index for remote quantification of biophysical characteristics of vegetation. *Journal of Plant Physiology*, *161*(2), 165–73.

Gitelson, A. A. (2011). Remote sensing estimation of crop biophysical characteristics at various scales. In P. S. Thenkabail, J. G. Lyon, & A. R. Huete (Eds.), *Hyperspectral Remote Sensing of Vegetation* (pp. 329–358).

Gitelson, A. A., Gritz, Y., & Merzlyak, M. N. (2003a). Relationships between leaf chlorophyll content and spectral reflectance and algorithms for non-destructive chlorophyll assessment in higher plant leaves. *Journal of Plant Physiology*, *160*(3), 271–82.

Gitelson, A. A., Kaufman, Y. J., & Merzlyak, M. N. (1996). Use of a green channel in remote sensing of global vegetation from EOS-MODIS. *Remote Sensing of Environment*, *58*(3), 289–298.

Gitelson, A. A., & Merzlyak, M. N. (1994). Spectral reflectance changes associated with autumn senescence of Aesculus hippocastanum L. and Acer platanoides L. leaves. Spectral features and relation to chlorophyll estimation. *Journal of Plant Physiology*, *143*, 286–286.

Gitelson, A. A., Stark, R., Grits, U., Rundquist, D., Kaufman, Y., & Derry, D. (2002). Vegetation and soil lines in visible spectral space: A concept and technique for remote estimation of vegetation fraction. *International Journal of Remote Sensing*, *23*(13), 2537–2562.

Gitelson, A. A., Viña, A., Arkebauer, T. J., Rundquist, D. C., Keydan, G. P., & Leavitt, B. (2003b). Remote estimation of leaf area index and green leaf biomass in maize canopies. *Geophysical Research Letters*, *30*(5), 1248.

Gitelson, A. A., Viña, A., Ciganda, V., Rundquist, D. C., & Arkebauer, T. J. (2005). Remote estimation of canopy chlorophyll content in crops. *Geophysical Research Letters*, *32*(8), L08403.

Gobron, N., Pinty, B., Verstraete, M., & Govaerts, Y. (1999). The MERIS Global Vegetation Index (MGVI): description and preliminary application. *International Journal of Remote Sensing*, *20*(9), 1917–1927.

Gobron, N., Pinty, B., Verstraete, M. M., & Govaerts, Y. M. (1997). A semidiscrete model for the scattering of light by vegetation. *Journal of Geophysical Research*, *102*(D8), 9431–9446.

González-sanpedro, M. C., Le Toan, T., Moreno, J., Kergoat, L., & Rubio, E. (2008). Seasonal variations of leaf area index of agricultural fields retrieved from Landsat data. *Remote Sensing of Environment*, *112*, 810–824.

Goodin, D. G., & Henebry, G. M. (1997). A Technique for Monitoring Ecological Disturbance in Tallgrass Prairie Using Seasonal NDVI Trajectories and a Discriminant Function Mixture Model. *Remote Sensing of Environment*, *61*, 270–278.

Govaerts, Y. M., Verstraete, M. M., Pinty, B., & Gobron, N. (1999). Designing optimal spectral indices: A feasibility and proof of concept study. *International Journal of Remote Sensing*, *20*(9), 1853–1873.

Guindin-Garcia, N., Gitelson, A. A., Arkebauer, T. J., Shanahan, J., & Weiss, A. (2012). An evaluation of MODIS 8- and 16-day composite products for monitoring maize green leaf area index. *Agricultural and Forest Meteorology*, *161*, 15–25.

Guyot, G., & Baret, F. (1988). Utilisation de la haute resolution spectrale pour suivre l'etat des couverts vegetaux. In T. D. Guyenne & J. J. Hunt (Eds.), *4th International Colloquium "Spectral Signatures of Objects in Remote Sensing"* (Vol. 287, pp. 279–286).

Haboudane, D., Miller, J. R., Pattey, E., Zarco-Tejada, P. J., & Strachan, I. B. (2004). Hyperspectral vegetation indices and novel algorithms for predicting green LAI of crop canopies: Modeling and validation in the context of precision agriculture. *Remote Sensing of Environment*, *90*(3), 337–352.

Haboudane, D., Miller, J. R., Tremblay, N., Zarco-Tejada, P. J., & Dextraze, L. (2002). Integrated narrow-band vegetation indices for prediction of crop chlorophyll content for application to precision agriculture. *Remote Sensing of Environment*, *81*(2-3), 416–426.

Hansen, M., DeFries, R., Dimiceli, C., Huang, C., Sohiberg, R., Zhan, X., & Townshend, J. (1998). Red and infrared space partitioning for detecting land cover change. *IGARSS'98. Sensing and Managing the Environment. 1998 IEEE International Geoscience and Remote Sensing. Symposium Proceedings. (Cat. No.98CH36174)*, *5*, 2512–2514.

Hanway, J. J. (1963). Growth Stages of Corn (Zea mays, L.)1. *Agronomy Journal*, *55*(5), 487.

Hatfield, J. L., Gitelson, A. A., Schepers, J. S., & Walthall, C. L. (2008). Application of Spectral Remote Sensing for Agronomic Decisions. *Agronomy Journal*, *100*(Supplement_3), S–117.

Hatfield, J. L., & Prueger, J. H. (2010). Value of Using Different Vegetative Indices to Quantify Agricultural Crop Characteristics at Different Growth Stages under Varying Management Practices. *Remote Sensing*, *2*(2), 562–578.

Hatfield, J. L., Prueger, J. H., & Kustas, W. P. (2004). Remote Sensing of Dryland Crops. In S. L. Ustin (Ed.), *Manual of Remote Sensing, Volumne 4, Remote Sensing for Natural Resource Management and Environmental Monitoring* (3rd ed., pp. 531–568).

Herrmann, I., Pimstein, A., Karnieli, A., Cohen, Y., Alchanatis, V., & Bonfil, D. J. (2011). LAI assessment of wheat and potato crops by VENμS and Sentinel-2 bands. *Remote Sensing of Environment*, *115*(8), 2141–2151.

Hmimina, G., Dufrêne, E., Pontailler, J.-Y., Delpierre, N., Aubinet, M., Caquet, B., De Grandcourt, a., Burban, B., Flechard, C., Granier, a., Gross, P., Heinesch, B., Longdoz, B., Moureaux, C., Ourcival, J.-M., Rambal, S., Saint André, L., & Soudani, K. (2013). Evaluation of the potential of MODIS satellite data to predict

vegetation phenology in different biomes: An investigation using ground-based NDVI measurements. *Remote Sensing of Environment*, *132*, 145–158.

Huang, N., Niu, Z., Zhan, Y., Xu, S., Tappert, M. C., Wu, C., Huang, W., Gao, S., Hou, X., & Cai, D. (2012). Relationships between soil respiration and photosynthesis-related spectral vegetation indices in two cropland ecosystems. *Agricultural and Forest Meteorology*, *160*, 80–89.

Huete, A. R. (2012). Vegetation Indices, Remote Sensing and Forest Monitoring. *Geography Compass*, *6*(9), 513–532.

Huete, A. R., Didan, K., Miura, T., Rodriguez, E. ., Gao, X., & Ferreira, L. . (2002). Overview of the radiometric and biophysical performance of the MODIS vegetation indices. *Remote Sensing of Environment*, *83*(1-2), 195–213.

Huete, A. R., Liu, H. Q., Batchily, K., & Van Leeuwen, W. (1997). A comparison of vegetation indices over a global set of TM images for EOS-MODIS. *Remote Sensing of Environment*, *59*(3), 440–451.

Hufkens, K., Friedl, M., Sonnentag, O., Braswell, B. H., Milliman, T., & Richardson, A. D. (2012). Linking near-surface and satellite remote sensing measurements of deciduous broadleaf forest phenology. *Remote Sensing of Environment*, *117*, 307–321.

Idso, S. B., & De Wit, C. T. (1970). Light relations in plant canopies. *Applied optics*, *9*(1), 177–84.

Jiang, Z., Huete, A. R., Didan, K., & Miura, T. (2008). Remote Sensing of Environment Development of a two-band enhanced vegetation index without a blue band. *Remote Sensing of Environment*, *112*, 3833–3845.

Jordan, C. F. . (1969). Derivation of Leaf-Area Index from Quality of Light on the Forest Floor. *Ecology*, *50*(4), 663–666.

Kanemasu, E. T. (1974). Seasonal canopy reflectance patterns of wheat, sorghum, and soybean. *Remote Sensing of Environment*, *3*(1), 43–47.

Kimes, D. S. (1983). Dynamics of directional reflectance factor distributions for vegetation canopies. *Applied Optics*, *22*(9), 1364–1372.

Kohavi, R. (1995). A Study of Cross-Validation and Bootstrap for Accuracy Estimation and Model Selection. In C. S. Mellish (Ed.), *International joint conference on artificial intelligence* (pp. 1137–1143).

Kollenkark, J. C., Daughtry, C. S. T., Bauer, M. E., & Housley, T. L. (1982). Effects of Cultural Practices on Agronomic and Reflectance Characteristics of Soybean Canopies1. *Agronomy Journal*, *74*(4), 751–758.

Kuusk, A. (1991). Determination of vegetation canopy parameters from optical measurements. *Remote Sensing of Environment*, *37*(3), 207–218.

Le Maire, G., Francois, C., SOUDANI, K., BERVEILLER, D., Pontailler, J.-Y., BREDA, N., GENET, H., DAVI, H., DUFRENE, E., & LEMAIRE, G. (2008). Calibration and validation of hyperspectral indices for the estimation of broadleaved forest leaf chlorophyll content, leaf mass per area, leaf area index and leaf canopy biomass. *Remote Sensing of Environment*, *112*(10), 3846–3864.

Lichtenthaler, H. K. K. (1987). Chlorophylls and carotenoids: Pigments of photosynthetic biomembranes. (L. Packer & R. Douce, Eds.)*Methods in Enzymology*, *148*(Plant Cell Membranes), 350–382.

Liu, H. Q., & Huete, A. R. (1995). A feedback based modification of the NDVI to minimize canopy background and atmospheric noise. *IEEE Transactions on Geoscience and Remote Sensing*, *33*(2), 457–465.

Liu, J., Pattey, E., & Jégo, G. (2012). Assessment of vegetation indices for regional crop green LAI estimation from Landsat images over multiple growing seasons. *Remote Sensing of Environment*, *123*, 347–358.

Lobell, D. B., & Asner, G. P. (2002). Moisture Effects on Soil Reflectance. *Soil Science Society of America Journal*, *66*(3), 722–727.

Myneni, R. B., Hall, F. G., Sellers, P. J., & Marshak, A. L. (1995). The interpretation of spectral vegetation indexes. *IEEE Transactions on Geoscience and Remote Sensing*, *33*(2), 481–486.

Myneni, R. B., Hoffman, S., Knyazikhin, Y., Privette, J. ., Glassy, J., Tian, Y., Wang, Y., Song, X., Zhang, Y., Smith, G. ., Lotsch, a, Friedl, M., Morisette, J. ., Votava, P., Nemani, R. ., & Running, S. . (2002). Global products of vegetation leaf area and fraction absorbed PAR from year one of MODIS data. *Remote Sensing of Environment*, *83*(1-2), 214–231.

Nguy-Robertson, A. L., Gitelson, A. A., Peng, Y., Viña, A., Arkebauer, T. J., & Rundquist, D. C. (2012). Green leaf area index estimation in maize and soybean: Combining vegetation indices to achieve maximal sensitivity. *Agronomy Journal*, *104*(5), 1336–1347.

Norman, J. M., Welles, J., & Walter, E. (1985). Contrasts among Bidirectional Reflectance of Leaves, Canopies, and Soils. *IEEE Transactions on Geoscience and Remote Sensing*, *GE-23*(5), 659–667.

Peng, Y., & Gitelson, A. A. (2011). Application of chlorophyll-related vegetation indices for remote estimation of maize productivity. *Agricultural and Forest Meteorology*, *151*(9), 1267–1276.

Peng, Y., Gitelson, A. A., Keydan, G. P., Rundquist, D. C., & Moses, W. (2011). Remote estimation of gross primary production in maize and support for a new paradigm based on total crop chlorophyll content. *Remote Sensing of Environment*, *115*(4), 978–989.

Pimstein, A., Eitel, J. U. H., Long, D. S., Mufradi, I., Karnieli, A., & Bonfil, D. J. (2009). A spectral index to monitor the head-emergence of wheat in semi-arid conditions. *Field Crops Research*, *111*(3), 218–225.

Pimstein, A., Karnieli, A., Bansal, S. K., & Bonfil, D. J. (2011). Exploring remotely sensed technologies for monitoring wheat potassium and phosphorus using field spectroscopy. *Field Crops Research*, *121*(1), 125–135.

Pimstein, A., Karnieli, A., & Bonfil, D. J. (2007). Wheat and maize monitoring based on ground spectral measurements and multivariate data analysis. *Journal of Applied Remote Sensing*, *1*(1), 013530.

Pinter, P. J., Hatfield, J. L., Schepers, J. S., Barnes, E. M., Moran, M. S., Daughtry, C. S. T., & Upchurch, D. R. (2003). Remote Sensing for Crop Management. *Photogrammetric Engineering and Remote Sensing*, *69*(6), 647–664.

R Development Core Team. (2010). R: A Language and Environment for Statistical Computing. (Austria, Ed.)*R Foundation for Statistical Computing Vienna Austria*.

Ranson, K. J., Daughtry, C. S. T., Biehl, L. L., & Bauer, M. E. (1985). Sun-view angle effects on reflectance factors of corn canopies. *Remote Sensing of Environment*, *18*(2), 147–161.

Richardson, A. D., Braswell, B. H., Hollinger, D. Y., Jenkins, J. P., & Ollinger, S. V. (2009). Near-surface remote sensing of spatial and temporal variation in canopy phenology. *Ecological Applications*, *19*(6), 1417–1428.

Richardson, A. D., Dail, D. B., & Hollinger, D. Y. (2011). Leaf area index uncertainty estimates for model–data fusion applications. *Agricultural and Forest Meteorology*, *151*(9), 1287–1292.

Ritz, C., & Streibig, J. C. (2008). Grouped Data. In C. Ritz & J. C. Streibig (Eds.), *Nonlinear Regression with R* (pp. 109–131).

Rondeaux, G., Steven, M., & Baret, F. (1996). Optimization of soil-adjusted vegetation indices. *Remote Sensing of Environment*, *55*(2), 95–107.

Rouse, J. W., Haas, R. H., Schell, J. A., & Deering, D. W. (1974). Monitoring vegetation systems in the Great Plains with ERTS. In S. C. Freden & M. A. Becker (Eds.), *Third ERTS Symposium* (Vol. 1, pp. 309–317).

Rundquist, D. C., Perk, R., Leavitt, B., Keydan, G. P., & Gitelson, A. A. (2004). Collecting spectral data over cropland vegetation using machine-positioning versus hand-positioning of the sensor. *Computers and Electronics in Agriculture*, *43*(2), 173–178.

Ryu, Y., Baldocchi, D. D., Verfaillie, J., Ma, S., Falk, M., Ruiz-Mercado, I., Hehn, T., & Sonnentag, O. (2010). Testing the performance of a novel spectral reflectance sensor, built with light emitting diodes (LEDs), to monitor ecosystem metabolism, structure and function. *Agricultural and Forest Meteorology*, *150*(12), 1597–1606.

Sakamoto, T., Gitelson, A. A., Nguy-Robertson, A. L., Arkebauer, T. J., Wardlow, B. D., Suyker, A. E., Verma, S. B., & Shibayama, M. (2012). An alternative method using digital cameras for continuous monitoring of crop status. *Agricultural and Forest Meteorology*, *154-155*, 113–126.

Sakamoto, T., Gitelson, A. A., Wardlow, B. D., Arkebauer, T. J., Verma, S. B., Suyker, A. E., & Shibayama, M. (2011). Application of day and night digital photographs for estimating maize biophysical characteristics. *Precision Agriculture*, *13*(3), 285–301.

Sakamoto, T., Shibayama, M., Takada, E., Inoue, A., & Morita, K. (2010). Detecting Seasonal Changes in Crop Community Structure using Day and Night Digital Images. *Photogrammetric Engineering and Remote Sensing*, *76*(6), 713–726.

Schaaf, C. B., & Strahler, a. H. (1993). Solar zenith angle effects on forest canopy hemispherical reflectances calculated with a geometric-optical bidirectional reflectance model. *IEEE Transactions on Geoscience and Remote Sensing*, *31*(4), 921–927.

Schmidt, M., & Lipson, H. (2009). Distilling free-form natural laws from experimental data. *Science (New York, N.Y.)*, *324*(5923), 81–5.

Sellers, P. J. (1985). Canopy reflectance, photosynthesis and transpiration. *International Journal of Remote Sensing*, *6*(8), 1335–1372.

Shapira, U., Herrmann, I., Karnieli, A., & Bonfil, D. J. (2013). Field spectroscopy for weed detection in wheat and chickpea fields. *International Journal of Remote Sensing*, *34*(17), 6094–6108.

Sivanpillai, R., & Ewers, B. E. (2013). Relationship between sagebrush species and structural characteristics and Landsat Thematic Mapper data. (A. Moody, Ed.)*Applied Vegetation Science*, *16*(1), 122–130.

Smith, A. M., Bourgeois, G., Teillet, P. M., Freemantle, J., & Nadeau, C. (2008). A comparison of NDVI and MTVI2 for estimating LAI using CHRIS imagery: a case study in wheat. *Canadian Journal of Remote Sensing*, *34*(6), 539–548.

Song, J. (1999). Phenological influences on the albedo of prairie grassland and crop fields. *International Journal of Biometeorology*, *42*(3), 153–157.

Soudani, K., Hmimina, G., Delpierre, N., Pontailler, J.-Y., Aubinet, M., Bonfil, D. J., Caquet, B., De Grandcourt, A., Burban, B., Flechard, C., Guyon, D., Granier, A., Gross, P., Heinesh, B., Longdoz, B., Loustau, D., Moureaux, C., Ourcival, J.-M., Rambal, S., Saint André, L., & Dufrêne, E. (2012). Ground-based Network of NDVI measurements for tracking temporal dynamics of canopy structure and vegetation phenology in different biomes. *Remote Sensing of Environment*, *123*, 234–245.

Squires, J. R., DeCesare, N. J., Olson, L. E., Kolbe, J. a., Hebblewhite, M., & Parks, S. a. (2013). Combining resource selection and movement behavior to predict corridors for Canada lynx at their southern range periphery. *Biological Conservation*, *157*, 187–195.

Streck, N. A., Rundquist, D., & Connot, J. (2002). Estimating Residual Wheat Dry Matter from Remote Sensing Measurements. *Photogrammetric Engineering and Remote Sensing*, *68*(11), 1193–1201.

Suyker, A. E., & Verma, S. B. (2010). Coupling of carbon dioxide and water vapor exchanges of irrigated and rainfed maize–soybean cropping systems and water productivity. *Agricultural and Forest Meteorology*, *150*(4), 553–563.

Suyker, A. E., Verma, S. B., Burba, G. ., Arkebauer, T. J., Walters, D. T., & Hubbard, K. G. (2004). Growing season carbon dioxide exchange in irrigated and rainfed maize. *Agricultural and Forest Meteorology*, *124*(1-2), 1–13.

Tian, Y., Woodcock, C. E., Wang, Y., Privette, J. L., Shabanov, N. V., Zhou, L., Zhang, Y., Buermann, W., Dong, J., Veikkanen, B., Hame, T., Andersson, K., Ozdogan, M., Knyazikhin, Y., & Myneni, R. B. (2002). Multiscale analysis and validation of the MODIS LAI productI. Uncertainty assessment. *Remote Sensing of Environment*, *83*(3), 414–430.

Verhulst, N., Govaerts, B., Nelissen, V., Sayre, K. D., Crossa, J., Raes, D., & Deckers, J. (2011). The effect of tillage, crop rotation and residue management on maize and wheat growth and development evaluated with an optical sensor. *Field Crops Research*, *120*(1), 58–67.

Verma, S. B., Dobermann, A., Cassman, K. G., Walters, D. T., Knops, J. M., Arkebauer, T. J., Suyker, A. E., Burba, G. G., Amos, B., Yang, H., Ginting, D., Hubbard, K. G., Gitelson, A. A., & Walter-Shea, E. A. (2005). Annual carbon dioxide exchange in

irrigated and rainfed maize-based agroecosystems. *Agricultural and Forest Meteorology*, *131*(1-2), 77–96.

Viña, A., & Gitelson, A. A. (2005). New developments in the remote estimation of the fraction of absorbed photosynthetically active radiation in crops. *Geophysical Research Letters*, *32*(17), L17403.

Viña, A., Gitelson, A. A., Nguy-Robertson, A. L., & Peng, Y. (2011). Comparison of different vegetation indices for the remote assessment of green leaf area index of crops. *Remote Sensing of Environment*, *115*(12), 3468–3478.

Viña, A., Gitelson, A. A., Rundquist, D. C., Keydan, G. P., Leavitt, B., & Schepers, J. (2004). Monitoring Maize (L.) Phenology with Remote Sensing. *Agronomy Journal*, *96*(4), 1139.

Wang, Q., Adiku, S., Tenhunen, J., & Granier, a. (2005). On the relationship of NDVI with leaf area index in a deciduous forest site. *Remote Sensing of Environment*, *94*(2), 244–255.

Watson, D. J. (1947). Comparative physiological studies on the growth of field crops: I. Variation in net assimilation rate and leaf area between species and varieties, and within and between years. *Annals of Botany*, *11*(1), 41–76.

Weiss, A., & Norman, J. M. (1985). Partitioning solar radiation into direct and diffuse, visible and near-infrared components. *Agricultural and Forest Meteorology*, *34*(2-3), 205–213.

Wu, J., Wang, D., & Bauer, M. (2007). Assessing broadband vegetation indices and QuickBird data in estimating leaf area index of corn and potato canopies. *Field Crops Research*, *102*(1), 33–42.

Yang, C.-M., & Chen, R.-K. (2004). Modeling Rice Growth with Hyperspectral Reflectance Data. *Crop Science*, *44*(4), 1283.

Zhang, X., Friedl, M. A., Schaaf, C. B., Strahler, A. H., Hodges, J. C. F., Gao, F., Reed, B. C., & Huete, A. R. (2003). Monitoring vegetation phenology using MODIS. *Remote Sensing of Environment*, *84*(3), 471–475.

Zygielbaum, A. I., Arkebauer, T. J., Walter-Shea, E. A., & Scoby, D. L. (2012). Detection and measurement of vegetation photoprotection stress response using PAR reflectance. *Israel Journal of Plant Sciences*, *60*(1), 37–47.

Zygielbaum, A. I., Gitelson, A. A., Arkebauer, T. J., & Rundquist, D. C. (2009). Non-destructive detection of water stress and estimation of relative water content in maize. *Geophysical Research Letters*, *36*(12), L12403.

Appendix A: Abbreviations

2-D – Two-dimensional

3-D – Three-dimensional

CALMIT – Center for Advanced Land Management Information Technologies

CC – Calibration coefficient

CI – Chlorophyll index

CV – Coefficient of variation

EVI2 – Enhanced vegetation index 2

$I_{UW(\lambda)}$ – Downwelling irradiance

MERIS – Medium resolution imaging spectrometer

MNB – Mean normalized bias

MODIS – Moderate resolution imaging spectroradiometer

NDVI – Normalized difference vegetation index

$R_{UW(\lambda)}$ – Upwelling radiance

REIP - Red edge inflection point

ρ_i – Reflectance at i band

m – Optical air mass

MTCI – MERIS terrestrial chlorophyll index

MTVI2 – Modified triangular vegetation index

OSAVI – Optimized soil-adjusted vegetation index

P – Pressure measured

P_0 – Pressure at sea level

PARin – Incoming photosynthetically active radiation

PARpotential – Potential photosynthetically active radiation for a give date

%PARpotential – Percentage of the potential photosynthetically active radiation

R^2 – Coefficient of determination

RMSE – Root Mean Square Error

SE – Standard Error

σ – Standard deviation

SR – Simple ratio

TVI – Triangular Vegetation Index

VI(s) – Vegetation Ind(ex/ices)

WDRVI – Wide dynamic range vegetation index

Appendix B: Additional data for determining stage of development

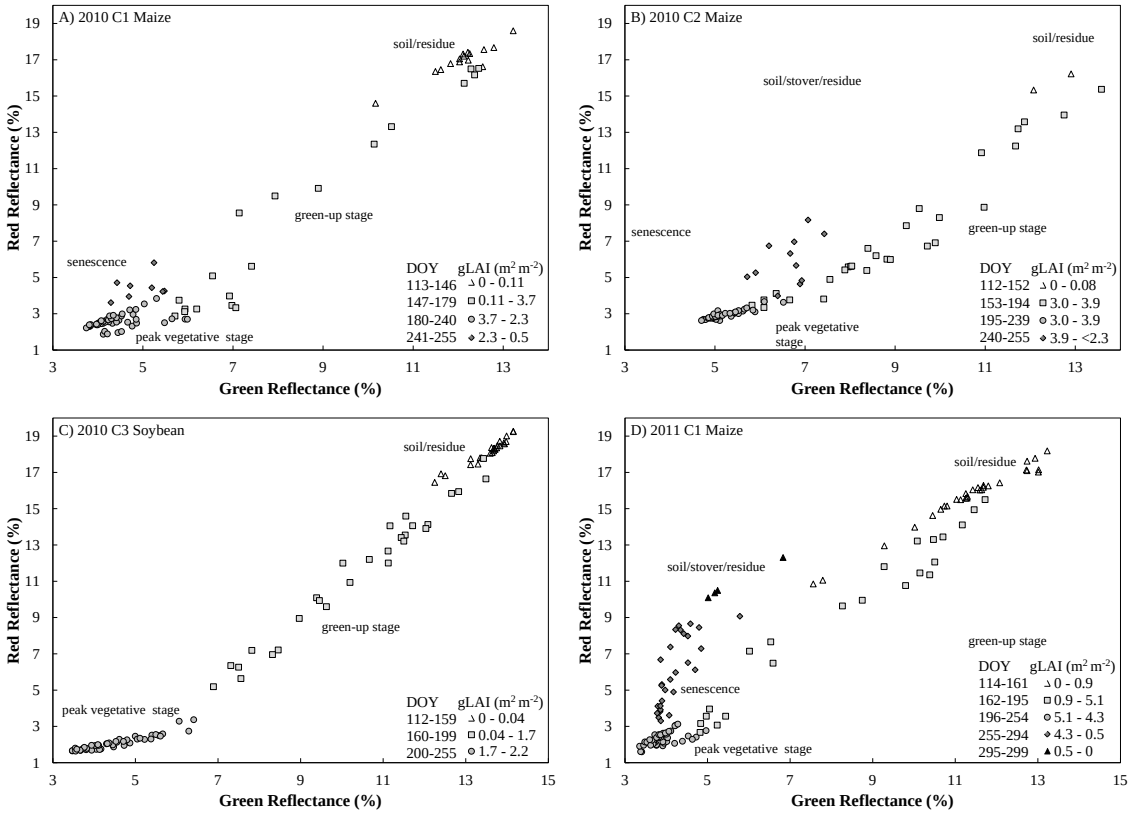

Figure B.1: Red vs. green reflectance relationships for the remainder of the sites from 2010-2012. Day of year (DOY) and the range of green LAI (green LAI) is indicated. For the peak vegetative stage (gray circles), the maximal green LAI will be larger than the values indicated in the range.

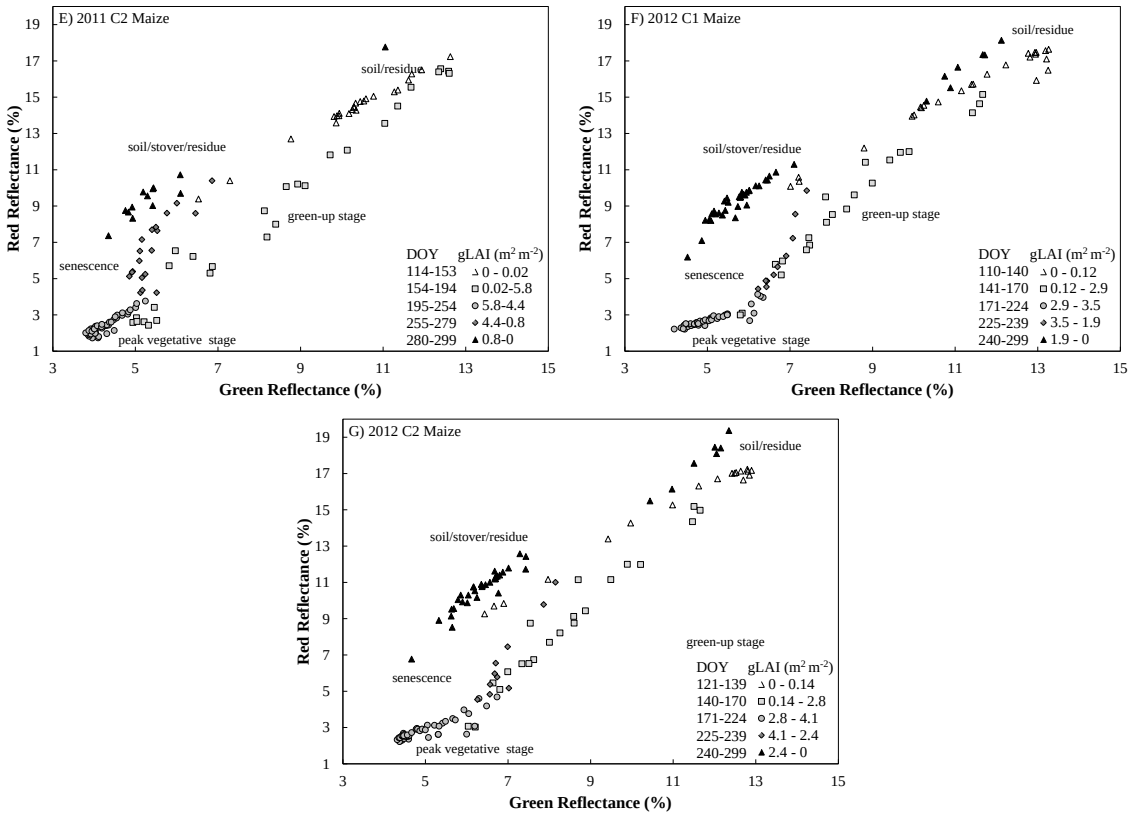

Figure B.1 (continued): Red vs. green reflectance relationships for the remainder of the sites from 2010-2012. Day of year (DOY) and the range of green LAI (green LAI) is indicated. For the peak vegetative stage (gray circles), the maximal green LAI will be larger than the values indicated in the range.

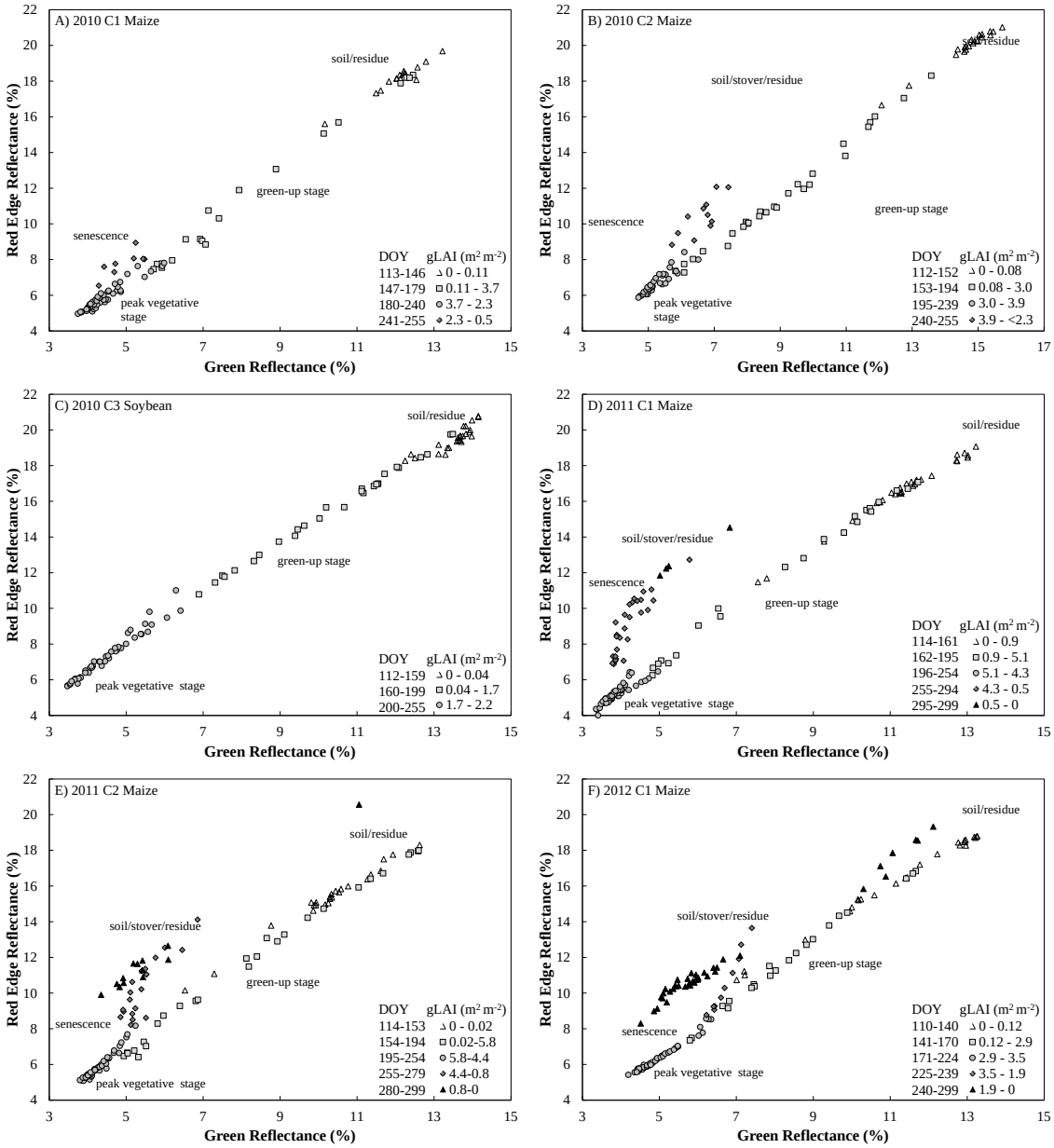

Figure B.2: Red edge vs. green reflectance relationships for the remainder of the sites from 2010-2012. Day of year (DOY) and the range of green LAI (green LAI) is indicated. For the peak vegetative stage (gray circles), the maximal green LAI will be larger than the values indicated in the range.

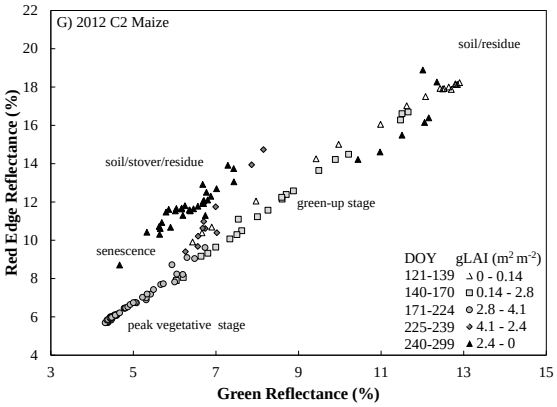

Figure B.2 (continued): Red edge vs. green reflectance relationships for the remainder of the sites from 2010-2012. Day of year (DOY) and the range of green LAI (green LAI) is indicated. For the peak vegetative stage (gray circles), the maximal green LAI will be larger than the values indicated in the range.

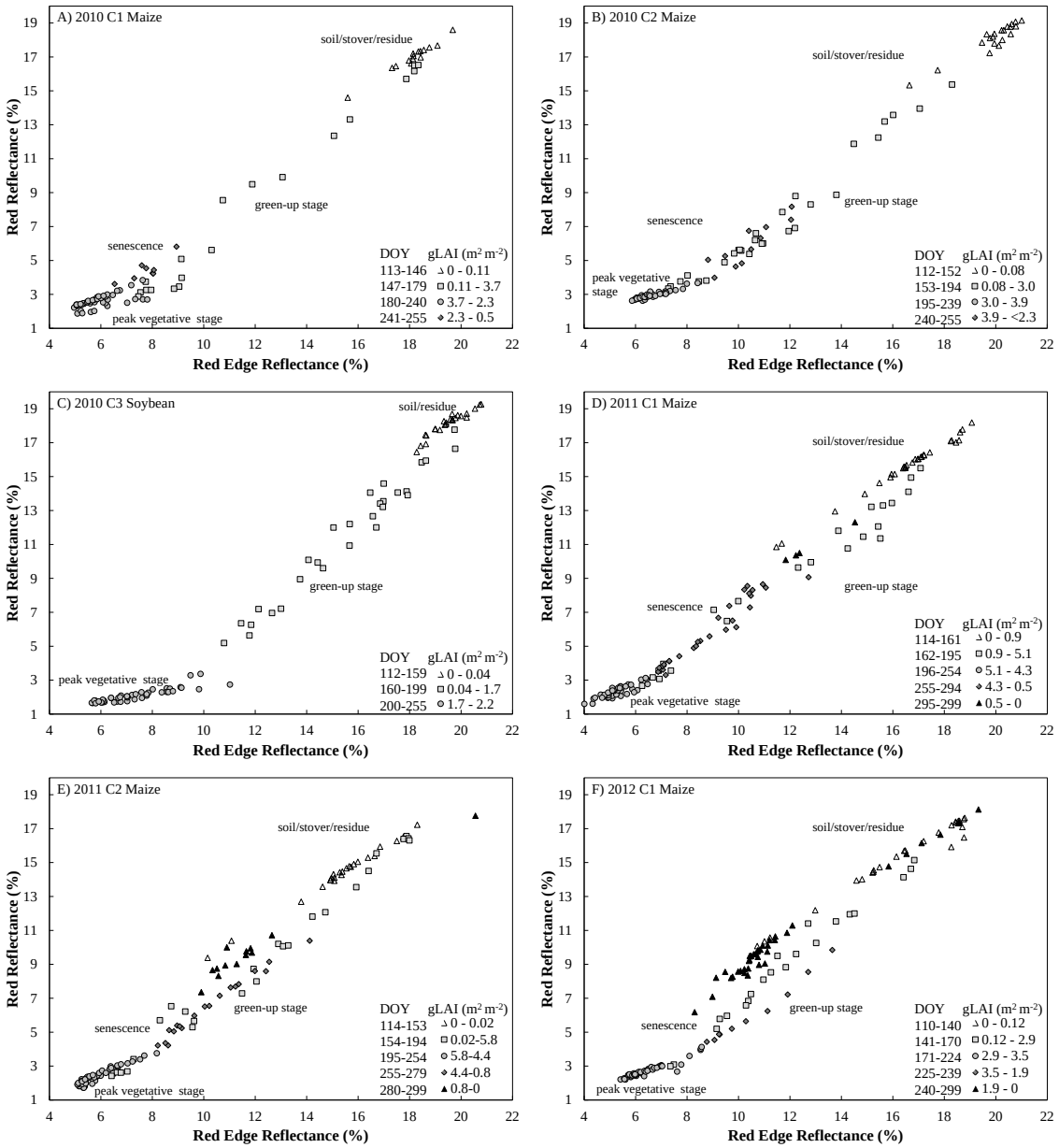

Figure B.3: Red vs. red edge reflectance relationships for the remainder of the sites from 2010-2012. Day of year (DOY) and the range of green LAI (green LAI) is indicated. For the peak vegetative stage (gray circles), the maximal green LAI will be larger than the values indicated in the range.

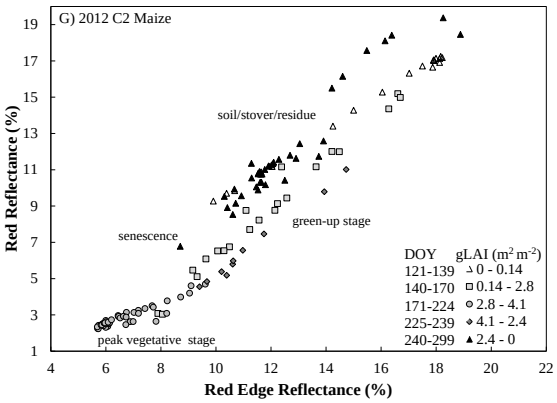

Figure B.3 (continued): Red vs. red edge reflectance relationships for the remainder of the sites from 2010-2012. Day of year (DOY) and the range of green LAI (green LAI) is indicated. For the peak vegetative stage (gray circles), the maximal green LAI will be larger than the values indicated in the range.

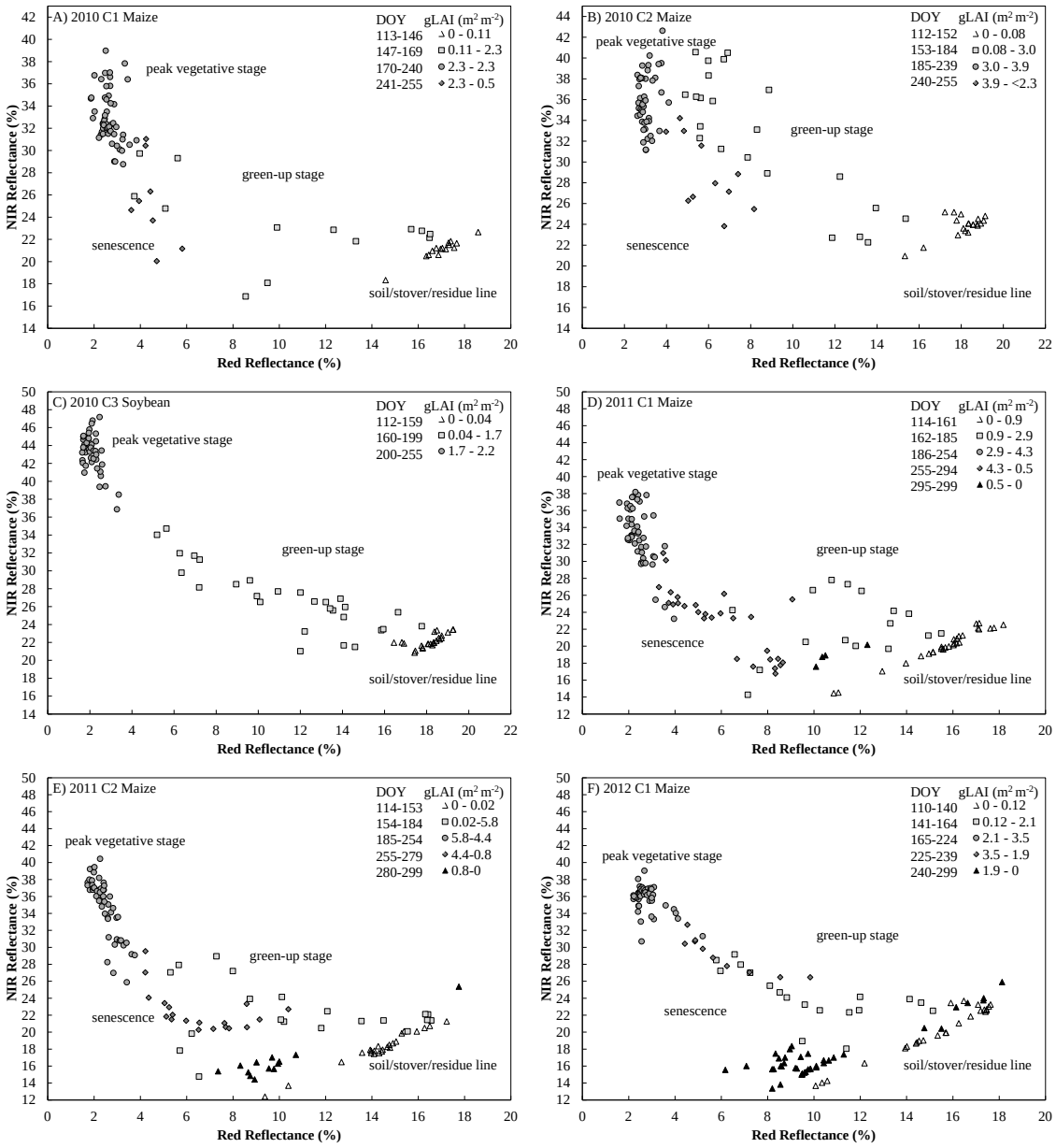

Figure B.4: NIR vs. red reflectance relationships for the remainder of the sites from 2010-2012. Day of year (DOY) and the range of green LAI (green LAI) is indicated. For the peak vegetative stage (gray circles), the maximal green LAI will be larger than the values indicated in the range.

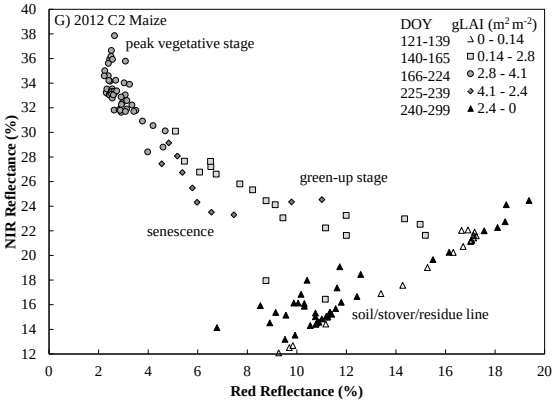

Figure B.4 (continued): NIR vs. red reflectance relationships for the remainder of the sites from 2010-2012. Day of year (DOY) and the range of green LAI (green LAI) is indicated. For the peak vegetative stage (gray circles), the maximal green LAI will be larger than the values indicated in the range.

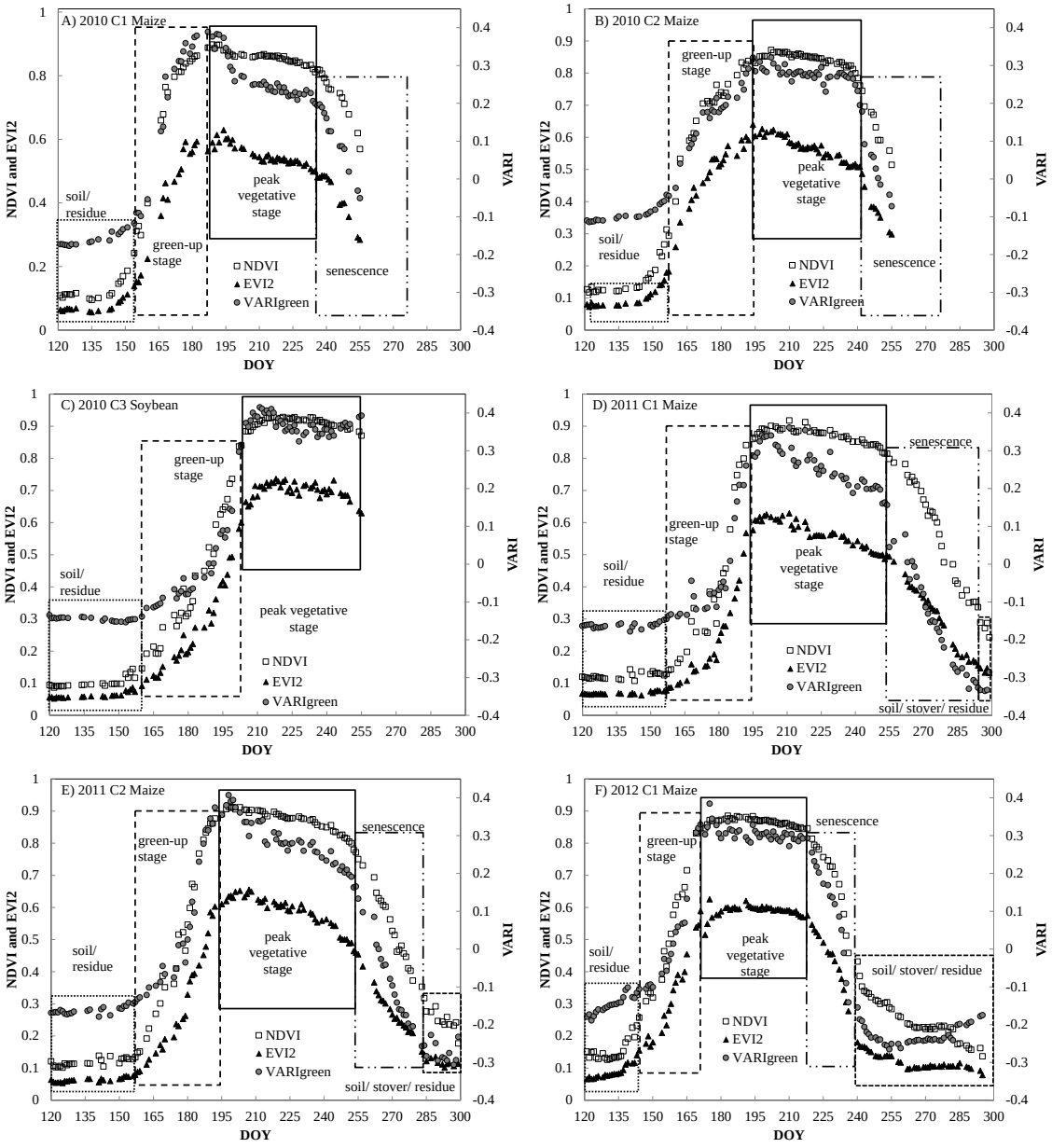

Figure B.5: Temporal behavior of three vegetation indices for the remainder of the sites from 2010-2012. Crop developmental stages identified in green vs. red reflectance relationships (Figure B.1) are labeled in each panel.

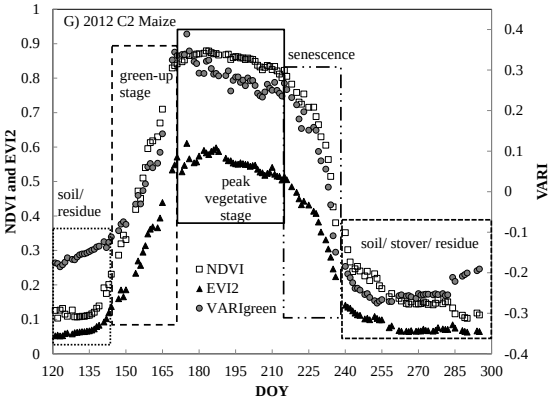

Figure B.5 (continued): Temporal behavior of three vegetation indices for the remainder of the sites from 2010-2012. Crop developmental stages identified in green vs. red reflectance relationships (Figure B.1) are labeled in each panel.